UNIVERSIDADE FEDERAL DE MINAS GERAIS
Curso de Pós-Graduação em Engenharia Metalúrgica e de Minas e Materiais

Tese de Doutorado

"Development of nano-sized Mn_3O_4 magnetic composites: application in wastewater treatment"

Autora: Gabriela Cordeiro Silva

Orientadora: Professora Virgínia S. T. Ciminelli

Co-orientador: Professora Angela de Mello Ferreira

Março de 2012

UNIVERSIDADE FEDERAL DE MINAS GERAIS

Curso de Pós-Graduação em Engenharia Metalúrgica e de Minas e Materiais

Gabriela Cordeiro Silva

"Development of nano-sized Mn_3O_4 magnetic composites: application in wastewater treatment"

Tese de Doutorado apresentada ao Curso de Pós-Graduação em Engenharia Metalúrgica e de Minas da Universidade Federal de Minas Gerais

Área de Concentração: Tecnologia Mineral

Orientadora: Professora Virgínia S. T. Ciminelli

Co-orientador: Professora Angela de Mello Ferreira

Belo Horizonte

Escola de Engenharia da UFMG

2012

Agradecimentos

Durante o desenvolvimento deste trabalho pude contar com a ajuda e o apoio de diversas pessoas as quais gostaria de agradecer.

Agradeço primeiramente a Deus pelas oportunidades que apareceram no meu caminho.

À professora Virgínia, por ter me orientado, pelas sugestões e críticas, pela avaliação do meu trabalho e pelos recursos e infra-estrutura disponibilizados.

Ao professor Wolfgang Höll e a todos os pesquisadores com os quais tive contato no KIT por me recepcionarem tão bem e motivaram a linha de pesquisa dessa tese.

Ao grupo de pesquisa do Laboratório de Hidrometalurgia pela convivência harmoniosa do dia-a-dia. À Ilda pela disposição e alegria. À Sica pelo bom humor e ajuda nas análises de meus resultados. À Cláudia pela convivência agradável e disposição em ajudar. À Christina, tia Chris, pela gentileza e eficiência. Aos companheiros, Fernando, Júlio, Gra, Adélia, Daniel, Clauson, Carol, Douglas e Rodrigo, pelo convívio amigável, troca de experiência e momentos de descontração. Aos funcionários do Laboratório de Análises Químicas pela disponibilidade em me atender. Ao Roberto pela boa vontade em fazer as imagens de MEV de minhas amostras.

Ao grupo de pesquisa do CEFET-MG por terem me acolhido tão bem. À Ângela pelo apoio e pelas dicas importantes. À Fabi e à Nath pela ajuda indispensável no laboratório e convívio amigável. Ao Paulo pelo trabalho e aprendizado com o Rietveld e medidas de DRX, e convivência agradável.

Aos professores e funcionários do Departamento de Metalurgia e de Minas em especial ao professor Wander, ao Eduardo, à Isabel e à Andréia pela boa vontade e pelas medidas de FTIR e DRX.

À Capes, ao INCT-Acqua, à Fapemig e ao CNPq pelo apoio financeiro e ao Laboratório Nacional de Luz Síncrotron e ao Centro de Microscopia pelo uso de suas instalações.

A todos os meus queridos amigos da graduação e às amigas de sempre, Caju, Sisa e Munique por ser uma fonte extra de energia.

À minha família que sempre me deu força e apoiou minhas decisões, em especial aos meus pais e a minha irmãzinha, que estão ao meu lado em todos os momentos, me aconselhando e incentivando.

Ao meu esposo, amor da minha vida, por seu carinho e compreensão nos momentos felizes e difíceis, e a sua família que passou a ser minha também.

Summary

List of Figures

List of Tables

List of Acronyms

AA	Azure A
AAS	Atomic Absorption Spectrometry
AB	Azure B
AC	Azure C
BET	Brunauer-Emmett-Teller
CCD	Charge Couple Device
CONAMA	Conselho Nacional do Meio Ambiente
DRIFTS	Diffuse Reflectance Infrared Fourier-Transformed Spectroscopy
EDS	Energy Dispersive Spectroscopy
EXAFS	Extended X-ray absorption fine structure spectroscopy
HGMS	High Gradient Magnetic Separation
ICP-OES	Inductively Coupled Plasma Optical Emission Spectrometry
ICDD	International Centre for Diffraction Data
IR	Infrared Spectroscopy
LNLS	Laboratório Nacional de Luz Síncrotron
MB	Methylene Blue
SEM	Scanning Electron Microscopy
TEM	Transmission Electron Microscopy
Th	Thionine
UV-vis	Ultraviolet-visible Spectroscopy
XAFS	X-ray Absorption Fine Structure Spectroscopy
XANES	X-ray Absorption Near Edge Structure
XRD	X-ray Diffraction

WHO	World Health Organization

Resumo

Compósitos com propriedades magnéticas foram sintetizados com sucesso por meio da deposição de óxido de manganês, Mn_3O_4, sobre partículas de magnetita. O óxido de manganês é obtido por precipitação usando O_2 como oxidante. As partículas de magnetita nos compósitos (~$40 m^2.g^{-1}$) formam aglomerados com as partículas de Mn_3O_4. A separação sólido-líquido é possível, por meio da aplicação de um campo magnético. A aplicação do compósito magnético na adsorção oxidativa de As(III) foi avaliada. Os ajustes das isotermas de sorção retornam valores de $b>1$ para a constante de Langmuir, demonstrando elevada afinidade dos compósitos por As(III), o que é desejado na remoção de contaminantes traços e sub-traços. A capacidade de adsorção máxima é $14 mg_{As}.g^{-1}_{sólido}$ ($0,0048 mmol_{As}.m^{-2}_{sólido}$). Durante o processo de adsorção e oxidação, o ferro não é liberado e parte do Mn^{2+} liberado para a solução, é adsorvido ou precipitado, ou ambos, o que implica em poucos contaminantes liberados e portanto, uma solução mais limpa. O espectro XANES dos compósitos carregados com As mostram que o arsênio adsorvido está na forma oxidada, As(V), demonstrando que o As(III) é oxidado com sucesso pelo Mn_3O_4. Dados espectrais de Raman e infravermelho das amostras carregadas com As (5,0 a $16 mg.g^{-1}$) sugerem a presença de bandas As-O referindo-se à formação de complexos monodentados e bidentados, elucidando a adsorção de arsênio na superfície do compósito. O compósito magnético de Mn_3O_4 foi também aplicado para oxidar e remover azul de metileno (MB) de soluções aquosas. Resultados de UV-vis mostram que o compósito de Mn_3O_4 é capaz de oxidar MB formando seus derivados parcial e totalmente desmetilados. A descoloração de 85% é alcançado em 60min, em pH 3. Para pH>3, a oxidação não ocorre, e apenas 50% do MB é adsorvido. Dessorção por metanol dos compostos orgânicos adsorvidos no compósito mostra que o derivado de MB totalmente desmetilado, a tionina, é o único composto adsorvido. Portanto, o presente trabalho simplifica a síntese de um compósito magnético de óxido de manganês para ser aplicado em sistemas ambientais, tanto como oxidante, quanto como adsorvente. Além disso, o trabalho acrescenta conhecimento sobre o modo das interações de As com Mn_3O_4 usando técnicas espectroscópicas vibracionais.

Abstract

Composites with magnetic properties have been successfully synthesized by means of the deposition of manganese oxide, Mn_3O_4, precipitated by using O_2 (an eco-friendly oxidant), onto magnetite particles. The magnetite particles in the composites (~$40m^2.g^{-1}$) form agglomerates with Mn_3O_4 particles. Solid-liquid separation by means of the application of a magnetic field is possible. The application of the magnetic composite in the oxidative adsorption of As^{3+} was evaluated. The arsenic sorption isotherm fits return values of b>1 for the Langmuir constant, demonstrating high affinity of the composites for As(III), which is desired for the removal of trace and sub-trace contaminants from water. The maximum adsorption capacity is ~$14mg_{As}.g_{solid}^{-1}$ ($0.0048mmol_{As}.m^{-2}_{solid}$). During the As oxidation-adsorption process, iron is not released and part of the Mn(II) released to solution is being adsorbed or precipitated, or both, which implies in a less contaminants release to solution. XANES of the As-loaded composites show that the arsenic adsorbed is in the oxidized arsenic form, As(V), demonstrating that As(III) is successfully oxidized by Mn_3O_4. Raman and IR spectral data of As-loaded (5.0 to $16mg.g^{-1}$) samples suggest the presence of As-O bands referring to the formation of inner-sphere monodentate and bidentate complexes, elucidating arsenic surface complexes on the composite. The magnetic Mn_3O_4 composite was also applied to oxidize and remove methylene blue (MB) from water. UV-vis results show that Mn_3O_4 composite is capable of oxidizing MB forming its partially and fully demethylated derivatives. Decolorization of 85% is achieved in 60min, at pH 3. For pH>3, oxidation does not occur and only 50% of the MB is adsorbed. Desorption by methanol of the organic compounds adsorbed in the composite have shown that the fully demethylated MB derivative, thionine, is the only adsorbed compound. Therefore, the present work simplifies the synthesis of a manganese oxide composite to be applied in environmental systems as both an oxidant and an adsorbent. Moreover, the work improves the knowledge about the mode of As interactions with Mn_3O_4 by using vibrational spectroscopic techniques.

Chapter 1 Introduction

1.1 Overview

The increased demand of quality water for human and industrial consumption, allied to stringent environmental laws has stimulated the development of materials and methods for the treatment of contaminated aqueous solutions. Adsorption and catalytic or direct oxidation are often involved in applied technologies for water treatment. As desired features, the adsorbent/catalyst should be low-cost, should have considerable contaminant uptake capacity or present high catalytic activity, and be easily recovered and regenerated for reuse. The performance of powder adsorbents/catalysts is sometimes limited when trace or sub-trace concentrations are concerned. In general, the best performance of the adsorbent/catalyst is associated with smaller particles, which possess large specific surface areas. Nanosized sorbents and catalysts have then been designed and evaluated in view of their superior sorption capacity and reactivity in these systems. However, the smaller the particles of the adsorbent/catalyst, the more difficult their separation from the aqueous solution is (Qu, 2008).

Magnetic separation is an effective technique for separating magnetic particles and has been used for several applications in areas such as biochemistry, analytical chemistry, mining and environmental engineering. It has the advantage of being rapid, easily applied in large scale operations and easily automated (Velsen van and Vos van der, 1991; Ebner et al., 1999). Therefore, the challenge of separating high specific surface area powder adsorbents/catalysts from solution could be addressed with the use of magnetic composites. Magnetic composites can be conveniently recovered by magnetic separation, avoiding the filtration steps, which may represent a barrier to the application of high performance advanced materials in environmental remediation processes and treatment of great volumes of aqueous solutions.

The literature has several works aiming the production of high performance adsorbents and catalysts (Qu, 2008). There are many works applying metal oxides to remove contaminants from waste-water or to catalyze reactions. Iron, aluminum, titanium and

manganese oxides are the most studied ones (Chaudhury et al., 2003; Ladeira and Ciminelli, 2004; Deschamps et al., 2005; Oliveira et al., 2006; Tripathy et al., 2006). Manganese oxides stand out for their properties, such as high surface areas and strong oxidation capacity, being mostly used at oxidation of many inorganic trace contaminants, volatile organic compounds and phenothiazine dyes (Driehaus et al., 1994; Stobbe et al., 1999; Sekine, 2002; Barret and Mcbride, 2005; Deschamps et al., 2005; Ahn et al., 2006; Chen et al., 2007; Chen and He, 2008; Dias et al., 2008; Chowdhury et al., 2009; Zaied et al., 2011; Chen et al., 2011). Magnetic manganese oxide composites can be seen as potential adsorbents/catalysts since they join the high sorptive and oxidation properties of manganese oxides with the recovery facility of magnetic materials. Therefore, the development of magnetic manganese oxide composites with high sorptive and catalytic capacities is a subject of relevance.

1.2 Magnetic composites

The magnetic particle technology has a high potential to be applied in sorption and catalysis systems, when joint with the use of magnetic separation process. The magnetic particles can be combined with functional groups or inorganic compounds yielding magnetic composites (Velsen van and Vos van der, 1991; Ebner et al., 1999). The main concern of magnetic separation processes is to generate magnetic forces on the magnetic particles large enough to overcome opposing forces, such as Brownian motion, viscous drag, and sedimentation. In a field gradient, there is a proportion between the magnetic force acting on a particle and the particle volume. Therefore, the magnetic attractive forces of ultrafine particles in a field gradient will not be large enough to overcome opposing forces, and no separation will occur. For the case of an isolated particle of magnetite, the critical size for separation is ~50nm, assuming very large applied fields that turns magnetic separations extremely expensive. In low magnetic gradients, the critical size of iron oxide magnetic particle for capture increases substantially (Yavuz et al., 2006).

Magnetite particles with diameter below 50nm exhibit a complex range of size-dependent behaviors, including a transition below ~40nm in size to single-domain

character, greater magnetic susceptibilities, and the emergence of superparamagnetic behavior. Magnetite particles are composed of small regions called magnetic domains (1-100μm), within each the local magnetization is saturated but not necessarily parallel. Domain walls are interfaces between regions in which the magnetization has different directions. As the grain size decreases, a critical size will be reached where the grain can no longer accommodate a wall. Below this critical size, the grain contains a single domain, which is uniformly magnetized to its saturation magnetization (Moskowitz, 1991). In external fields, the single-domain nanoparticles aggregate effectively forming larger and more magnetically responsive particles. Magnetite nanocrystals less than ~16nm in diameter behave as superparamagnets. Superparamagnetic particles have no remanence, which turns their interaction with the external field reversible, thus facilitating their removal from the column matrix in low-field magnetic separators. Therefore, for optimum magnetic separations at low fields, the largest magnetite nanoparticles that still show superparamagnetic properties should be used (Yavuz et al., 2006).

A series of magnetic composites, which could be separated by magnetic separation technology, have been prepared to remove a wide range of contaminants from water. Magnetic carbon composites, chitosan and alginate-bound magnetic adsorbents, magnetic synthetic polymers, magnetic clays and magnetic metal oxides, which exhibit a large specific surface area or selective functional groups, have been developed and possess great potential to remove organic and inorganic pollutants in sorption processes due to the high sorption capacities and conveniently magnetic separation (references in Table 1-1).

Most of the works shown in Table 1-1 use the magnetic composites to remove heavy metals or dyes. Very few works investigate the removal of anions and oxyanions. Moreover, most of the composites still suffer from complex synthetic procedures and high cost. The development of less costly and environmentally friendly magnetic composites, which require less reagents, lower temperature and shorter time for their synthesis, should be investigated as an alternative replacement of commercial materials used in water treatment, such as activated carbon (Gupta et al., 2009).

Table 1-1: List of some magnetic adsorbents found in the literature.

Magnetic Adsorbent	Specific Surface Area ($m^2 g^{-1}$)	Contaminant	Sorption capacity	Reference
Magnetic carbon composite	1885	organic dyes	83-91%	Si et al.,2012
	658	organic dyes	13.15 and 22mg.g^{-1}	Sun et al., 2011
	148	As(V) and As(III)	5.83 and 13.10mg.g^{-1}	Chandra et al., 2010
Magnetic chitosan	-	Methyl orange	1651mg.g^{-1}	Hu et al., 2012
	-	Cu^{2+}, acid dyes	20mg.g^{-1}	Chang and Chen (2005a, 2005b)
	-	Co^{2+}	27.4mg.g^{-1}	Chang et al., 2006a
	-	Fluoride	15.08mg.g^{-1}	Ma et al., 2007
	-	Au^{3+} and Ag^{1+}	3.79 and 1.93mmol.g^{-1}	Donia et al., 2007
Magnetic alginate	174	Ni^{2+}	0.52mmol.g^{-1}	Ngomsik et al., 2006
	312.94	As(V) and Cu^{2+}	6.75 and 60.24mg.g^{-1}	Lim and Chen, 2007
	313	Cu^{2+}	0.99mmol.g^{-1}	Lim et al., 2008
	-	organic dyes	(2.4 - 15.9) x10^{-3}mmol.g^{-1}	Rocher et al., 2008
Magnetic synthetic polymer	-	Cu^{2+}, Cd^{2+}, Pb^{2+}	6.5, 20.3, 41.6mg.g^{-1}	Denizli et al., 1998
	0.065	Cu^{2+}	2.26eq.kg^{-1}	Dahlke et al., 2006
Magnetic clay	55	Ni^{2+}, Cu^{2+}, Cd^{2+},Zn^{2+}	40, 50, 74, 75mg.g^{-1}	Oliveira et al., 2003
	353	Cr^{3+}, Cu^{2+}, Zn^{2+}	49, 87, 114mg.g^{-1}	Oliveira et al., 2004
	134	Pb^{2+}, Cu^{2+}	0.51, 0.71mmol.g^{-1}	Peng et al., 2006
Magnetic metal oxides and hydroxides	(MnO_2)	As(V), As(III)	0.68mg.g^{-1}	Dlugosch, 2001
	(Fe_3O_4)	U^{6+}	52mg.g^{-1}	Fan et al., 2012
	42, 76 ($Al(OH)_3$)	Fluoride	38, 8g.kg^{-1}	Chang et al., 2006b
	79.6 (ZrO_2)	Sulfate	9.29, 9.78g.kg^{-1}	Chang et al., 2008
	92 (MnO_2)	Cd^{2+}	35mg.g^{-1}	Rosas et al., 2010

576.4 (MnO_2)	Congo Red	85-94%	Zhai et al., 2009
70, 96 (MnO_x)	Methylene Blue	44.2%, 90%	Chen et al., 2011

1.3 Manganese oxides

Manganese (Mn) is the third most abundant transition metal and the 10th most abundant element on the Earth's crust. Close to the Earth's surface, Mn is effortlessly oxidized, giving rise to more than 30 identified Mn oxide/hydroxide minerals. These oxides occur in three different oxidation states: +2, +3, and +4. These are the major players in the story of mineralogy and geochemistry of Mn in the upper crust and the major sources of industrial Mn. High levels of Mn are found in the soils of the Iron Ore Province (IOP) of Minas Gerais State, in the form of different manganese oxides (Carvalho Filho et al., 2011). Mn oxides/hydroxides are highly chemically active and strong scavengers of heavy metals. Manganese is not toxic; however, it causes problems in drinking water, such as turbidity and precipitation in pipes, which leads to a bad taste of the water (Dlugosch, 2001; Martins and Lima, 2001). The EPA limit for soluble Mn in drinking water is 0.05mg.L^{-1}. In Brazil, CONAMA establishes that the limit for soluble Mn is 0.5mg.L^{-1} in drinking water and 1.0mg.L^{-1} in effluents (CONAMA, 2011). The redox chemistry of manganese II-IV have significant roles and impact in the environment, such as oxidation of metal oxides and organic compounds, thus the study of Mn oxide precipitation and dissolution rates and mechanisms involved are relevant (Martin, 2005). Manganese is difficult to remove. It needs highly oxidizing and high pH (above 9) conditions for manganese oxide/hydroxide formation (Lovett, 1992; Johnson and Younger, 2005; Johnson and Hallberg, 2005; Martin, 2005). This precipitation condition results in high consumption of an alkaline reagent (often Ca^{2+} based) and in formation of large amounts of sludge to be disposed of.

Fig. 1-1 shows the Eh-pH diagrams for 10^{-5}mol.L^{-1} and 10^{-3}mol.L^{-1} Mn_T at 25ºC, where Mn_T is the sum of all the manganese aqueous and solid species. The manganese concentration was chosen based on the CONAMA limits for manganese in effluents and the values usually found in effluents before treatment (CONAMA 2011). $[Mn(H_2O)_6]^{2+}$

is the unique dominant species at a wide Eh-pH range (Fig. 1-1). By increasing pH, Mn^{2+} precipitates. Moreover, by increasing Mn concentration, pH for precipitation decreases. Eh-pH diagrams establish the thermodynamically favorable pathways for transformations, but to predict the transformation rates, a kinetic analysis is required. Kinetic analysis of manganese transformations in natural waters shows that the manganese dissolution rate is slow. Similarly, the precipitation rate is quite slow in the absence of catalysis. The least thermodynamically favored solid is the first solid to form. This phenomenon is called Ostwald`s rule of stages (Martin, 2005).

In natural waters, aqueous Mn^{2+} is oxidized by reaction with dissolved O_2. The reaction rate becomes appreciable only for pH>8 and it proceeds through the aqueous $Mn(OH)_2$ species (homogeneous oxidation). Mn^{2+} oxidation rate is catalyzed by metal oxide surfaces terminated by hydroxyl groups (>OH), which bind Mn^{2+}. The ($>O_2Mn$) complexes promote fast oxidation (heterogeneous oxidation), just as OH ligands do. The catalysis occurs both on foreign surfaces and for the special case of autocatalysis, where the product of the oxidation accelerates the reaction rate (Martin, 2005). None of the catalysts for Mn oxidation are as effective as Mn oxides (Lovett, 1992; Johnson and Younger, 2005). The rate of abiotic Mn oxidation is dependent on both the concentration of Mn^{2+} ions and the quantity of Mn oxide present. The oxidation of Mn^{2+} begins through adsorption on mineral surfaces. After the initial oxidation the newly formed site becomes the most reactive for continuation of the adsorption-oxidation process (Lovett, 1992; Johnson and Younger, 2005).

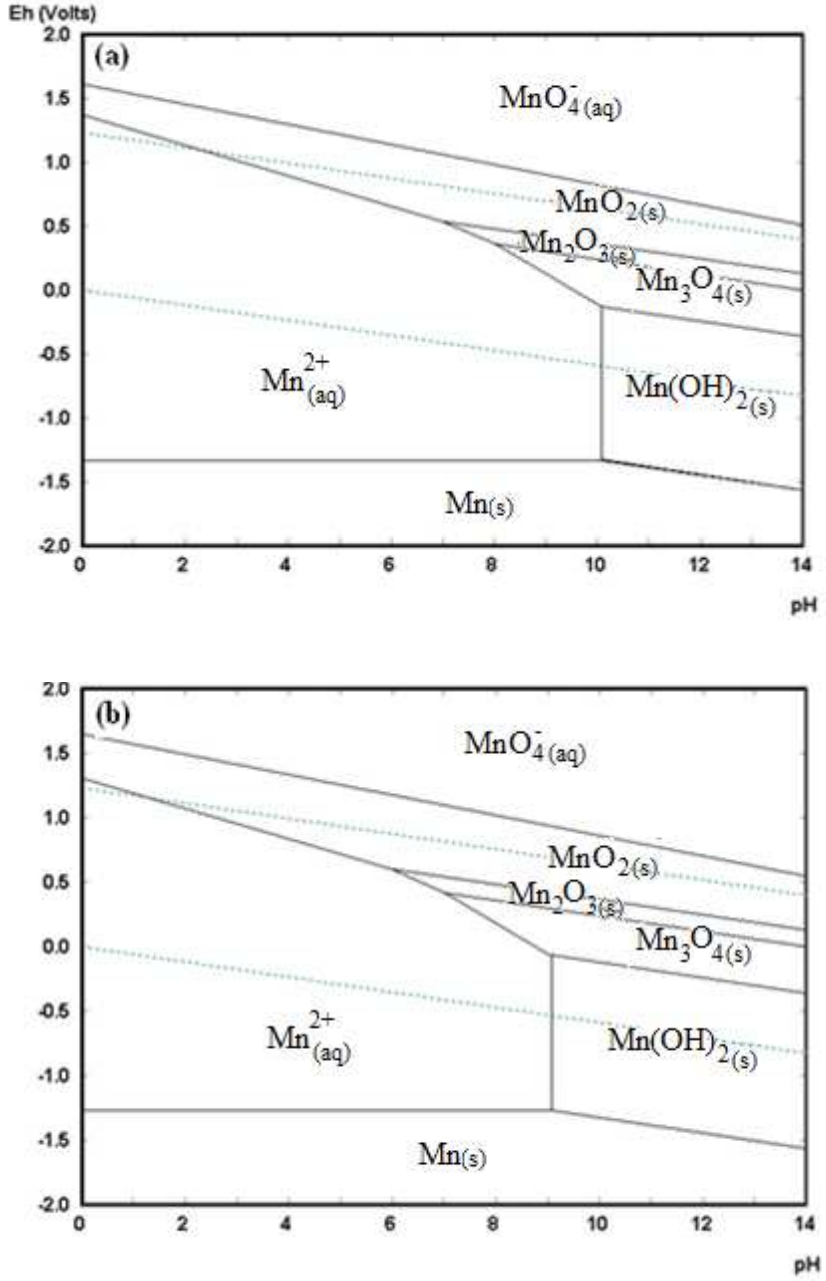

Fig. 1-1: Eh-pH diagrams of manganese species for (a) $[Mn_T] = 10^{-5}mol.L^{-1}$ and (b) $[Mn_T] = 10^{-3}mol.L^{-1}$. The water stability field is shown for pO_2=1.0atm and pH_2=1.0atm (HSC 6) (Appendix).

When the contacting aqueous solution is strongly undersaturated, manganese oxides dissolve. The more acidic is the pH, the greater are the dissolution rates. The rates depend on crystalline phase, initial chemical or physical preparation and often pass through initial transients of rapid dissolution. Proton-promoted, ligand-promoted, reductive, and synergistic dissolutions are parallel pathways of increasing dissolution rates. Reductive dissolution is faster than ligand-promoted dissolution; and proton-promoted dissolution is the slowest of all. Protons attach to the oxygen in the hydroxyl groups that bridge the metals, removing electron density and weakening the bond strength of the metal-oxygen linkage. Ligands bind to the surface groups of manganese oxides forming inner-sphere complexes and, thus, increasing dissolution rates. The greater the ligand surface concentration and the ligand binding strength, the greater the increase in dissolution rate. Manganese oxide dissolution is rapidly accelerated by reductants. A surficial Mn^{2+} ion locked inside an oxide lattice is formed when an electron is transferred to a Mn^{3+}/Mn^{4+} oxide and rapid depolymerization occurs followed by Mn^{2+} release to the aqueous phase. Manganese oxides are reduced by common organic matter, such as ascorbic acid, hydrogen sulfide, and phenols, and also by inorganic compounds, such as arsenite. Moreover, dissolution rate increases above the sum of individual dissolution rates when some species interact cooperatively. This is called synergistic dissolution (Martin, 2005).

1.4 Potential applications of magnetic manganese oxide composites

One of the most important applications of manganese oxides is oxidation. Manganese oxides serve as highly active thermally stable catalysts for oxidation or direct oxidants of a variety of volatile organic compounds, such as formaldehyde, methane, oxalic acid, phosphonic acid and diphenyl ether (Stobbe et al., 1999; Sekine, 2002; Barret and Mcbride, 2005; Ahn et al., 2006; Chen et al., 2007; Chen and He, 2008), of phenothiazine dyes, such as methylene blue and its partially and fully *N*-demethylated derivatives (Chowdhury et al., 2009; Chen et al., 2011; Zaied et al., 2011) and of some inorganic compounds, such as arsenite, Cr^{3+} oxide and Se^{4+} oxide (Stumm and Morgan, 1981; Oscarson et al., 1981, 1983; Eary and Rai, 1987; Driehaus et al., 1994; Scott and Morgan, 1995; Deschamps et al., 2005; Dias et al., 2008).

Over the last few decades, adsorption has gained increased importance as an effective purification and separation technique used in wastewater treatment. The removal of heavy metals from metal-laden tap or waste water is considered an important application of adsorption processes using a suitable adsorbent (Han et al., 2006; Tripathy et al., 2006). Manganese oxide has been described as a good adsorbent for heavy metals such as Cd^{2+}, Co^{2+}, Pb^{2+}, Cu^{2+}, Ni^{2+} and Zn^{2+} from aqueous solutions or waste water due to its relatively high surface area, micro porous structure, and hydroxyl functional groups capable of reacting with metals, phosphate and other specifically sorbing ions (Han et al., 2006; Tripathy et al., 2006).

Only a few works have been focusing on magnetic manganese oxide composites to be used in water treatment (Dlugosch, 2001; Zhai et al., 2009; Rosas et al., 2010; Chen et al., 2011). Most of these works focus on manganese dioxides (Dlugosch, 2001; Zhai et al., 2009; Rosas et al., 2010) and only one work (Chen et al., 2011) investigates manganese oxides with higher standard reducing potential, such as Mn_3O_4 and Mn_2O_3. However, in the aforementioned work, the Mn_3O_4 and Mn_2O_3 are synthesized using high temperature (250^{o}C) and long time (24h). Furthermore, the combined effect of oxidation/sorption is not investigated.

Considering the aforementioned context, the development of a less complex synthesis (temperature, reagents, time) of magnetic manganese oxide composites with high standard reducing potential manganese oxide phases, such as Mn_3O_4, to be investigated for their combined oxidation/sorption property in stirred, solid-aqueous environmental systems to remove both inorganic and organic contaminants is subject of relevance.

1.5 Characterization Techniques

1.5.1 X-Ray Diffraction (XRD)

X-ray diffraction of powders is a technique frequently used for phase identification of a crystalline material and can provide information on unit cell dimensions, space group and quantitative analysis by Rietveld refinement. X-ray diffraction technique is based on constructive interference of monochromatic X-rays and a crystalline sample when conditions satisfy Bragg's Law ($n\lambda=2d \sin\theta$), which relates the wavelength of electromagnetic radiation to the diffraction angle and the lattice spacing in a crystalline sample. The random orientation of powdered materials makes it possible to attain all diffraction directions of the lattice by scanning the sample through a range of 2θ angles, allowing the identification of the minerals present by comparison with standard reference patterns (Dutrow and Clark, 2012).

X-ray powder diffraction is most widely used for the determination of unknown crystalline materials, which is critical to studies in geology, environmental science, material science, engineering and biology. In environmental science X-ray diffraction analysis are often used to identify phases (i.e., composition) in precipitates (Caetano et al., 2009) and residues (Pantuzzo and Ciminelli, 2010). Many other applications are possible, such as determination of unit cell dimensions and crystal structures, quantitative analysis, degree of crystallinity and crystallite size calculations, characterization of thin films (by small angle X-ray diffraction) and textural measurements (Dutrow and Clark, 2012; Majuste et al., 2012; Ribeiro et al., 2012). Ribeiro et al. (2012) have used X-ray diffraction to characterize the structure of a nanosized semiconducting oxide. The values of average particle sizes and microstrains could be calculated and Rietveld refinement procedure applied to obtain the unit cell structure. Rietveld refinement is a technique devised by Hugo Rietveld for use in the characterization of crystalline materials. The "Rietveld Method" creates a virtual separation of the overlapping peaks in powder X-ray diffraction diagrams, allowing an accurate determination of the structure. A widely used application of the method is quantitative phase analysis (Rietveld, 1969; Wei et al., 2012). Quantitative phase

analyses by Rietveld refinement can be used even to address the amorphous content of materials (Jansen et al., 2011).

1.5.2 Vibrational Spectroscopy

Vibrational spectroscopy includes infrared (IR) and Raman spectroscopy and provides characteristic fundamental vibrations that are employed for the elucidation of molecular structure. Raman and IR spectroscopy are complementary techniques and measure the vibrational modes of a molecule. Although some vibrations may be active in both Raman and IR, these two forms of spectroscopy arise from different processes and different selection rules. In general, Raman spectroscopy is best at symmetric vibrations of non-polar groups while IR spectroscopy is best at the asymmetric vibrations of polar groups (Larkin, 2011).

IR spectroscopy measures transitions between molecular vibrational energy levels as a result of the absorption of mid-IR radiation. Raman spectroscopy is a two-photon inelastic light-scattering event. Here, the incident photon is of much greater energy than the vibrational quantum energy, and loses part of its energy to the molecular vibration with the remaining energy scattered as a photon with reduced frequency (Larkin, 2011).

Raman and IR spectroscopy have been used in the identification of phases and compounds contained in rocks, minerals, corrosion products, tailings and industrial wastes (Ladeira and Ciminelli, 2004; Dias et al., 2008; Caetano et al., 2009; Guimarães et al., 2009; Silva et al., 2009; Caldeira et al., 2010; Müller et al., 2010; Majuste et al., 2012; Duarte et al., 2012). In the environmental area, Raman spectroscopy allows microanalysis, contributing to define the speciation of the chemical element and the identification of molecules (types of bonds involved) (Teixeira and Ciminelli, 2005; Teixeira et al., 2007; Dias et al., 2008; Müller et al., 2010; Duarte et al., 2012). Diffuse reflectance infrared spectroscopy (DRIFTS) can also be used to identify surface-bound complexes (Guimarães et al., 2007; Caldeira et al., 2010; Müller et al., 2010). Raman and IR spectroscopy analysis presents the benefits of the identification of less crystalline and amorphous phases, and small amounts of material (Teixeira et al., 2007;

Dias et al., 2008; Müller et al., 2010; Duarte et al., in press). Raman spectroscopy is a nondestructive technique that requires no sample preparation. With this technique, diatomic homonuclear molecules, aqueous solutions and heterogeneous complex mixtures can be analyzed. In Micro-Raman, the spectrometer has a microscope that is used to select the area to be analyzed (even single particles) (Ferraro et al., 2003). Most of the minerals or compounds have a unique Raman spectrum, composed by narrow and well defined bands associated to local or net vibrations. The technique also allows the identification of oxyanions (i.e., SO_4^{2-}, CO_3^{2-}, PO_4^{3-}, AsO_4^{3-}, and others), as these are good in dispersing the light, and may be present in the form of compounds adsorbed in a matrix (Teixeira et al., 2007; Dias et al., 2008; Müller et al., 2010; Duarte et al., 2012).

1.5.3 Mössbauer Spectroscopy

Mössbauer spectroscopy is a versatile technique that can be used to provide information in many areas of science. The technique is widely used to examine the valence state of iron, which is found in nature as Fe^0 (metal), Fe^{2+}, and Fe^{3+}, as well as the type of coordination polyhedron occupied by iron atoms (trigonal, tetrahedral, octahedral, etc.) (Silva et al., 2009; Vasconcelos et al., 2010; Solti et al., 2012), and also in the identification of Fe oxide phases and characterization of synthesized nanoparticles (Rodriguez et al., 2010; Silva et al., 2012)

Mössbauer spectroscopy has an extremely fine energy resolution and can detect even subtle changes in the nuclear environment of the relevant atoms. Typically, there are three types of nuclear interactions that are observed, Isomer Shift (or chemical shift), Quadrupole Splitting and Hyperfine Splitting (or Zeeman Splitting). The Isomer Shift reflects the chemical bonding of the atoms and is related to the electron density at the nucleus; the Quadrupole Splitting reflects the interaction between the nuclear quadrupole and the surrounding electric field gradient; the Hyperfine Splitting is a result of the interaction between the nucleus and any surrounding magnetic field. The combination of these parameters is used to identify the valence state and site occupancy of Fe in a given site and individual mineral (Silva et al., 2009; Vasconcelos et al., 2010). Additional information in the form of a value for the magnetic field can help with

identification of some phases if the phase is magnetically ordered (Rodriguez et al., 2010). Mössbauer spectroscopy is also also used to identify minerals (Silva et al., 2012). Nevertheless, this application is limited, since many different minerals can have site geometries that are the same and their Mössbauer spectra and the parameters will also be the same (Gütlich, 2012). In addition to identification, the relative intensities of the various peaks reflect the relative concentrations of compounds in the sample and can be used for semiquantitative analysis (Navarra et al., 2010; Presniakov et al., 2012). Also, since ferromagnetic phenomena are size-dependent, in some cases spectra can provide insight into the crystallite size and grain structure of a material (Rocha et al., 2012).

1.5.4 Electron Microscopy (SEM and TEM)

Electron microscopy uses a beam of electrons to illuminate samples and produce magnified images. Electron microscopes achieve better than 50pm resolution and magnifications of up to about 10,000,000 times and use electrostatic and electromagnetic "lenses" to control the electron beam and focus it to form an image. Electron microscopy is used to observe a wide range of biological and inorganic samples. Industrially, the electron microscope is often used for quality control and failure analysis (Erni et al., 2009).

Transmission electron microscopy (TEM) uses a high voltage electron beam to create an image. The electrons are transmitted through the sample that is in part transparent to electrons and in part scatters them out of the beam. When it emerges from the sample, the electron beam carries information about its structure. The image is detected by the CCD and is displayed on a monitor. High-resolution transmission electron microscopy (HRTEM) has allowed the production of images with resolution below 0.5Å (50pm) and magnifications above 50 million times (Erni et al., 2009). The ability to determine the positions of atoms within materials has made the HRTEM an important tool for nano-technologies research and development (O'Keefe et al., 2005; Chandra et al., 2010).

Unlike the TEM, the scanning electron microscopy (SEM) produces images by probing the samples with a focused electron beam that is scanned across a rectangular area of the specimen. The electron beam loses energy interacting with the samples, which is converted into heat, low-energy secondary electrons and high-energy backscattered electrons, light or X-ray emissions, which provide signals carrying information about the properties of the sample surface, such as its topography and composition. The image resolution of a SEM is about an order of magnitude poorer than that of a TEM. The SEM image relies on surface processes rather than transmission and, therefore, it is able to image bulk samples up to many centimetres in size and has a great depth of field, producing images that are good representations of the three-dimensional shape of the sample (McMullan, 1993). There is a variety of SEM called environmental scanning electron microscope (ESEM), which produces images of sufficient quality and resolution with the samples being wet or contained in low vacuum or gas (McMullan, 1993; Rosas et al., 2010).

1.5.5 Ultraviolet-visible Absorption Spectroscopy (UV-vis)

UV-vis absorption spectroscopy typically probes electronic transitions from valence bands or low molecular electronic levels into the conduction bands or unoccupied orbitals of solids or molecules. UV-vis absorption spectroscopy is used broadly to study chemistry in solutions and is routinely used in analytical chemistry for the quantitative determination of different analytes, such as transition metal ions, highly conjugated organic compounds, and biological macromolecules. However, it is not commonly employed for the study of liquid/solid interfaces, since weak UV-vis absorption signals from species at liquid/solid interfaces are easily obscured by the much more intense broad bands due to the liquid phase (Zaera, *in press*).

The Beer-Lambert law states that the absorbance of a solution is directly proportional to the concentration of the absorbing species in the solution and the path length. Thus, for a fixed path length, UV-vis spectroscopy can be used to determine the concentration of the absorber in a solution. It is necessary to know the rate of absorbance changes with concentration. This can be taken from references (tables of molar extinction

coefficients), or more accurately, determined from a calibration curve (Solomons, 1996).

Many studies of adsorption kinetics using UV-vis absorption spectroscopy rely on the indirect measurement of the concentration of the adsorbate molecules in solution before/after the uptake, mainly the ones related to dye adsorption and degradation (Chowdhury et al., 2009; Chen et al., 2011; Zaied et al., 2011). UV-vis absorption spectroscopy can also be used to obtain more detailed kinetics, or even fast dynamic, information. For this, the absorption of light of fixed energy, often from a pulsed laser, is followed as a function of time; the use of picosecond lasers affords the study of the dynamics of fast electronic transitions this way (Zaera, *in press*).

1.5.6 X-ray Absorption Spectroscopy (XAS)

When X-rays hit a sample, they can be scattered or absorbed and excite the electrons bound in an atom. At certain energies, the absorption increases drastically and gives rise to the absorption edge. Each such edge occurs when the energy of the incident photons is just sufficient to produce a photoelectron. When the photoelectron leaves the absorbing atom, its wave is backscattered by the neighbouring atoms. The X-ray absorption spectrum can be divided into 2 regions: X-ray absorption near edge structure (XANES), which comprehends the range of energy until 30eV above the edge; and extended X-ray absorption fine structure (EXAFS), which starts approximately from 30eV above the edge and continues. In the XANES region, transitions of core electrons to non-bound levels with close energy occur, a sudden raise of absorption is observed and informations of oxidation state and electronic structure of the absorber atom are obtained. In the EXAFS region, the photoelectrons have high kinetic energy, and single scattering by the nearest neighbouring atoms normally dominates. Informations of coordination number, interatomic distances and nature of the neighbors of the absorber atom are obtained by EXAFS (Newville, 2004).

1.6 Relevance and Objectives

High surface area and powerful oxidants metal oxides, such as manganese oxides, are of great interest in the removal of trace contaminants from aqueous solutions due to their adsorption, oxidation and chemical catalysis properties. Magnetic separation is a consolidated technology that can be applied to remove ultrafine particles from aqueous solutions. Therefore, magnetic manganese oxide composites have potential to be applied in advanced water treatment systems, since they combine the sorptive, oxidative and catalytic properties of ultrafine manganese oxide particles with the recovery facility of magnetic separation technology.

The few works that developed magnetic manganese oxide composites to be used in water treatment (Dlugosch, 2001; Zhai et al., 2009; Rosas et al., 2010; Chen et al., 2011) have focused on manganese dioxides or other manganese oxide phases, such as Mn_3O_4 and Mn_2O_3, which are synthesized by complicated routes using high temperature and long time. Moreover, the combined oxidation/sorption effect of using the manganese oxide composites to remove organic and inorganic contaminants from water is overlooked.

In this context, the present work aims to synthesize magnetic composites by precipitating manganese oxides in the presence of magnetite particles by using an environmentally friendly oxidant, such as oxygen from the air. The magnetic manganese oxide composites should have high affinity and be able to remove trace and sub-trace contaminants. Moreover, the composites should present combined oxidation/sorption property eliminating the need of a pre-oxidation process. The following specific objectives are proposed: (i) less complex (temperature, reagents, time) synthesis of stable manganese oxide magnetic composites; (ii) evaluation of the magnetic composites that combine oxidation/sorption capacities in stirred, solid-aqueous environmental systems to remove both inorganic and organic contaminants. As selected case studies, arsenite oxidative adsorption and dye degradation are investigated.

1.7 Thesis Structure

The Thesis is organized in 6 chapters. In Chapter 1 the work is contextualized by means of a review on magnetic composites, manganese oxides and potential applications for manganese oxide composites. A brief description of the characterization techniques applied, as well as the relevance and objectives are also presented.

In Chapter 2, the synthesis of manganese oxide composites with commercial magnetite by two different routes - one using permanganate as oxidant and the other using air - are described and the different products are compared by means of characterization techniques and As(III) removal tests. The best route was shown to be the one which used air as oxidant and yielded Mn_3O_4 as the unique Mn oxide phase with no exposed magnetite particles.

In Chapter 3 the magnetic composites (Mn_3O_4/Fe_3O_4) synthesized by the best route according to Chapter 2, but with three different magnetic particles (commercial, ball-milled commercial and synthesized), are evaluated for the removal of As(III) from aqueous solutions. Part of the results of this chapter was published as a paper by the journal *"Materials Research"*. The Mössbauer analyses were carried out at Centro Brasileiro de Pesquisas Físicas (CBPF) by Dr. Pablo Muñoz. XANES measurements were performed at *Laboratório Nacional de Luz Síncroton* (LNLS) in collaboration with Drª Maria Sylvia Dantas and Drª Graziele Duarte from UFMG.

Chapter 4 investigates the mechanism of arsenic immobilization in the Mn_3O_4 magnetic composite (with synthesized magnetite nanoparticles) by Raman and IR spectroscopy. This is a paper accepted for publication by the journal *"Spectrochimica Acta Part A"*. The Raman analyses were carried out at Universidade Federal de Minas Gerais (UFMG), at the Department of Metallurgical and Materials Engineering under supervision of Drª Maria Sylvia S. Dantas. IR analyses were carried out at the same department by Dr. Eduardo Henrique Martins Nunes at the Laboratory of Ceramic Materials supervised by Prof. Wander Luiz Vasconcelos.

In Chapter 5 UV-vis spectroscopy is used to evaluate the degradation of methylene blue by the Mn_3O_4 magnetic composites (with synthesized magnetite nanoparticles). The degradation tests and UV-vis analyses were carried out at Centro Tecnológico de Minas Gerais (CEFET-MG), at the Chemistry Department. The XRD analyses were also performed at CEFET-MG with collaboration of Dr. Paulo Renato Paiva. The results will be submitted to the journal *"ACS Nano"*.

Finally, Chapter 6 brings the final considerations of the project, including the main conclusions and the suggestions to future works.

Chapter 2 Synthesis of manganese oxide magnetic composites: Evaluation of different synthesis parameters

2.1 Introduction

The use of inorganic magnetic micro- or nano-composites technology to minimize environmental problems has received considerable attention. Magnetic inorganic composites can be used to remove contaminants from aqueous effluents and the loaded material can be separated from the medium by a simple magnetic process. Activated carbon, carbon nanotubes, clay materials and zeolites have been combined with maghemite or magnetite to produce magnetic composites (Peng et al., 2006; Fan et al., 2012; Si et al., 2012).

Manganese oxides, which stand-out for their high oxidation potential and surface areas, are commonly used to remove organic and inorganic contaminants, such as dyes and arsenite, by oxidative adsorption (Dias et al., 2008; Vaclavikova et al., 2008; Zhang et al., 2010; Zaied et al., 2011). Magnetic materials prepared from manganese oxide can be produced by means of the oxidation of manganese ions due to the action of an oxidizing agent in presence of magnetic particles such as magnetite (Rosas et al., 2010). The most commonly used oxidizing agent to precipitate manganese oxides is potassium permanganate ($KMnO_4$). $KMnO_4$ can oxidize Mn^{2+} directly to Mn^{4+} producing manganese dioxides (MnO_2). Manganese dioxides are usually used to remove heavy metals from water due to their high surface areas. These compounds have also been employed to oxidize As(III) to As(V), thus improving As(III) removal from water (Dias et al., 2008; Rosas et al., 2010; Vaclavikova et al., 2008). Other manganese oxides, such as Mn_3O_4 (Mn^{2+}/Mn^{3+} oxide) and Mn_2O_3 (Mn^{3+} oxide) have been mostly used in organic degradation due to their high standard redox potentials (Chowdhury et al., 2009). These manganese oxides are usually obtained by calcination and solvothermal methods (Yang et al., 2006). Aqueous Mn^{2+} is oxidized by dissolved O_2 in natural waters at pH>8 through the aqueous $Mn(OH)_2$ species or by metal oxide surfaces terminated by hydroxyl groups (>OH), which bind Mn(II) (Martin, 2005). Therefore,

dissolved O_2 could be an environmentally friendly oxidant to produce magnetic manganese oxide composites. The present work proposes a method for the production of manganese oxide magnetic composites with O_2 as the oxidant. The performance of these composites has been compared with that of the material produced with the addition of potassium permanganate. Both products have been characterized with respect to surface areas (BET) and manganese oxide phases (Raman Spectroscopy). Moreover, their oxidation and adsorptive capacities have been evaluated in the removal of As(III) from water.

2.2 Experimental

2.2.1 Synthesis of the manganese oxide magnetic composites

The synthesis of the manganese oxide magnetic composites was based on the oxidation of manganese ions by permanganate (Eq. 2-1) (Rosas et al., 2010) and oxygen, O_2, at room temperature, in presence of commercial magnetite, Fe_3O_4 (Fig. 2-1).

$$3MnCl_{2(aq)} + 2KMnO_{4(aq)} + 4KOH_{(aq)} = 5MnO_{2(s)} + 6KCl_{(aq)} + 2H_2O \qquad (2\text{-}1)$$

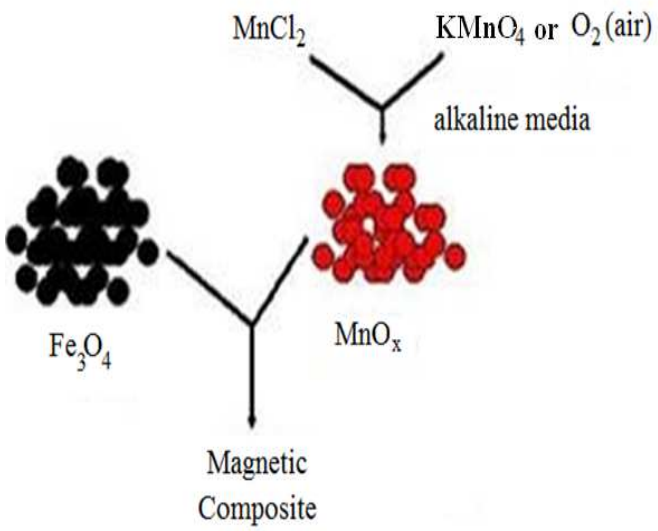

Fig. 2-1: Schematic representation of the manganese oxide magnetic composites synthesis.

Magnetite, provided from Sigma-Aldrich (<5μm, 98%), was described as synthetic iron oxide, Fe_3O_4. After the synthesis, the resulting magnetic composites were separated from the solutions and washed using deionized water with a conductivity of 18.2μ.cm^{-1} obtained with a Milli-Q water purification system (Milipore). Solutions of 1.0mol.L^{-1} $MnCl_2.4H_2O$, 1.0mol.L^{-1} KOH and 0.2mol.L^{-1} $KMnO_4$ were used for the preparation of the composites. $KMnO_4$ and $MnCl_2.4H_2O$ were standardized by using sodium oxalate and an already standardized $KMnO_4$ solution, respectively. The pH and the Eh (redox potential) were constantly monitored during synthesis (713 pHMeter, Metrohm). All chemicals were of analytical grade and used without further purification.

The syntheses of the composites prepared with $KMnO_4$ (sample 0, Table 2-1) were carried out by mixing, in 500mL of deionized water, 23mL of potassium permanganate with 14mL of KOH (initial pH 12) in the presence of 1.0g of magnetite particles. 14mL of $MnCl_2$ was added and the mixture was stirred (700rpm) during 30min (final pH 4.0) (Rosas et al., 2010).

For the preparation of the composite by using O_2 (samples 1 to 3, Table 2-1), 1000mL of deionized water pre-saturated with O_2 by flowing air was put in contact with different volumes (5, 15 and 45mL) of $MnCl_2.4H_2O$ in presence of 1.0g of magnetite particles. The Eh-pH diagrams (species and thermodynamic data are listed in the Appendix) for the Mn-H_2O system (Fig. 2-2) show that the oxidation of aqueous Mn^{2+} with dissolved O_2 is stable at pH>8. Therefore, the reaction was carried out under alkaline conditions (pH 8.0 to pH 12) by addition of KOH, and constant input of air (567L.h^{-1}) and stirring (700rpm) during 30min. Since the Eh-pH diagrams for conditions of samples 1, 2 and 3 are mainly the same, the Eh-pH diagram chosen to be shown in Fig. 2-2 is for the synthesis conditions of sample 3.

Table 2-1 summarizes the parameters investigated in the synthesis of the magnetic composite and illustrates typical results. When 5.0mL of $MnCl_2$ and 10mL of KOH are mixed (sample 1, Table 2-1), the pH drops from 10.2 to 7.6 and Eh increases from 0.22V to 0.48V. To decrease magnetite particles exposure in the composite, the $MnCl_2$ volume added was triplicate. As an attempt to keep similar pH conditions of the

synthesis with permanganate, the volume of KOH was also increased (sample 2, Table 2-1). The final pH reach 11.5 and the Eh varied from 0.1V to 0.2V. With the aim to further improve the coverage of the magnetite particles, the volume of $MnCl_2$ was increased (sample 3, Table 2-1). The pH and Eh remained constant at ~12 and at 0.1V.

Table 2-1: Summary of the synthesis parameters.

Oxidant	Sample	KOH volume (mL)	$MnCl_2$ volume (mL)	Initial pH/Eh (V)	Final pH/Eh (V)	Surface Area ($m^2.g^{-1}$)
$KMnO_4$	0	14	14	12.0/ -	12.0/ -	59
O_2	1	10	5.0	10.2/0.22	7.6/0.48	28
	2	30	15	12.0/0.10	11.5/0.20	47
	3	100	45	12.0/0.10	12.0/0.10	39

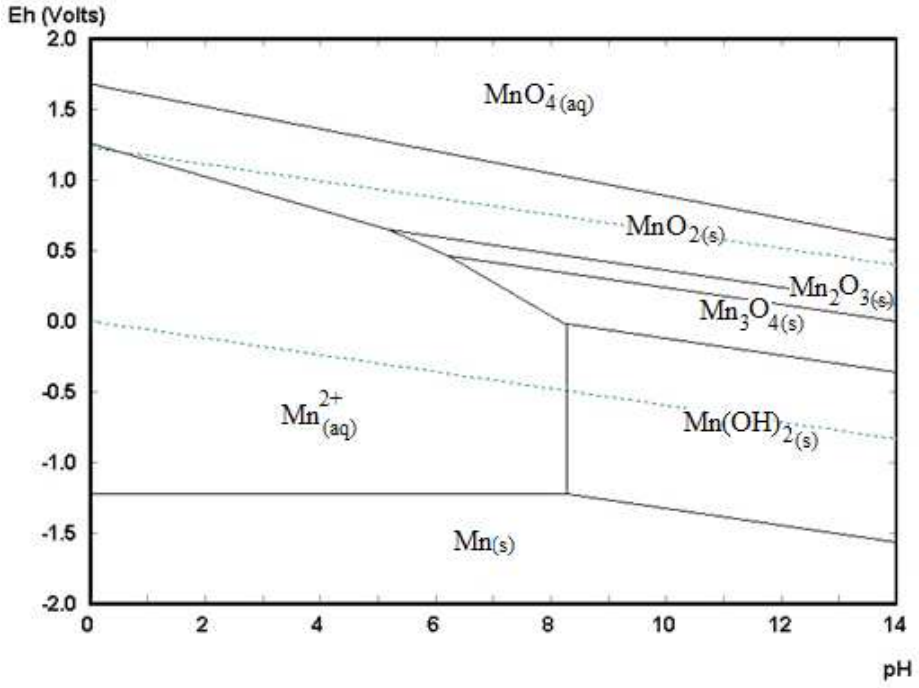

Fig. 2-2: Eh-pH diagram (298K) constructed using the conditions of magnetic composite synthesis with O_2: 45mL of $MnCl_2$ ($[Mn_T] = 4.0x10^{-2}mol.L^{-1}$). The water stability field is shown for $pO_2 = 1.0atm$ and $pH_2 = 1.0atm$ (HSC 6) (Appendix).

2.2.2 Characterization of the materials

Characterization of magnetic composites were obtained by Raman spectroscopic analysis on a Horiba Jobin Yvon LABRAM-HR 800 spectrograph, equipped with a 633nm helium-neon laser, 20mW of power, coupled to an Olympus BHX microscope equipped with lenses of 10, 50 and 100X. Raman-scattered radiation was collected with 600g.mm^{-1} grating, in a 180° backscattering configuration. The spectra were collected in a frequency range of 100 to at least 1100cm^{-1} with a step size of 1.1cm^{-1}. In order to suppress extra noise and to obtain sufficiently accurate results, a N_2 cooled charge couple device (CCD) detector was used as the detecting device. To reduce noise ratio, spectra were acquired at acquisition time of one minute twenty times. X-ray diffraction analyses (XRD) were performed on a Philips-PANalytical PW 1710 X-ray difractometer, using a copper anode (Cu $K\alpha_1$ radiation) and graphite crystal monochromator. Analyses were run by step-scanning from 4^o to 90^o 2θ, increments of 0.06 2θ and continuous count time of 1s. Measurements of the specific surface area were made by the BET (Brunauer-Emmett-Teller) – Multipoint method using a nitrogen gas sorption analyzer NOVA 1000 Quantachrome. Prior to the measurements the samples were massed, degassed by placing them into a glass cell under vacuum for at least 24h at 100ºC, and massed again. The BET analyzer was configured and its Dewar flask filled with liquid nitrogen and set into place. Each degassed sample was load and the results of the analysis collected.

2.2.3 Arsenic oxidation and removal

In the batch arsenic sorption experiments, 0.2g of the adsorbent material (magnetic composite) were added into the 250mL Pyrex erlenmeyers flasks, filled with 100mL of As(III) solution, and the vessels sealed with laboratory parafilm (Pechiney plastic packaging, USA). The As(III) stock solution was prepared by dissolving $AsNaO_2$ (Fluka) in Milli-Q water. Agitation at 200rpm was provided by a thermostatic shaker, manufactured by New Brunswick Scientific Edison, USA. The temperature was maintained at (25±0.5)ºC. All the experiments were carried out at initial pH 5.0 with initial As(III) concentration of 10mg.L^{-1}. After 24h, the pH of the solutions was

measured and the samples were separated from the liquid. The filtrates were assayed for total arsenic directly by flame Atomic Inductively Coupled Plasma Optical Emission Spectrometry, ICP-OES (Perkin-Elmer Optima 7300 DV). The tests were carried out in triplicate.

2.3 Results and Discussion

Fig. 2-3(a) shows the XRD diagram of the magnetic composite synthesized by using permanganate. The diffraction pattern of the solid has shown the lines corresponding to the diffraction pattern of commercial magnetite powder and a broad peak in the region 20-30 degrees, indicating the presence of an amorphous phase. Raman technique is useful for identification of manganese oxides, especially for samples with poor crystallinity. Fig. 2-3(b) shows the Raman spectra in two different regions of the composite. Spectrum A is quite similar to the spectrum of magnetite and spectrum B is characteristic of manganese oxides having the birnessite-type structure (δ-MnO_2). The birnessite-type manganese oxides (δ-MnO_2) are a group of layered manganese dioxides, which can be found in nature or synthesized. They present a layered structure consisting of edge-sharing MnO_6 octahedra, with water molecules and metal cations occupying the interlayer region (Julien et al., 2003). Birnessite- type MnO_2 present low Raman activity. They show three major bands at 500-510, 575-585 and 625-650cm^{-1}. The two high-wavenumber bands dominate all spectra, while bands in the low-frequency region exhibit weak intensity. The Raman band at 625-650cm^{-1} can be viewed as the symmetric stretching vibration ν_2 (Mn-O) of MnO_6 groups and the band located at 575-585cm^{-1} is usually attributed to the ν_3 (Mn-O) stretching vibration in the basal plane of [MnO_6] sheets. Significant spectral modifications can be observed as a function of the nature of ions located within the basal MnO_6 sheets. Nevertheless, the general similarity of the Raman spectra suggests that different birnessites can be characterized by the same basic structure (Julien et al., 2003, 2004). The synthesized birnessite-type magnetic composite has shown a relatively high specific surface area of 59$m^2.g^{-1}$ and As(III) removal tests have shown a loading of ~0.04$mg.m^{-2}$ (Table 2-2).

The Raman spectra of the magnetic composites synthesized with O_2 are shown in Fig. 2-4. For sample 1, the Raman spectrum shows the presence of Mn_2O_3 (bixbyite), MnOOH (groutite) and Mn_3O_4 (hausmannite). Bixbyite is a sesquioxide that has two polymorphs, the cubic α–Mn_2O_3 and the tetragonal γ–Mn_2O_3. Hausmannite is a spinel manganese oxide containing Mn^{2+} ions in tetrahedral coordination and Mn^{3+} ions in distorted octahedral coordination. Groutite also presents oxygen atoms forming distorted octahedra around the Mn^{3+} atoms (Julien et al., 2004). The composite (sample 1) shows specific surface area of $28 m^2.g^{-1}$ and an As loading of $\sim 0.06 mg.m^{-2}$ (Table 2-2). For sample 2, Raman spectrum presents bands related to Mn_2O_3, MnOOH, Mn_3O_4 and also MnO_2 (Fig. 2-4). The MnO_2 phase formed is R-MnO_2 (ramsdellite), a metastable form of MnO_2 (Julien et al., 2004). The surface area of the composite (sample 2) increased to $47 m^2.g^{-1}$ and the As uptake is $\sim 0.03 mg.m^{-2}$ (Table 2-2). For the magnetic composites described (samples 1 and 2), micro-Raman spectra of some regions show the presence of characteristic magnetite Raman bands (data not shown), which indicates that the magnetic particles are exposed. However, for sample 3, Raman spectra of different regions only showed the characteristic Raman bands of Mn_3O_4 (Fig. 2-3 and Fig. 2-4), which indicates that the magnetic particles are not exposed. Moreover, sample 3 presents a surface area of $39 m^2.g^{-1}$ and the highest specific As uptake of ($\sim 0.10 mg.m^{-2}$, Table 2-2). Therefore, Mn_3O_4 plays an important role in As uptake, since the composite that shows the best As uptake ($\sim 0.10 mg.m^{-2}$), sample 3 (Table 2-2), is the one composed of Mn_3O_4 as the only Mn oxide phase (Fig. 2-4).

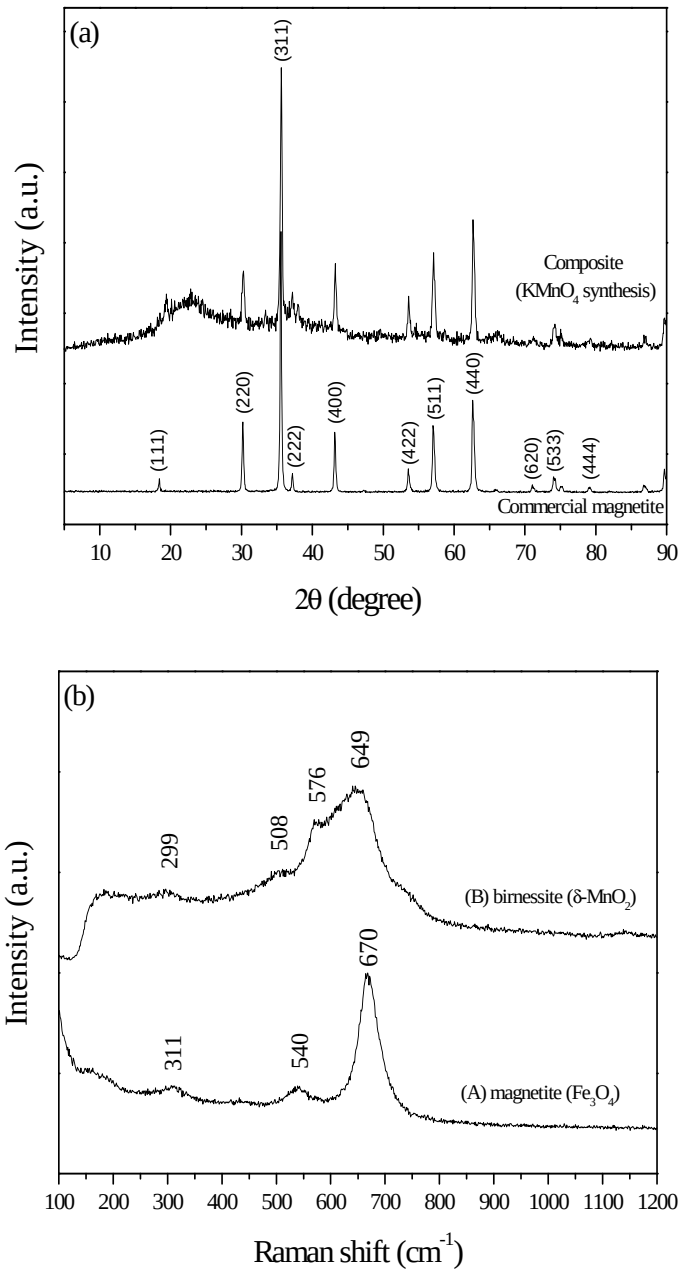

Fig. 2-3: (a) X-ray powder diffraction pattern and (b) Raman spectra (two different regions) of the magnetic composite synthesized by using permanganate.

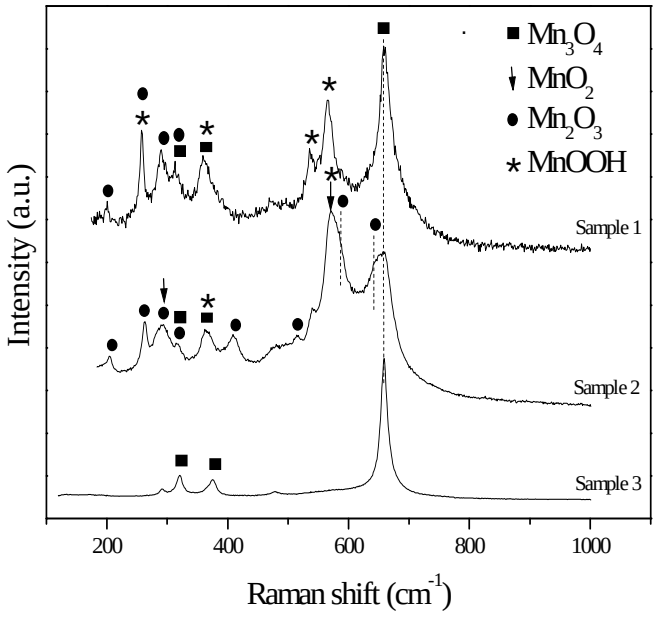

Fig. 2-4: Raman spectra of the magnetic composites synthesized with O_2 (samples 1, 2 and 3 - Table 2-1).

Table 2-2: Summary of the As(III) removal tests results.

Oxidant	**Sample**	**As(III) uptake ($mg.m^{-2}$)**
$KMnO_4$	0	0.041±0.003
O_2	1	0.059±0.006
	2	0.034±0.006
	3	0.103±0.005

Plots of the redox potential (Eh) versus pH for MnO_2, Mn_2O_3, MnOOH and Mn_3O_4 (Eqs. 2-2 to 2-5) with a Mn^{2+} concentration of $4.0x10^{-4}mol.L^{-1}$ (based on the Mn^{2+} release during As sorption tests) are shown in Fig. 2-5. It can be seen that at pH<7 Mn_3O_4 presents higher redox potential than Mn_2O_3 and MnO_2, and at pH<10 Mn_3O_4 presents higher redox potential than MnOOH, therefore being more effective to oxidize As(III) to As(V) in acidic media. In the present As oxidation and removal tests pH increases from 5.0 to 7.0, remaining in the range where Mn_3O_4 presents the highest redox potential compared to the other studied manganese oxides. Therefore, the greater As uptake by sample 3, could be explained by Mn_3O_4 higher redox potential in acidic media, which favors a rapid oxidation of As(III) to As(V) improving As adsorption.

$$MnO_2 + 4H^+ + 2e^- = Mn^{2+}_{(aq)} + 2H_2O \ (Eh^0_{298} = 1.225V) \quad (2\text{-}2)$$
$$Eh_{298} = 1.225 - 0.0295 \log[Mn^{2+}] - 0.118\ pH$$

$$Mn_2O_3 + 6H^+ + 2e^- = 2Mn^{2+}_{(aq)} + 3H_2O \ (Eh^0_{298} = 1.497V) \quad (2\text{-}3)$$
$$Eh_{298} = 1.497 - 0.059 \log[Mn^{2+}] - 0.177\ pH$$

$$2MnOOH + 6H^+ + 2e^- = 2Mn^{2+}_{(aq)} + 4H_2O \ (Eh^0_{298} = 1.542V) \quad (2\text{-}4)$$
$$Eh_{298} = 1.542 - 0.059 \log[Mn^{2+}] - 0.177\ pH$$

$$Mn_3O_4 + 8H^+ + 2e^- = 3Mn^{2+}_{(aq)} + 4H_2O \ (Eh^0_{298} = 1.824V) \quad (2\text{-}5)$$
$$Eh_{298} = 1.824 - 0.0885 \log[Mn^{2+}] - 0.236\ pH$$

$$H_2AsO_4^- + 2e^- + 3H^+ = H_3AsO_3 + H_2O \ (Eh^0_{298} = 0.641V) \quad (2\text{-}6)$$
$$Eh_{298} = 0.641 - 0.0885\ pH$$

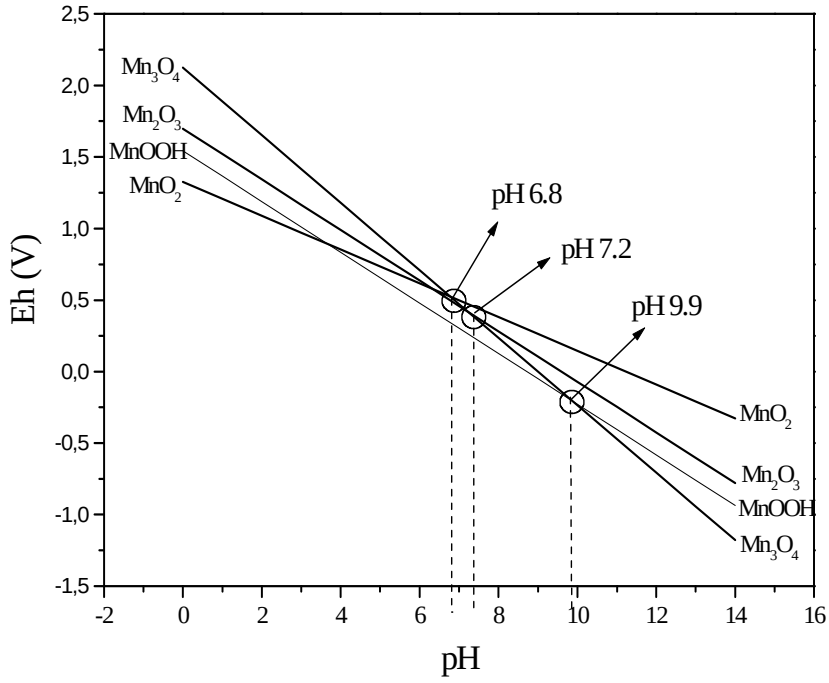

Fig. 2-5: Eh versus pH curves of manganese oxides reductive reactions considering $[Mn^{2+}] = 4x10^{-4}mol.L^{-1}$.

2.4 Conclusion

Different experimental conditions for the synthesis of manganese oxide magnetic composite have been evaluated. The produced materials have been tested for As(III) oxidation and removal, a typical commercial application of manganese oxides. The diffraction pattern and Raman spectrum of the composite synthesized with $KMnO_4$ have shown the presence of magnetite (Fe_3O_4) and birnessite-type structure phase (δ-MnO_2); the magnetite particles were partially exposed. The synthesized birnessite-type magnetic composite has shown a relatively high specific surface area of $59m^2.g^{-1}$ and As(III) removal of $\sim 0.04mg.m^{-2}$. The synthesis with O_2 produced MnOOH, Mn_2O_3 and Mn_3O_4 precipitates according to the Raman analyses. The composite specific surface area, magnetite coverage as well as As loading varied according to synthesis conditions. By controlling Eh and pH, magnetic composites with not exposed magnetite particles and specific surface areas of $39m^2.g^{-1}$ were synthesized; arsenic uptake was $\sim 0.10mg.m^{-2}$. Therefore, it is shown that is possible to replace $KMnO_4$ by O_2 in manganese oxide

precipitation. The synthesis conditions can be adjusted to produce different manganese oxide phases. The Mn_3O_4 magnetic composites obtained in the synthesis with oxygen from the air - an environmentally friendly and available oxidant if compared with permanganate - has proved to be an efficient material to remove As(III) from water.

Chapter 3 Preparation and application of a magnetic composite (Mn_3O_4/Fe_3O_4) for removal of As(III) from aqueous solutions

3.1 Introduction

The presence of arsenic in drinking water is of great concern due to its toxicity and carcinogenic potential. Arsenic concentration below 10μg L^{-1} is the World Health Organization's (WHO) recommendation for drinking water supplies (Mohan and Pittman, 2007). The increasing water quality demand for human consumption and industrial support, coupled with stringent environmental legislation, has stimulated the development of new materials and methods for the treatment of arsenic-contaminated aqueous solutions. Adsorption processes are commonly applied to water treatment. As desired features, adsorbents should be low-cost and should present a considerable contaminant adsorption capacity. When trace or sub-trace concentrations are of concern, powder adsorbents with small-sized particles and a large specific surface area are required. Separating small-sized particles of a highly specific surface area from a solution is a challenge that can be addressed with the use of magnetic adsorbents. Magnetic adsorbents can be conveniently recovered by magnetic separation, in turn avoiding the filtration steps, which represent a barrier to the application of high-performance, small-sized materials in environmental remediation processes and in the treatment of great volumes of aqueous solutions. Some investigations have shown that magnetic iron oxides, such as magnetite nanoparticles, lead to the efficient removal of arsenic from contaminated water (Yavuz et al., 2006). Nevertheless, the instability of these magnetic nanoparticles represents a problem, as magnetite is highly susceptible to oxidation when exposed to the atmosphere. To face this problem, magnetite nanoparticles are being combined with other compounds or covered by an active compound (Qu, 2008; Rosas et al., 2010; Chen et al., 2011). In both cases the magnetic property of magnetite is preserved.

The oxidation state and chemical speciation of arsenic play a determining role in its toxicity, mobility, and bioavailability in soil–water systems, the As(III) species being

the most toxic and mobile. Under oxidizing conditions, $H_2AsO_4^-$ is the dominant inorganic arsenic species at low pH (from pH 2.0 to pH 6.9), while at higher pH, $HAsO_4^{2-}$ becomes dominant. The inorganic species H_3AsO_4 and AsO_4^{3-} may be present in extremely acidic and alkaline conditions, respectively. Under reducing conditions at a pH of less than approximately 9.2, the neutral As(III) species, H_3AsO_3, predominates (Smedley and Kinniburgh, 2002). The most used arsenic removal techniques, such as adsorption on activated alumina and coprecipitation with ferric salts, are often more effective for As(V) than for As(III) removal, given that the predominant As(III) species at circumneutral pH is the uncharged H_3AsO_3, while for As(V) the predominant species are the charged $H_2AsO_4^-$ and $HAsO_4^{2-}$ (Smedley and Kinniburgh, 2002). Therefore, an oxidation step is often used to improve arsenic removal and fixation. Manganese oxides are known as effective oxidizers of As(III) to As(V) in natural environments and in water treatment units (Smedley and Kinniburgh, 2002; Deschamps et al., 2005; Ladeira and Ciminelli, 2004; Vaclavikova et al., 2008; Dias et al., 2008). Among the series of manganese oxides, Mn_3O_4 is particularly known to be an effective and inexpensive catalyst in various oxidation and reduction reactions (Parsons et al., 2009; Zhang et al., 2010). The use of powder magnetic manganese oxide composites as adsorbents may combine the excellent adsorptive and oxidation properties of manganese oxide with good performance recovery of magnetic separation techniques. Nevertheless, very few works have been focusing on magnetic manganese oxide composites to be used in water treatment (Rosas et al., 2010; Chen et al., 2011). Moreover, in these published works, the magnetic composites are often synthesized by precipitation of manganese oxide, when in presence of magnetite, by using relatively costly oxidants, such as potassium permanganate and hydrogen peroxide. Considering the aforementioned context, the present work aims to synthesize relatively low-cost magnetic Mn_3O_4 composites, with chemical stability and physical integrity, in stirred solid-aqueous systems. The magnetic sorbent is applied to As(III) removal in environmental systems.

3.2 Experimental

All chemicals were of analytical grade and used without further purification. All solutions were prepared with deionized water with a conductivity of $18.2 \mu S.cm^{-1}$

obtained with a Milli-Q water purification system (Millipore). To remove contaminants that had been potentially adsorbed onto the glass and plastic walls, all vessels and instruments were cleaned by soaking in detergent solution, then in 1M HNO_3 solution, and subsequently in deionized water, in each case for at least 24 hours. All parts of the spectroscopic equipment used to extract and fill the sample cells were cleaned and rinsed properly with acetone. The pH electrode (713 pHMeter, Metrohm) was calibrated everyday with three pH buffers (pH 4.0, 7.0, and 10.0).

3.2.1 Synthesis of the magnetic manganese oxide composites

For the preparation of the composite, 1000mL of deionized water was placed in contact with 1.0g of different obtained magnetite particles and 45mL of 1.0mol L^{-1} $MnCl_2.4H_2O$ (Sigma-Aldrich) solution at pH 12 (1.0mol.L^{-1} KOH – Sigma-Aldrich) in a 2000mL Pyrex beaker under stirring (mechanical stirrer, Fisatom 713 D) and constant air input (aquarium pump Power 500). This same reaction was also carried out in the absence of magnetite particles for comparison. The resulting solid was separated from the liquid by using a neodymium magnet (180x100x35mm, Imatec *Produtos Magnéticos Ltda*) and washed using deionized water. The solutions were analyzed by Atomic Absorption Spectrometry, AAS (Perkin Elmer Analyst A300), for iron and manganese content. Commercial magnetite microparticles (< 5μm) (mag1) were furnished by Sigma-Aldrich. Magnetite nanoparticles covered by hematite (mag2) were obtained by ball-milling of commercial magnetite microparticles during 4 hours. Magnetite nanoparticles (mag3) were prepared by mixing N_2 saturated water solution of Fe^{3+}: Fe^{2+} (2:1) and adding KOH solution (5.0mol.L^{-1}) at 70°C (Oliveira et al., 2004; Peng et al., 2005; Mürbe et al., 2008).

3.2.2 Evaluation of the sorbents chemical stability and physical integrity

The chemical stability of the composites is associated with the dissolution of solid constituents, while the physical integrity of the composites is associated with the detachment of the different solid phases. The chemical stability and physical integrity tests consisted of batch experiments in which 0.2g of the magnetic composites were

placed in contact with 100mL aqueous solutions in different pH values (from 2.0 to 12) in 250mL Pyrex vessels sealed with laboratory parafilm (Pechiney plastic packaging, USA) and stirred for 24h in a thermostatic shaker (New Brunswick Scientific Edison, USA) at room temperature. The solids were separated from the solution by a neodymium magnet, while the supernatant solutions were vacuum-filtered through 0.22µm membrane filters (Fisher Scientific). The membrane filters were weighed on a precision balance (Mettler AE 200) before and after filtration to estimate the detachment. The solution was analyzed by AAS for Mn and Fe contents, whereas the solids were analyzed by EDS for Mn and Fe contents. The tests were carried out in duplicate.

3.2.3 Spectroscopic and image analyses techniques

Raman spectroscopic and X-ray diffraction (XRD) analyses were carried out for solid identification. Raman spectra were collected on a Horiba Jobin Yvon LABRAM-HR 800 spectrograph, equipped with a 633 nm helium-neon laser, 20mW of power, attached to an Olympus BHX microscope equipped with 10X, 50X, and 100X lenses. The diffractograms were obtained on a Philips-PANalytical PW 1710 X-ray diffractometer equipped with a texture chamber. The lattice constants of magnetite samples were calculated by using the following equation:

$$\frac{1}{d^2} = \frac{h^2+k^2+l^2}{a_0^2} \qquad (3\text{-}1)$$

where d is the d-spacing; h,k,l are the Miller indices; and a_0 is the cubic lattice constant.

A Thermo Noram (Quest) spectrometer with energy dispersive X-ray analysis (EDS) was used for elemental detection in the Center of Microscopy at the *Universidade Federal de Minas Gerais* (UFMG). X-ray absorption near-edge structure (XANES) spectra of the As K-edge (11868eV) were obtained to determine arsenic oxidation states at As-loaded solids using the synchrotron facilities at the *Laboratório Nacional de Luz Síncrotron* (LNLS), in Campinas, Brazil, at the XAFS2 workstation in the transmission

mode under operation conditions of 1.37GeV and beam currents of approximately 250mA. The spectra were collected at room temperature using a Si (111) double crystal monochromator with an upstream vertical aperture of 0.3mm and calibrated with Au L_1-edge (11918eV). The samples were fixed onto acrylic holders, sealed with Kapton tape film, placed at an angle to the incident beam. Energy calibration was monitored during data collection by acquiring reference Au foil spectra simultaneously. $AsNaO_2$ (Fluka) and $AsHNa_2O_4.7H_2O$ (Fluka) were used as As(III) and As(V) standards, respectively. Mössbauer spectroscopy data were collected on a conventional constant acceleration Mössbauer spectrometer (Halder) in transmission mode with a ^{57}Co (Rh) source to identify the composite's magnetic phase. Measurements of the specific surface area were made by the BET (Brunauer-Emmett-Teller) – Multipoint method using a nitrogen gas sorption analyzer NOVA 1000 Quantachrome.

3.2.4 Arsenic immobilization

In the batch arsenic sorption experiments, 0.2g of the adsorbent materials (magnetic composites or manganese oxide) was added into the 250mL Pyrex erlenmeyers flasks, filled with 100mL of As(III) solution at initial pH 5.0, and the vessels sealed with laboratory parafilm (Pechiney plastic packaging, USA). The As(III) stock solution was prepared by dissolving $NaAsO_2$ (Fluka) in Milli-Q water. Initial As(III) concentrations varied from 1.0 to 50mg.L^{-1}. Agitation at 200 rpm was provided by a thermostatic shaker (manufactured by New Brunswick Scientific Edison, USA). The temperature was maintained at (25.0±0.5)ºC. After 24h, the pH of the solutions was measured, and the samples were separated from the liquid by using a magnet. The filtrate was directly assayed for total arsenic, iron and manganese using inductively coupled plasma optical emission spectrometry, ICP-OES (Perkin-Elmer Opttima 7300 DV). The tests were carried out in duplicate.

3.3 Results and Discussion

3.3.1 Evaluation of the composites chemical stability and physical integrity

The supernatants obtained after the magnetic separation of the solid samples stirred in pH 10 and pH 12 aqueous solutions were turbid (brown yellow) and had to be vacuum-filtered twice through a 0.22µm membrane filter (Fisher Scientific) to achieve clarification. EDS results have shown the presence of only manganese in the fine filtrate particles, indicating that the physical integrity of the magnetic composites were compromised in these pH values (22% of Mn_3O_4 was separated from magnetite particles). When stirring at pH values from 3.0 to 9.0, no turbidity could be observed in the supernatants obtained after magnetic separation, which indicates that the physical integrity was preserved (less than 1% of Mn_3O_4 was separated from the magnetite particles). Significant manganese dissolution (49%) could only be observed in pH 2.0. In pH values from 3.0 to 9.0, less than 1% of manganese was dissolved. Iron dissolution was not detected (< 10µg.L^{-1}). It can be concluded that the composites have shown a good chemical stability and physical integrity in pH values ranging from 3.0 to 9.0, which is the commonly used range for arsenic adsorption in water treatment units.

3.3.2 Sorbents characterization

The values of specific surface areas for magnetite, manganese oxide, and magnetic manganese oxide composite samples are shown in Table 3-1. The different magnetite particles presented different specific surface areas. Sample mag3 presented the highest value, which was expected from the preparation route followed. The smallest specific surface area belongs to mag1, which is the commercial magnetite. The commercial magnetite increased its specific surface area approximately six times after being milled (mag2). The different composites present similar specific surface areas, indicating that different magnetite particles (with different specific surface areas) do not interfere in the Mn_3O_4 precipitation and Mn_3O_4 particles are contributing more in the composites' specific surface areas. These results suggest the formation of agglomerates where the dominantly Mn_3O_4 particles are somehow covering the magnetite particles.

Table 3-1: BET surface areas of the samples.

Samples	Specific surface area ($m^2.g^{-1}$)
mag1	6
mag2	37
mag3	92
Mnmag1	39
Mnmag2	41
Mnmag3	40
Mn_3O_4	54

Fig. 3-1 shows the XRD diagrams of the samples. Samples mag1 and mag3 show peaks corresponding to a cubic structure of Fe_3O_4 (ICDD, 89-0691 - magnetite structure, $Fd\bar{3}m$) with lattice constants a_0=8.37Å and a_0=8.34Å, respectively (Fig. 3-1a). Sample mag1 presents a lattice constant lower but closer to the lattice constant for bulk magnetite (a_0=8.3918Å) (Mürbe et al., 2008) than sample mag3. The decrease in unit cell parameters of magnetite indicates that Fe^{2+} is being oxidized to Fe^{3+} in both samples. Sample mag1 shows sharp peaks while sample mag3 shows broad peaks, indicating that mag3 has smaller crystallite size, which favors oxidation. Sample mag2 shows broad peaks corresponding to a rhombohedral structure of α-Fe_2O_3 (ICDD, 89-0599 - hematite structure, $R\bar{3}c$) and a few peaks corresponding to a cubic structure of Fe_3O_4 (ICDD, 89-0691) with lattice constant a_0=8.35Å (Fig. 3-1a). The synthesis of Mn_3O_4, in both the absence and presence of magnetite, can be confirmed by the presence of diffraction peaks corresponding to a tetragonal structure of Mn_3O_4 (ICDD, 24-0734 - hausmannite structure, I41/amd (Fig. 3-1b). The diffraction peaks of pure Mn_3O_4 are broader than the diffraction peaks of the composites. This result indicates that the synthesis in the presence of magnetite favors the formation of a more ordered Mn_3O_4 material with a single phase of manganese oxide. The diffraction pattern of the Mnmag1 composite has also shown some peaks that correspond to the diffraction

pattern of commercial magnetite with lattice constant a_0=8.36Å, as was expected from the bulk.

Raman spectra of the composites and manganese oxide (Fig. 3-2a) have confirmed the presence of Mn_3O_4 (Han et al., 2006; Tian et al., 1997). The Raman spectrum of bulk Mn_3O_4 ($MnMn_2O_4$ in spinel notation) is characterized by a very sharp peak at 654cm^{-1}. This peak corresponds to the Mn-O breathing vibration of divalent manganese ions in tetrahedral coordination. Two smaller peaks are located at 300-310 and 350-360cm^{-1}. Bulk Mn_3O_4 also presents a weak signal at 485cm^{-1} (Julien et al., 2004). However, these values may shift to higher values as grain sizes decrease due to the phonon confinement effect (Xu et al., 2005). Lack of magnetite contribution in the spectra of the composites indicates coverage of magnetic particles by Mn_3O_4 particles. Samples mag1 and mag3 show the Raman bands related to magnetite, while mag2 shows the Raman bands of hematite with the main Raman band of magnetite between 660 and 670cm^{-1} (Fig. 3-2b).

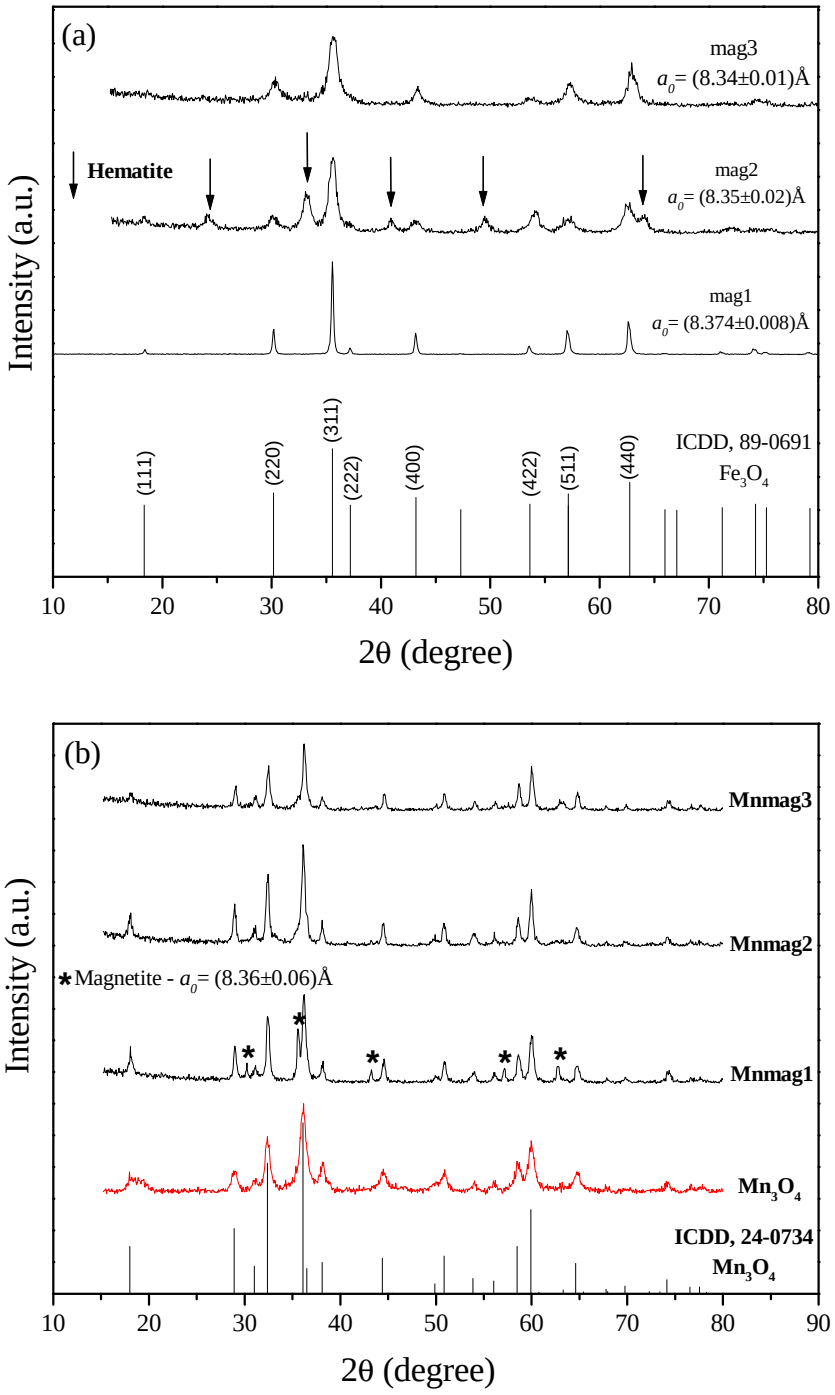

Fig. 3-1: Powder X-ray diffraction pattern of: (a) magnetite particles (mag) and (b) synthesized Mn_3O_4 and Mn_3O_4 magnetic composites (Mnmag).

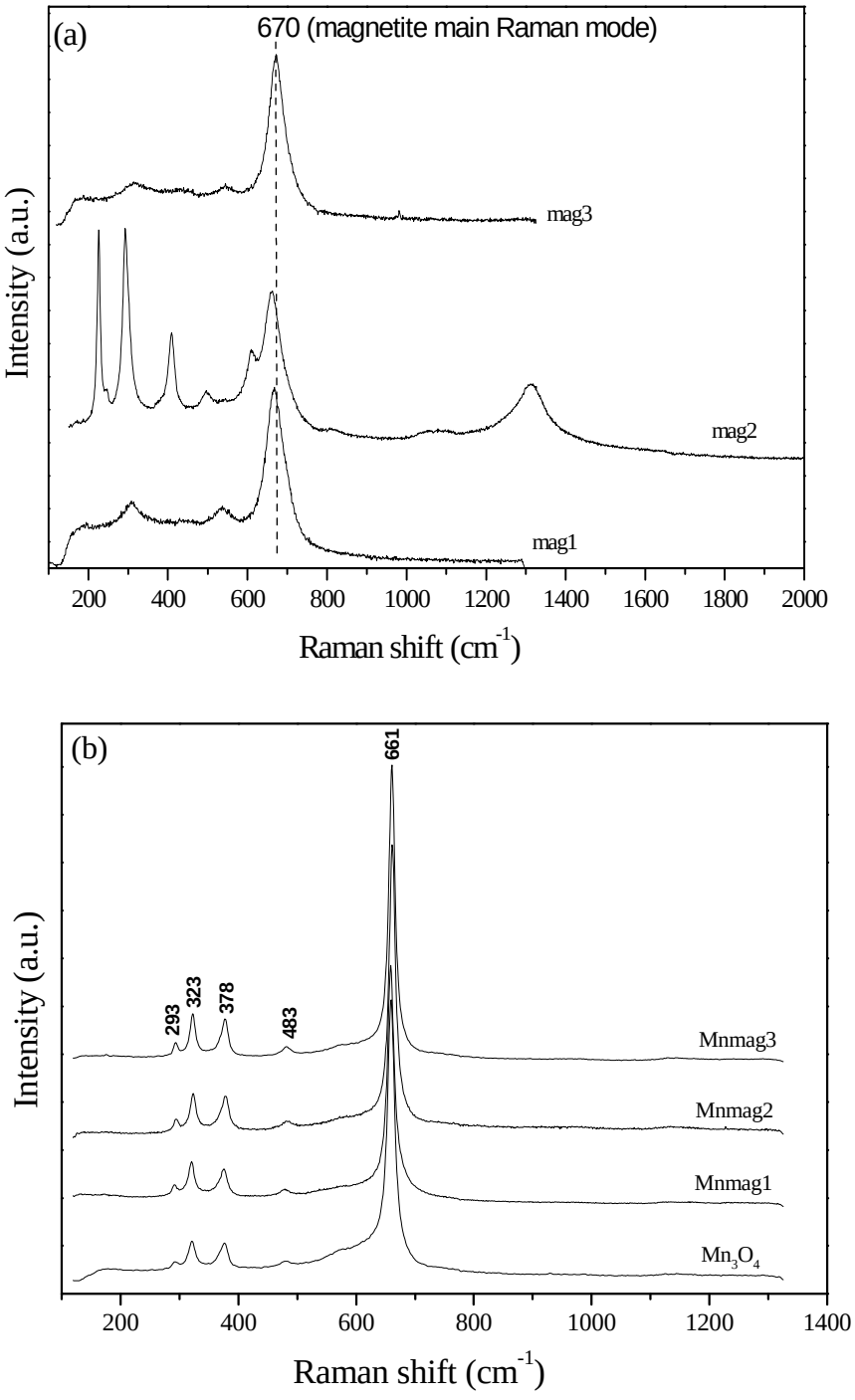

Fig. 3-2: Raman spectra of: (a) magnetite particles (mag); (b) Mn_3O_4 and magnetic Mn_3O_4 composites (Mnmag).

Mössbauer results indicate oxidation of Fe^{2+} to Fe^{3+}, since the ratios of the areas of octahedral and tetrahedral sites of commercial magnetite (mag1) and the Mnmag1 composite are less than 2.00 (Table 3-2, Fig. 3-3). There is a gap-free miscibility row between maghemite (γ-Fe_2O_3) and magnetite (Fe_3O_4), which can be written as $Fe_{3-\nu}\square_\nu O_4$ with $0 \leq \nu \leq 1/3$ and $\square$ as vacancy. Maghemite is reached at $\nu = 1/3$. The number of vacancies can be determined from Mössbauer data. From the area ratio x of the octahedral subspectra (O) and tetrahedral subspectra (T) follows that $\nu = (2-x)/(5x+6)$ (Ramdani et al., 1987). For commercial magnetite (mag1) ($x = 1.14$), $\nu = 0.07$, and for the Mnmag1 composite ($x = 1.25$), $\nu = 0.06$. The ν values are closer to 0 than to 1/3 indicating that the oxidation is not significant and does not compromise magnetic separation.

Table 3-2: Mössbauer hyperfine parameters of commercial magnetite and Mnmag1 magnetic composite.

MAGNETITE			**COMPOSITE**		
	mag (O)	**mag (T)**		**mag (O)**	**mag (T)**
IS (mm/s)	0.54	0.19	**IS (mm/s)**	0.55	0.2
QS (mm/s)	0.00	-0.02	**QS (mm/s)**	0.01	-0.02
B_{HF} (T)	45.78	49.22	**B_{HF} (T)**	45.79	49.34
Area (%)	53.3	46.7	**Area (%)**	55.53	44.47
$A_{(O)}/A_{(T)}$ (*x*)	1.14		**$A_{(O)}/A_{(T)}$ (*x*)**	1.25	

IS: isomer shift; **QS:** quadrupole splitting; **B_{HF}:** hyperfine field; **T:** tetrahedral sites; **O:** octahedral sites.

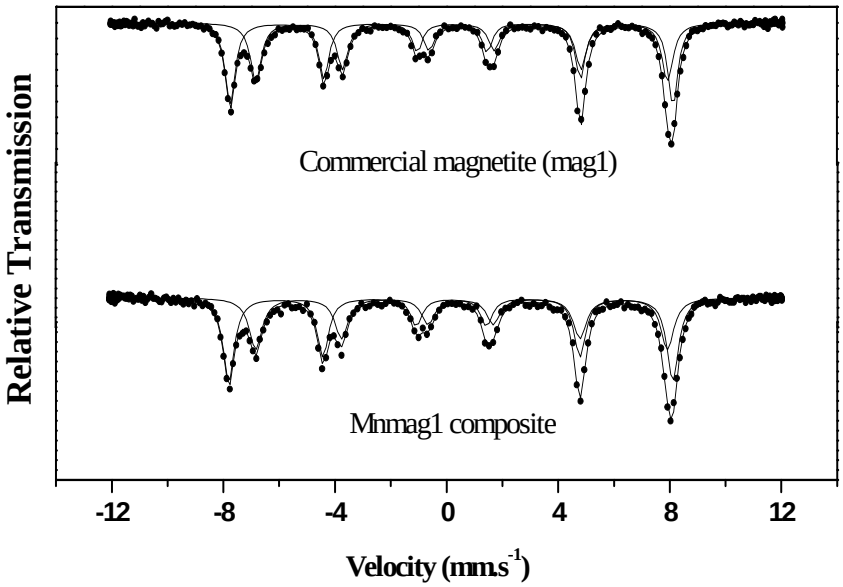

Fig. 3-3: Mössbauer spectra of commercial magnetite and the Mnmag1 magnetic composite measured at 300K.

3.3.3 Arsenic immobilization experiments

In the As(III) sorption experiments with the composite and manganese oxide samples, the pH values of the solutions increased from 5.0 to 7.0 and from 5.0 to 6.0, respectively, indicating that H^+ ions are being consumed. The As(III) sorption isotherms are shown in Fig. 3-4. The maximum sorption capacity and affinity of arsenic ions were evaluated from the isotherms by Langmuir (3-2), Freundlich (3-3) and combined Langmuir and Freundlich (3-4) models expressed as follows:

$$q = \frac{bq_m C_e}{1+bC_e} \tag{3-2}$$

$$q = kC_e^{(\frac{1}{n})} \tag{3-3}$$

$$q = \frac{bq_m C_e^{(\frac{1}{n})}}{1+bC_e^{(\frac{1}{n})}} \tag{3-4}$$

where q is the amount of arsenic adsorbed per unit surface area of adsorbent ($mg.m^{-2}$), C_e is the equilibrium concentration of arsenic ($mg.L^{-1}$), b is the constant related to the free energy of adsorption ($L.mg^{-1}$), q_m is the maximum adsorption capacity ($mg.m^{-2}$), k is the Freundlich constant, indicative of the relative adsorption capacity of the adsorbent ($mg.m^{-2}$), and ($1/n$) is the adsorption intensity.

The isotherms best fitting results based on the lowest χ^2 values are listed in Table 3-3. The maximum sorption capacity is ~14$mg_{As.}g_{solid}^{-1}$ (0.0048$mmol_{As}.m^{-2}_{solid}$) for the composites, 20$mg_{As.}g_{solid}^{-1}$ (0.0049$mmol_{As}.m^{-2}_{solid}$) for Mn_3O_4 sample and 17$mg_{As.}g_{solid}^{-1}$ (0.0024$mmol_{As}.m^{-2}_{solid}$) for Fe_3O_4 nanoparticles (mag3). The values for the composites and for Mn_3O_4 sample are higher than for Fe_3O_4 nanoparticles, and are comparable to the value ($14.7mg.g^{-1}$) found for a raw material rich in Fe_2O_3 and MnO_2 with a specific surface area of $40.8m^2\ g^{-1}$ (0.0048$mmol_{As}.m^{-2}_{solid}$) (Deschamps et al., 2005), and are considered high when compared to other synthetic manganese dioxides found in the literature, such as birnessite (~0.0029$mmol_{As}.m^{-2}_{solid}$), for the same range of initial arsenic concentration (less than $50mg.L^{-1}$) (Vaclavikova et al., 2008). The composite and the Mn_3O_4 samples have shown high and similar affinity for As(III). High affinity adsorbents are desired for the removal of trace and sub-trace contaminants, as is true in the removal of arsenic from water.

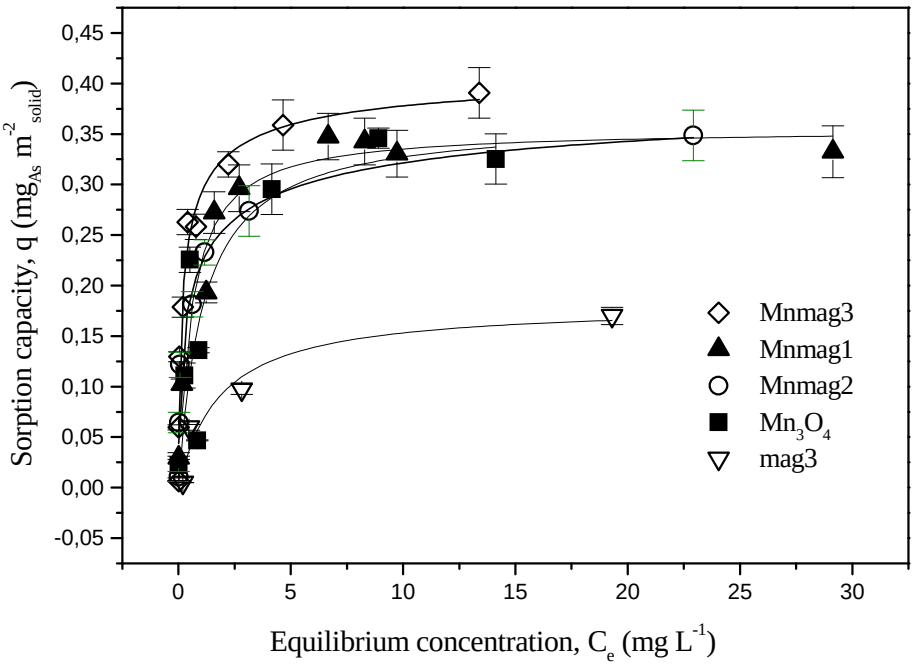

Fig. 3-4: Adsorption isotherms of As(III) on Mn_3O_4, on the Mn_3O_4 magnetic composites (Mnmag) and on the synthesized magnetite sample (mag3). Best fittings are shown. Experimental conditions: pH 5.0, 200rpm, 24h, (25.0±0.5)ºC. Error bars represent the error calculated considering an error of 5% in concentration.

Table 3-3: Isotherm parameters for As(III) on the composites and Mn_3O_4 sample.

Composite	**q_e (mg.m^{-2})**	**b (L.mg^{-1})**	**n**	**Best fit**	**χ^2**
Mnmag1	(0.36 ± 0.02)	(1.7 ± 0.5)	-	Langmuir	0.00071
Mnmag2	(0.41 ± 0.07)	(1.2 ± 0.5)	(1.0 ± 0.4)	Langmuir-Freundlich	0.00054
Mnmag3	(0.42 ± 0.05)	(2 ± 1)	(1.5 ± 0.7)	Langmuir-Freundlich	0.00073
Mn_3O_4	(0.37 ± 0.05)	(0.9 ± 0.4)	-	Langmuir	0.00399
mag3	(0.18 ± 0.03)	(0.5 ± 0.3)	-	Langmuir	0.00044

The reactions that would most likely occur during the sorption of arsenate in Mn_3O_4 tests are the oxidation of arsenite to arsenate and a reductive dissolution of Mn_3O_4, in turn releasing Mn^{2+} into the solution (3-4) as well as causing the adsorption of arsenate ions onto hausmannite (3-5) (Vaclavikova at al., 2008).

$$Mn_3O_4 + H_3AsO_3 + 5H^+ = 3Mn^{2+} + H_2AsO_4^- + 3H_2O \quad (3\text{-}4)$$

$$>Mn\text{-}[OH] + H_2AsO_4^- + H^+ = >Mn\text{-}[AsO_4] + H_2O \quad (3\text{-}5)$$

According to equation (3-4), there should be three times more Mn released than As oxidized. Manganese and iron release were analysed during the sorption tests. Iron was not detected (< 10μg.L^{-1}). A relation between Mn release and As sorption is shown in Fig 3-5. It can be seen that, in initial concentrations of above 20mg.L^{-1}, there is more As sorbed than Mn released. Fig. 3-6 compares the As K-edge XANES spectra of the composites and Mn_3O_4 sample after arsenic removal tests with arsenic salts used as standards, indicating that the As adsorbed is in the oxidized arsenic form, As(V). Therefore, it can be concluded that part of the Mn^{2+} in solution is being adsorbed or precipitated, or both. This will be confirmed by ongoing Raman and Extended X-Ray Absorption Fine Structure (EXAFS) analyses.

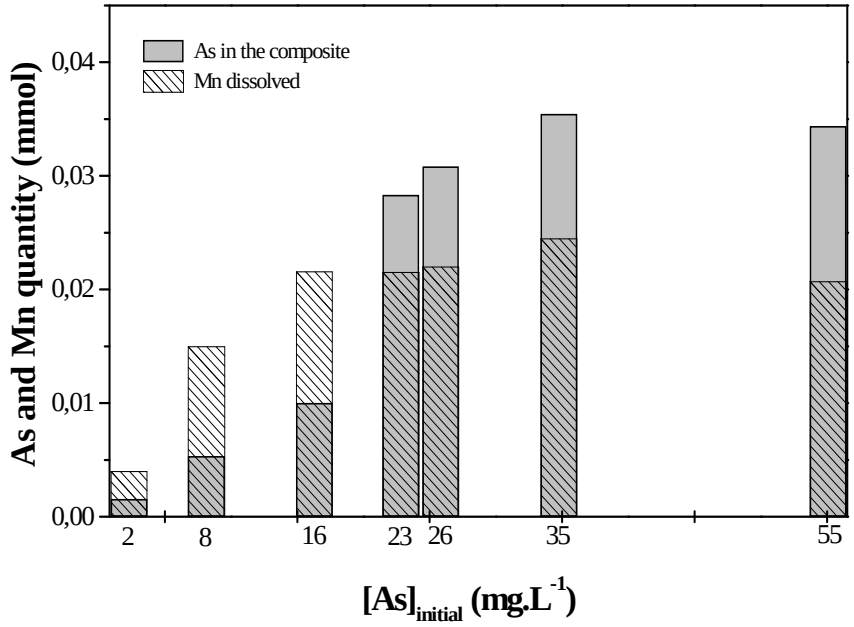

Fig. 3-5: Relation between arsenic in the Mnmag1 composite and Mn in solution.

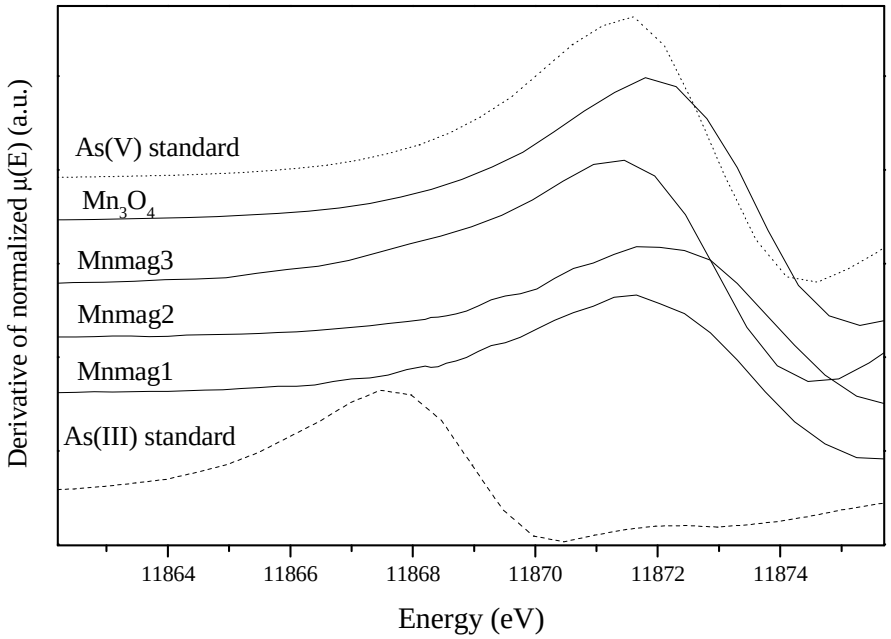

Fig. 3-6: Derivative of As K-edge XANES spectra of the Mnmag composites and synthesized Mn_3O_4 sample (after contact with As(III) solution); As(III) and As(V) standards ($AsNaO_2$ and $AsHNa_2O_4.7H_2O$, respectively).

Mechanisms of As(III) oxidation by Mn-oxides can be quite complex, involving several simultaneous reactions. Some investigations suggest that the oxidation of As(III) to As(V) using manganese dioxide involves the reduction of Mn^{4+} to Mn^{3+}, followed by Mn^{3+} to Mn^{2+}, consistent with one electron transfer reactions (Vaclavikova et al., 2008; Driehaus et al., 1994; Scott and Morgan, 1995; Nesbitt et al., 1998; Manning et al., 2002). Many works on the complexation of arsenite and arsenate by manganese dioxide using XAFS show that As(III) is oxidized to As(V), while only arsenate is adsorbed onto MnO_2 surfaces (Manning et al., 2002; Foster et al., 2003; Lafferty et al., 2010). The majority of these works show that arsenate is adsorbed on the edge of MnO_2, binding to the Mn^{4+} octahedron in bidentate binuclear form (Manning et al., 2002; Foster et al., 2003). A more recent work has shown that arsenate can bind to the Mn^{4+} octahedron in both monodentate mononuclear and bidentate binuclear forms, as well as to the Mn^{3+} octahedron in both monodentate mononuclear and bidentate mononuclear forms (Lafferty et al., 2010). A work from our group has shown that during As(III) sorption onto a manganese dioxide (Na-birnessite, $Na_{0.55}Mn_2O_4.1.5H_2O$), hausmannite (Mn_3O_4) is the intermediate product of reductive dissolution of manganese dioxide, whereas arsenate is adsorbed by Mn_3O_4. Moreover, it has been demonstrated that the precipitation of a Mn^{2+} arsenate, $Mn_3(AsO_4)_2$, occurs for high arsenic concentrations (above 160mg.L^{-1}) (Dias et al., 2008). However, no detailed study has been carried out to show how arsenic is complexed on the surface of hausmannite.

3.4 Conclusion

The results of the synthesis of manganese oxide (Mn_3O_4) magnetic composite have demonstrated that stable magnetic adsorbents with high affinity for As(III) solutions can be generated. The composites have shown good chemical stability and physical integrity in pH values ranging from 3.0 to 9.0, which is commonly used range for arsenic adsorption in water treatment units. The composites surface areas are closer to that of the manganese oxide area, thus indicating that the magnetic particles were well covered by manganese oxide particles. Mn_3O_4 magnetic composites have shown high affinity for arsenic and represent a practical approach to the separation of arsenic from water. The As adsorbed onto the composites was in oxidized arsenic form, As(V). Moreover, the

magnetic property of magnetite, which is attached to the active Mn_3O_4, allows the removal of the sorbent particles from the solution.

Chapter 4 Raman and IR spectroscopic investigation of As-loaded Mn_3O_4 magnetic composites

4.1 Introduction

Arsenite and arsenate adsorption in metal oxides is one of the processes that control arsenic distribution in the environment. Manganese oxides are effective oxidants in the transformation of As(III) to As(V) and allow a stronger fixation and removal of greater amounts of arsenic at pH below 7. In particular, manganese dioxides are the most reported manganese oxides in literature used in water treatment (Deschamps et al., 2005; Bochkarev et al., 2010; Yin et al., 2011). The oxidation of As(III) to As(V) by manganese dioxides is suggested to involve the reduction of Mn^{4+} to Mn^{3+} and, futher, of Mn^{3+} to Mn^{2+} (Driehaus et al., 1994; Scott and Morgan, 1995; Nesbitt et al., 1998; Manning et al., 2002; Dias et al., 2008). Many works on the complexation of arsenite and arsenate in manganese dioxides using XAFS show that As(III) is oxidized to As(V) and only arsenate is found as the adsorbed species on MnO_2 (Manning et al., 2002; Foster et al., 2003; Deschamps et al., 2005; Lafferty et al., 2010). The majority of these works shows that arsenate is adsorbed in the edge of MnO_2, binding to the Mn^{4+} octahedra in bidentate binuclear form (Manning et al., 2002; Foster et al., 2003). A more recent work (Lafferty et al., 2010) has shown that arsenate can bind to the Mn^{4+} octahedra in a monodentate mononuclear form and to the Mn^{3+} octahedra in a bidentate mononuclear form. Dias et al. (2008) have shown that during As(III) sorption in a manganese dioxide (Na-birnessita, $Na_{0.55}Mn_2O_4.1.5H_2O$), hausmannite (Mn_3O_4), a manganese oxide very common in soils, is the intermediate product of reductive dissolution of manganese dioxide and arsenate is adsorbed in Mn_3O_4 surface. Moreover, it has been demonstrated that precipitation of a Mn^{2+} arsenate, $Mn_3(AsO_4)_2$, occurs for high arsenic concentrations (above 160mg.L^{-1}). Hausmannite [Mn_3O_4 or $(Mn^{2+})(Mn^{3+})_2O_4$] is a spinel manganese oxide with structural distortions caused by Jahn-Teller effect, having Mn^{2+} ions in tetrahedral coordination and Mn^{3+} ions in distorced octahedral coordination. Magnetic Mn_3O_4 composites combine the oxidative property of Mn_3O_4 with the magnetic property of ferromagnetic iron oxides, such as magnetite (Fe_3O_4) and maghemite (γ-Fe_2O_3), which will help the solid-liquid separation

process that follows arsenic sorption. We have synthesized low-cost magnetic Mn_3O_4 composites to remove As(III) from water and have shown that the magnetic composite presents high affinity for As(III), with maximum sorptive capacity of 14mg.g^{-1} (0.0048mg.m^{-2}) (Chapter 3). However, no detailed study has been carried out to show how arsenic is complexed on the surface of hausmannite. The present work aims to understand the mechanism of arsenic immobilization in a magnetic Mn_3O_4 composite by Raman and IR spectroscopy.

4.2 Experimental

All chemicals were of analytical grade and used without further purification. All solutions were prepared with deionized water with a conductivity of 18.2µS.cm^{-1} obtained with a Milli-Q water purification system (Millipore).

4.2.1 Synthesis of the studied Mn_3O_4 and Mn_3O_4 magnetic composites

Samples of Mn_3O_4 magnetic composites were prepared under alkaline conditions at room temperature (25±2°C) by adding 45mL of 1.0mol.L^{-1} manganese chloride ($MnCl_2.4H_2O$ - Sigma-Aldrich) solution in 1000mL Milli-Q water saturated with O_2 in the presence of 0.5g of previously synthesized magnetite nanoparticles. Under vigorous stirring and air bubbling 1.0mol.L^{-1} KOH were added to increase the initial pH to pH 12. Almost at the same moment a brown solid precipitated. Magnetite nanoparticles were prepared by mixing N_2 saturated water solution of Fe^{3+}: Fe^{2+} (2:1) with 5.0mol.L^{-1} KOH (Sigma-Aldrich) solution at 70°C.

4.2.2 Adsorption experiments

The adsorption studies were performed batchwise. The As solutions were prepared by dissolving sodium (meta)arsenite ($NaAsO_2$, purity >99%, Fluka) in Milli-Q water. The adsorption studies were carried out in 250 mL Pyrex vessels sealed with laboratory parafilm (Pechiney plastic packaging, USA). In the experiments 0.2g of the adsorbent were added to the Erlenmeyer flasks, filled with 100mL arsenic solution containing

different amounts of arsenic. The Mn_3O_4 magnetic composites were exposed to As concentrations from 1.0mg.L^{-1} to 50mg.L^{-1} and also 1000mg.L^{-1}. Agitation at 200rpm was provided by a thermostatic shaker, manufactured by New Brunswick Scientific Edison, USA. Agitation rate, pH and temperature were controlled in all sorption experiments; temperature was maintained at (25±5^{o}C) and pH 5.0, respectively. In order to produce an adequate reference material for the spectroscopic measurements, blank samples were prepared in Milli-Q water under the same pH conditions as the experiments with As. After 24 hours, the pH of the solutions was measured and the solids of each flask were separated by a magnet and the supernatant solution vacuum-filtered through a 0.22μm membrane filter (Fisher Scientific). Subsequently, the solids were rinsed with Milli-Q water. The filtrate was assayed for total arsenic directly by inductively coupled plasma optical emission spectrometry, ICP-OES (Perkin-Elmer Opttima 7300 DV).

4.2.3 Spectroscopic analysis

Raman spectra were obtained on a Horiba Jobin Yvon LABRAM-HR 800 spectrograph, equipped with a 633nm helium-neon laser, 20mW of power, attached to an Olympus BHX microscope equipped with 10X, 50X, and 100X lenses. Raman-scattered radiation was collected with 600g.mm^{-1} grating, in a 180° backscattering configuration. The spectra were collected in a frequency range of 100 to at least 1100cm^{-1} with a step size of 1.1cm^{-1}. In order to suppress extra noise and to obtain sufficiently accurate results, a N_2 cooled charge couple device (CCD) detector was used as the detecting device. To reduce noise ratio, spectra were acquired at acquisition time of three minutes twenty times. Raman spectra were recorded of all freshly prepared samples, as well as of As-loaded samples.

A Perkin Elmer, Paragon 1000 spectrometer was used for IR spectra collection. The sample scans ranged from 400 to 4000cm^{-1} with 4.0cm^{-1} resolution and were obtained as 128 scans. IR spectra were obtained as dry samples mixed with KBr corresponding to 8mg of sample in approximately 40mg of spectral grade KBr. In IR spectroscopy it is of importance to work with dried samples, since minor amounts of humidity disturbs the

IR signal. Thus, before sample preparation, KBr was kept in an oven (130±2°C) for at least 24 hours. The samples were stored at room temperature (25±2°C) in a desiccator, filled with silica gel. The KBr was grained along with each sample manually by using a mortar and pestle. Subsequently, the mixture was filled into the sample cup with attention to homogeneity and leveled surface, and absence of clusters. The collected Raman and IR data were baseline-corrected and curve-fitted to obtain quantitative band parameters, such as peak maxima, widths, intensities and areas, by using the software Peakfit 4.0.

4.3 Results and Discussion

The Raman spectrum of Mn_3O_4 magnetic composite shows the main bands reported in literature for Mn_3O_4 with vibrational characteristics of crystalline materials: bands of small widths and high intensity (Fig. 3-3(b), Mnmag3). Lack of magnetite contribution in the spectra of the composite indicates covering of magnetic particles by Mn_3O_4.

The As(III) sorption isotherm (initial As concentrations from 1.0mg.L^{-1} to 50mg.L^{-1}) for the Mn_3O_4 magnetic composite is shown in Fig. 3-5 (Mnmag3 curve). The sample shows high affinity for As with maximum sorption capacity of 14mg.g^{-1} (0.0048mg.m^{-2}). Raman spectra were obtained for As adsorbed onto the synthesized Mn_3O_4 magnetic composite sample. As a result of the adsorption process the obtained spectra present distinct differences in the region from 750 to 950cm^{-1}. The results are compiled in Fig. 4-1 and the peak fitting of the spectra is shown in Fig. 4-2. All reacted samples with As loading varying from 5 to 16mg.g^{-1} (Fig. 4-1(a), Fig. 4-2 and Table 4-1) exhibit, in their Raman spectra, bands centering at ~830cm^{-1} and ~900cm^{-1}, which are related to arsenic adsorption, since they do not appear in the spectrum of blank sample (Fig. 4-2 and Table 4-1). XANES results show that the As adsorbed in the samples with 5 to 35mg.g^{-1} of arsenic loading is at the oxidized arsenic form, As(V) (Fig. 4-3). Therefore, arsenate not arsenite species are complexed to the Mn_3O_4 surface in the composite.

The vibrational spectra of As complexes seem to be more difficult to interpret than those of protonated aqueous As species. Arsenic complexes may exhibit shifts in As-

OM (M=Metal) symmetric vibrations, according to the type of interactions, such as ion-pair, monodentate complex, bidentate complex or polymer formation. Furthermore, these vibration shifts are specific to the type of complexed metal (Myneni et al., 1998). Müller et al. (2010) recorded Raman spectra from As(V) aqueous solutions at various pH conditions and have shown that the AsO_4^{3-} species presents a strong line at 811cm^{-1} and a small line at 785cm^{-1}, which are assigned to the symmetric and asymmetric stretching vibrations of As-O, respectively. The results of Müller et al. (2010) for As(V) adsorbed onto iron oxides show only a band at ~840cm^{-1}, which was related to a shift of the As-O symmetric vibration of AsO_4^{3-}. Dias et al. (2008) have shown that during As(III) sorption in a manganese dioxide (Na-birnessita, $Na_{0.55}Mn_2O_4.1.5H_2O$), Mn_3O_4 is the intermediate product of reductive dissolution of manganese dioxide and a band at 830cm^{-1} in the Raman spectra is associated to the presence of arsenate adsorbed in Mn_3O_4 surface. Comparing the obtained Raman spectra of As(V) adsorption (Fig. 4-1(a), Fig. 4-2 and Table 4-1) with the results obtained by Müller et al. (2010) and Dias et al. (2008) (unique bands centered at 840 and 830cm^{-1}, respectively), one can conclude that the bands found in this work, at ~830cm^{-1} and ~900cm^{-1}, which present similar intensities, are also due to the symmetric vibration of As-O in inner-sphere surface complexes. However, the presence of two bands instead of one is probably related to different type of interactions. Lafferty et al. (2010) has shown that arsenate can bind to Mn^{3+} octahedra in both bidentate and monodentate mononuclear forms (Fig. 4-4). Therefore, the band at ~900cm^{-1} could be associated to bidentate mononuclear forms, while the band at 830cm^{-1} could be associated to monodentate mononuclear forms, since in bidentate mononuclear forms (As-Mn distance of 2.78Å - Lafferty et al., 2010) the As-O vibration is expected to occur in higher frequencies than in the monodentate mononuclear forms (As-Mn distance of 3.35Å - Lafferty et al., 2010) due to the smaller distances between Mn^{3+} and As(V). Raman spectroscopy mainly exhibits bands resulting of symmetric vibrations, differently from IR spectroscopy, which provides primarily bands due to asymmetric vibrations. Both are important to characterize surface complexes. Hence, IR spectroscopy was applied to the 14$mg.g^{-1}$ As loaded synthesized Mn_3O_4 magnetic composite. The recorded IR spectrum of As(V) adsorption onto the sample is compiled in Fig. 4-5. Fitting the spectral data suggests the presence of three bands at ~737, 774 and 835cm^{-1} and two bands at ~899 and 915cm^{-1}

(Fig. 4-6 and Table 4-2). The bands may result from splitting of asymmetric vibration related to symmetry reduction. The AsO_4^{3-} molecule with T_d symmetry presents one frequency for the symmetric stretching vibration and one for the asymmetric stretching vibrations. When the symmetry is reduced to C_{2v} (one oxygen of AsO_4^{3-} is bound - monodentate complexes), the frequency of the symmetric stretching vibration increases and the asymmetric stretching vibrations present two frequencies. Moreover, when the symmetry is reduced to C_{3v} (two oxygens of AsO_4^{3-} are bound - bidentate complexes), the frequency of the symmetric stretching vibration increases more and the asymmetric stretching vibrations present three frequencies (Müller et al., 2010).Therefore, the presence of five bands related to asymmetric vibrations in IR spectra suggests the formations of both monodentate and bidentate complexes, confirming the Raman results.

Dias et al. (2008) have shown that precipitation of a Mn^{2+} arsenate, $Mn_3(AsO_4)_2$, occurs at high arsenic loading, such as those occurring close to saturation (*i.e.* maximum loading capacity of the sorbent). In our work, the only evidence of precipitation occurs for the sample with the highest As loading (35mg.g^{-1}) (Fig. 4-1(b)). As it can be seen in the Raman microscope image shown in the inset of Fig. 4-1(b), the sample presents some translucent crystals. For this sample, only a band at ~850cm^{-1} appears, with much higher intensity than the bands at ~830cm^{-1} and ~900cm^{-1} that appear in the samples with lower As loadings (Fig. 4-1). The precipitate presents As-O symmetric vibration frequency between 830 and 900cm^{-1} probably because each arsenate ion in $Mn_3(AsO_4)_2$ is bonded to two Mn^{2+} in both monodentate and bidentate mononuclear forms.

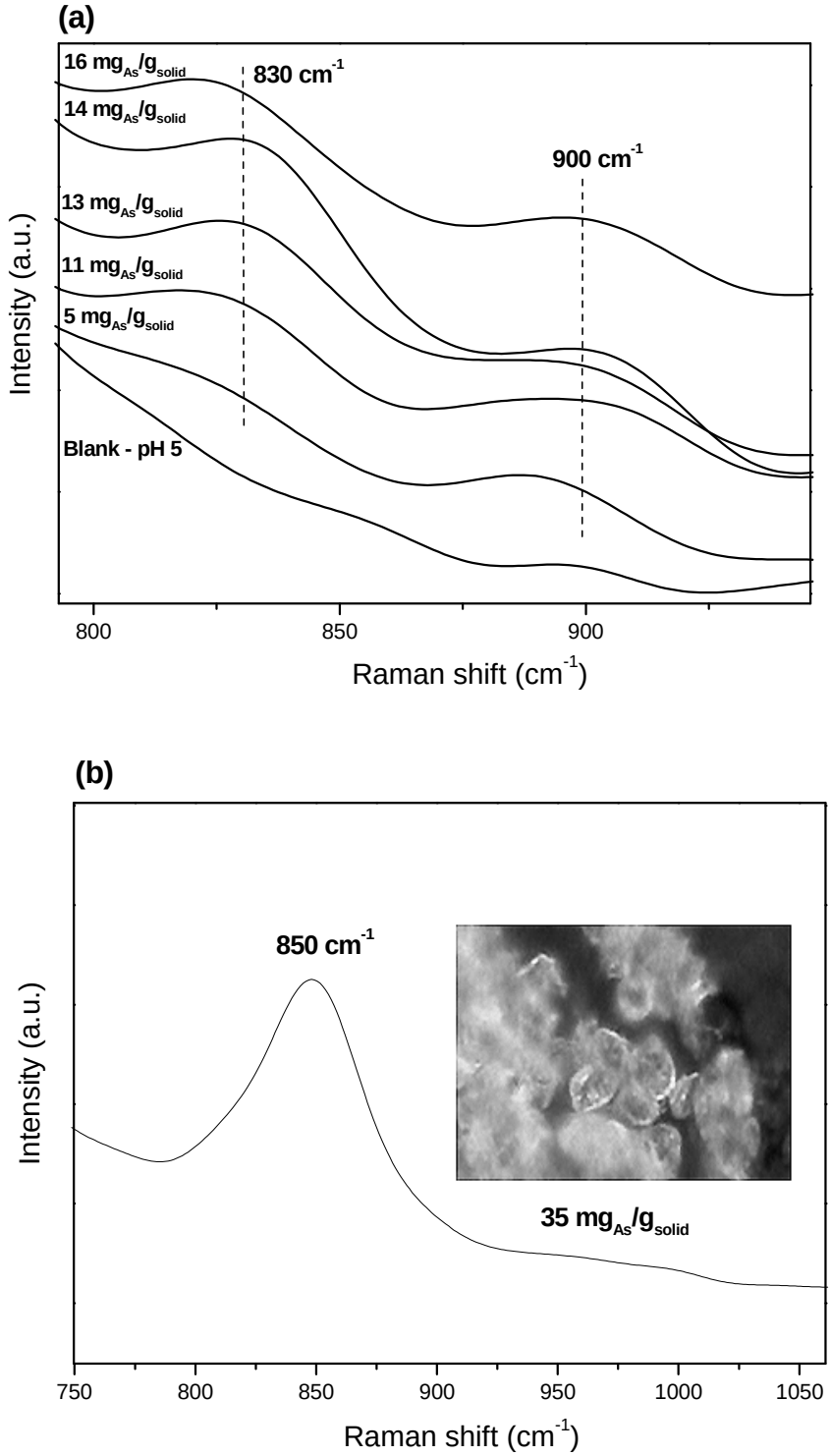

Fig. 4-1: Raman spectra of the magnetic Mn_3O_4 composite after As(III) sorption tests: (a) Blank sample (solid in contact with a pH 5 solution) and As-loaded samples from $5mg_{As}.g_{solid}^{-1}$ until $16mg_{As}.g_{solid}^{-1}$; (b) Sample containing $35mg_{As}.g_{solid}^{-1}$; inset showing a Raman microscope image of the sample.

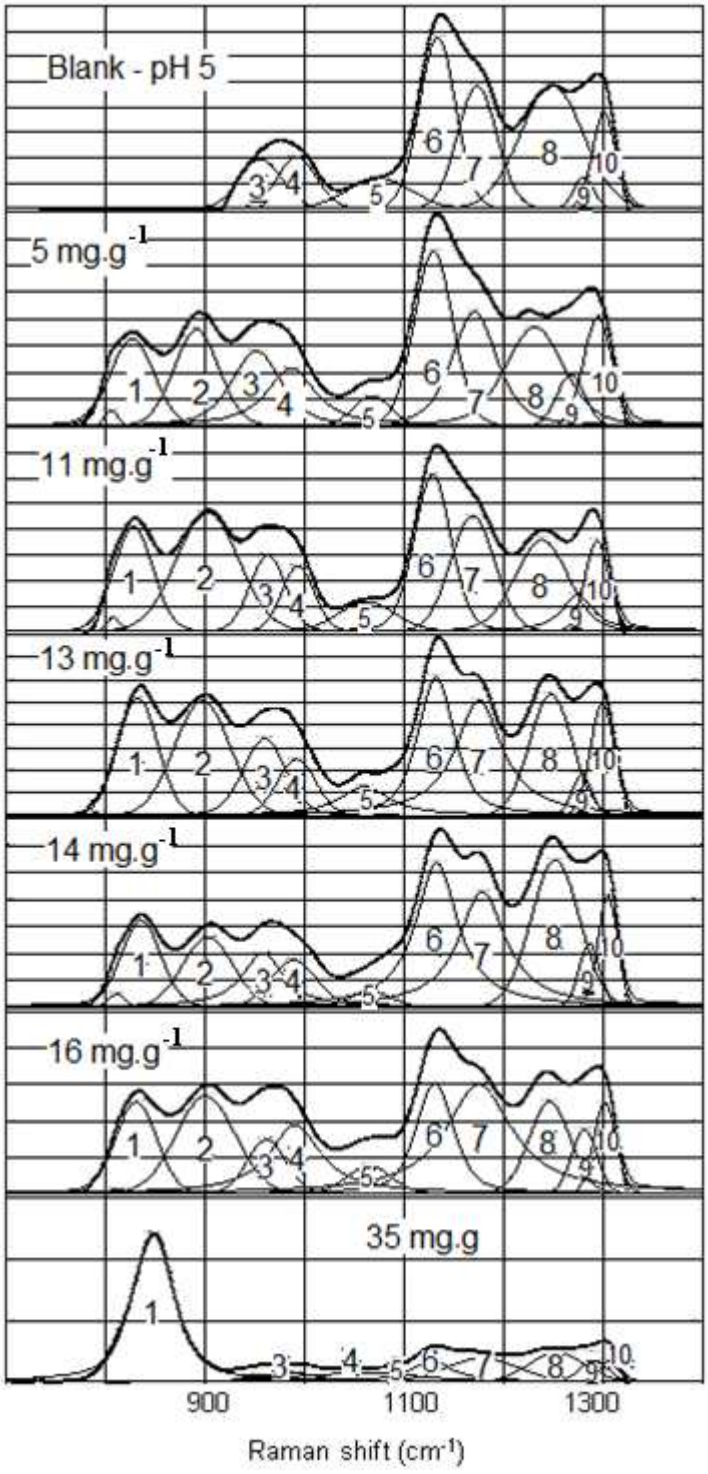

Fig. 4-2: Raman spectra peak fitting of the blank sample and As-loaded samples. Peaks are numbered from 1 to 10 and are described in Table 4-1.

Table 4-1: Raman peaks of As-loaded samples.

SAMPLES	PEAKS (cm^{-1})									
	1	2	3	4	5	6	7	8	9	10
Blank	-	-	956.4	992.8	1075.3	1133.9	1173.7	1248.3	1280.4	1300.7
5mg.g^{-1}	**827.3**	**892.0**	952.2	987.2	1068.3	1129.8	1171.0	1231.1	1267.5	1294.6
11mg.g^{-1}	**828.5**	**900.9**	963.7	994.1	1063.3	1129.0	1169.2	1237.8	1273.6	1293.6
13mg.g^{-1}	**832.9**	**898.0**	960.3	992.5	1060.6	1132.5	1175.4	1247.5	1278.6	1299.0
14mg.g^{-1}	**836.2**	**903.3**	958.6	989.8	1066.6	1133.3	1178.8	1251.8	1286.0	1304.6
16mg.g^{-1}	**830.8**	**901.2**	962.5	991.1	1064.9	1131.3	1175.4	1246.1	1280.9	1302.0
35mg.g^{-1}	**848.3**	-	956.7	994.0	1055.3	1128.3	1178.3	1253.1	1290.6	1306.2

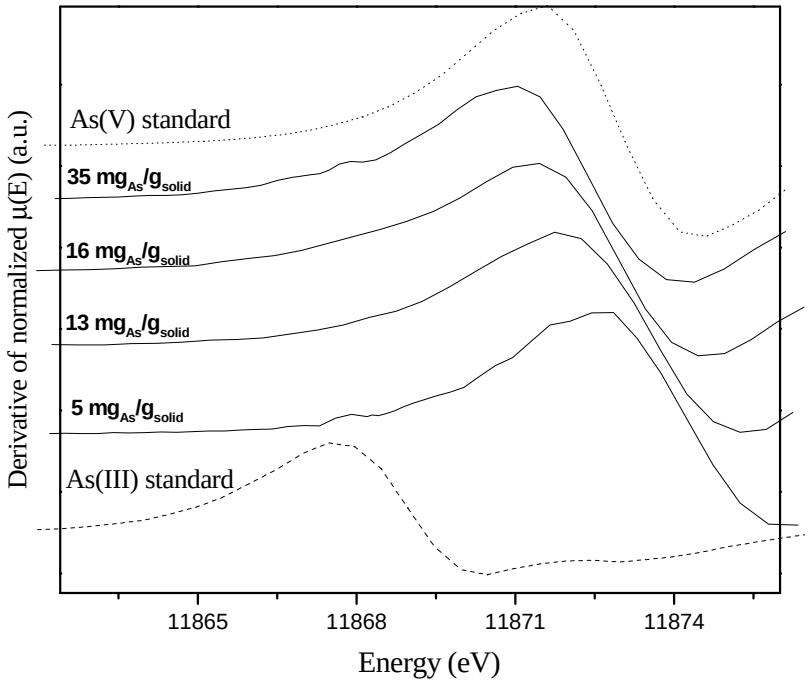

Fig. 4-3: Derivative of As K-edge XANES spectra of the As-loaded samples (after contact with As(III) solution); As(III) and As(V) standards ($AsNaO_2$ and $AsHNa_2O_4.7H_2O$, respectively).

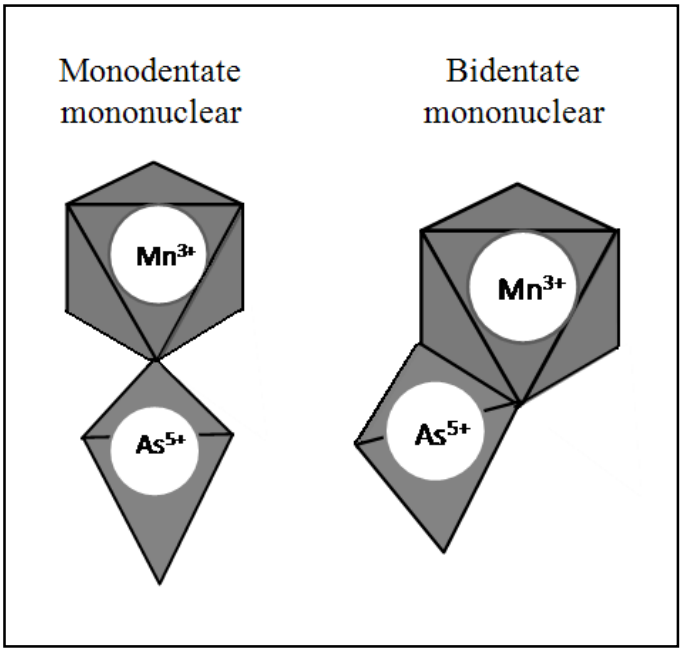

Fig. 4-4: Schematic representations of monodentate and bidentate mononuclear forms of As(V) complexed to Mn^{3+} octahedra.

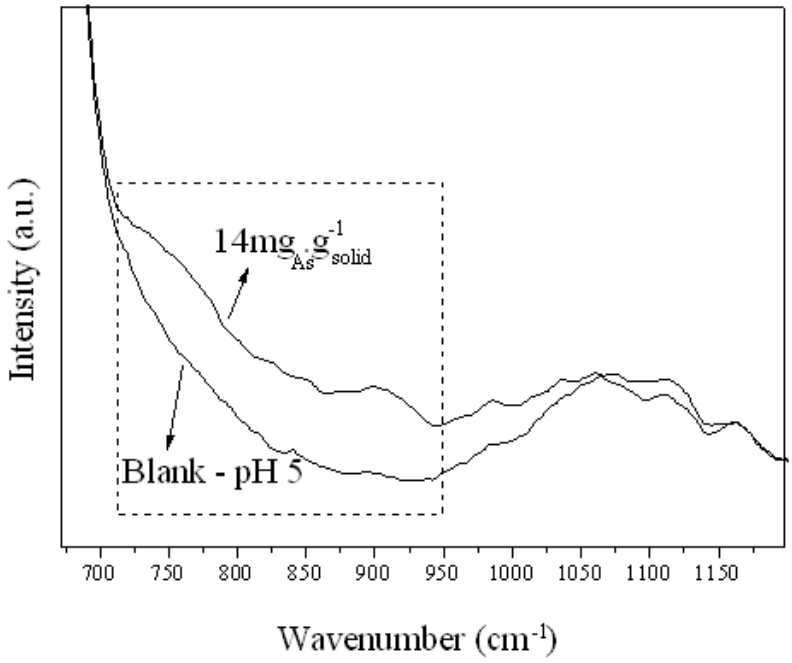

Fig. 4-5: IR spectra of the magnetic Mn_3O_4 composite containing $14mg_{As}.g_{solid}^{-1}$ and blank sample.

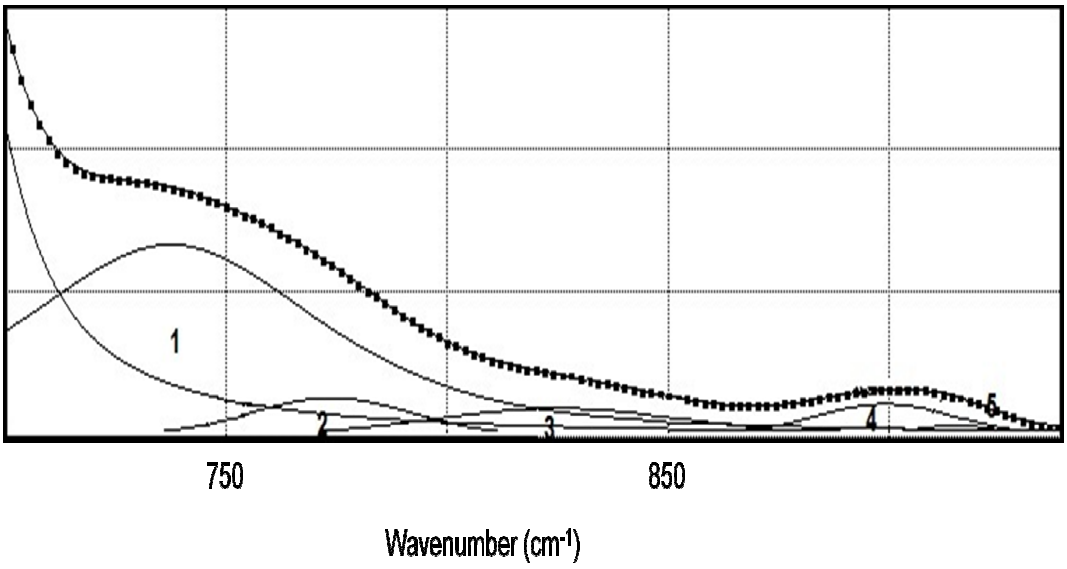

Fig. 4-6: Peak fitting of the IR spectrum of the sample containing $14mg_{As}.g_{solid}^{-1}$. Peaks are numbered from 1 to 5 and are described in Table 4-2.

Table 4-2: IR peaks of $14mg_{As}.g_{solid}^{-1}$ sample.

PEAKS (cm^{-1})				
1	2	3	4	5
737.5	773.6	825.0	898.8	914.8

4.4 Conclusion

The sorption of As on the synthesized Mn_3O_4 magnetic composite samples was investigated using Raman and IR spectroscopy. XANES results have shown that the As adsorbed in the samples is at the oxidized arsenic form, As(V). Raman spectra of adsorbed As(V) species onto Mn_3O_4 occur at about $830cm^{-1}$ and $900cm^{-1}$. IR spectral data suggests the presence of three bands at ~737, 774 and $835cm^{-1}$ and two bands at ~899 and $915cm^{-1}$. The results are in agreement with monodentate and bidentate mononuclear complexation models. The obtained Raman spectral data for the highest As loading ($35mg.g^{-1}$) result in a distinct band at about $850cm^{-1}$. In the Raman

microscope image of this sample, the presence of translucent crystals could be detected. These findings indicate the precipitation of manganese arsenate at high As loadings.

Chapter 5 Mn_3O_4 Magnetic Nanocomposites for Degradation of Methylene Blue

5.1 Introduction

Water pollution is one of the major challenges faced by global society. The development of new materials and methods for water treatment has received growing interest in remedying environmental problems. Dye waste is an important source of water contamination since the presence of dyes in water reduces light penetration hindering photosynthesis in aquatic plants apart from the undesirable coloring of streams. Many textile industries use dyes generating a colored wastewater and causing damage to the ecological system. Therefore, treating of dye effluents prior to their discharge is essential (Grau, 1991). Manganese oxides are powerful oxidants due to their high reducing potential. It has already been reported that Mn^{3+} and Mn^{4+} oxides and hydroxides can oxidize many inorganic and organic compounds (Stobhe et al., 1999; Xu et al., 2008; Abdelazez et al., 2010; Kima et al., 2010; Rhadfia et al., 2010). Mn_3O_4 (hausmannite) is a complex oxide of Mn containing both di- and tri-valent manganese that presents higher standard redox potential (1.824V) than other manganese oxides (1.225V for MnO_2 and 1.497V for Mn_2O_3) (Chapter 2). In view of strong oxidative characteristic of Mn_3O_4, they have been evaluated as effective oxidants for the degradation of dyes in water, since oxidation of dyes usually requires the use of strong electron acceptors with reducing potential higher than 1.0V (Chowdhury et al., 2009; Katafias et al., 2011; Zaied et al., 2011). The introduction of magnetic properties in Mn_3O_4 can improve its separation from dye effluents. Magnetic materials can be conveniently recovered by magnetic separation, in turn avoiding the filtration steps, which represent a barrier to the application of high performance, small-sized materials in environmental remediation processes and the treatment of great volumes of aqueous solutions. To face this problem, magnetite nanoparticles are being combined with other compounds or covered by an active compound (Qu, 2008; Rosas et al., 2010; Chen et al., 2011). In both cases the magnetic property of magnetite is preserved. Here, we report the application in methylene blue degradation of a magnetic composite based on Mn_3O_4 synthesized at room temperature and by using air as an oxidant. The composite

have already been tested in As(III) oxidative adsorption and showed great results (Chapter 3).

5.2 Experimental

All chemicals were of analytical grade and used without further purification. All solutions were prepared with deionized water with a conductivity of 18.2µS.cm^{-1} obtained with a Milli-Q water purification system (Millipore). To remove contaminants that had been potentially adsorbed onto the glass and plastic walls, all vessels and instruments were cleaned by soaking in detergent solution, then in 1.0mol.L^{-1} HNO_3 solution, and subsequently in deionized water, in each case for at least 24 hours. All parts of the spectroscopic equipment used to extract and fill the sample were cells cleaned and rinsed properly with acetone. The pH electrode (713 pH Meter, Metrohm) was calibrated prior to use with three pH buffers (pH 4.0, 7.0, and 10.0).

5.2.1 Synthesis of magnetite nanoparticles (mag3 – Chapter 3)

Magnetite particles were prepared by a chemical precipitation route. An aqueous solution prepared with 400mL of deionized water, 9.61g of $Fe_2(SO_4)_3.5H_2O$ (97%, Aldrich), 7.13g of $FeSO_4.7H_2O$ (RegentPlus^{TM}, ≥ 99.0% - Aldrich) and 100mL of a 5.0mol.L^{-1} KOH (Sigma-Aldrich) solution was stirred under N_2 atmosphere at 70°C for 2h. The black suspension was filtered, washed with water several times, and finally dried in an oven at 45°C (Oliveira et al., 2004; Peng et al., 2005; Mürbe et al., 2008).

5.2.2 Synthesis of magnetic Mn_3O_4 composite (Mnmag3 - Chapter 3)

For the preparation of the composite, 1000mL of deionized water was placed in contact with 1.0g of previously synthesized magnetite nanoparticles and 45mL of 1.0mol.L^{-1} $MnCl_2.4H_2O$ (Sigma-Aldrich) solution at pH 12 (1.0mol.L^{-1} KOH - Sigma-Aldrich) in a 2000mL Pyrex beaker under stirring (mechanical stirrer, Fisatom 713 D) and constant air input (aquarium pump Power 500) during 30min. This same reaction was also carried out in the absence of magnetite nanoparticles for comparison. A brown colored

solid was separated from solution by a neodymium magnet (180x100x35mm, Imatec Produtos Magnéticos Ltda), washed with deionized water solution and dried in a dessicator at room temperature.

5.2.3 Methylene Blue (MB) Degradation

Decolorization experiments were conducted in a glass beaker, typically containing 68mL of $1.4x10^{-5}mol.L^{-1}$ MB dye solution and 50mg of Mn_3O_4 nanoparticles or Mn_3O_4 magnetic composite (Mnmag3 from Chapter 3). The mixture was allowed to react at room temperature under stirring. The progress of decolorization was assessed by UV-vis spectroscopic measurements of the mixture at different time intervals (5min to 3h). To investigate the effect of pH on the decolorization process, experiment was performed at pH 3.0, 4.0 and 6.0 keeping the amount of Mn_3O_4 and the dye constants. The effect of duplicating and reducing the composite mass was also investigated (25 and 100mg of Mnmag). The tests were conducted in duplicate. Absorbance ranging from 0.3 to 1.0 is less susceptible to stray light and noise problems and hence becomes the preferred absorbance range for UV-vis analyses. Therefore, the MB concentration was chosen to obtain initial absorbance of 1.0.

5.2.4 Analysis Instruments

Raman spectroscopic and X-ray diffraction (XRD) analyses were carried out for solid identification. Raman spectra were collected on a Horiba Jobin Yvon LABRAM-HR 800 spectrograph, equipped with a 633nm helium-neon laser, 20mW of power, attached to an Olympus BHX microscope equipped with 10X, 50X, and 100X lenses. Raman-scattered radiation was collected with $600g.mm^{-1}$ grating, in a 180° backscattering configuration. The spectra were collected in a frequency range of 100 to at least $1100cm^{-1}$ with a step size of $1.1cm^{-1}$. In order to suppress extra noise and to obtain sufficiently accurate results, a N_2 cooled charge couple device (CCD) detector was used as the detecting device. To reduce noise ratio, spectra were acquired at acquisition time of three minutes twenty times.

The diffractograms were obtained on a Shimadzu 7000 X-ray diffractometer, using a copper anode (Cu $K\alpha_1$ radiation) and graphite crystal monochromator. Analyses were run by step-scanning from 4^o to 90^o 2θ, increments of 0.02 2θ and count time of 3s. Lattice parameters were refined using the GSAS 2001 software. The crystallite size was estimated using the Crystallite Size/Lattice Strain Calculation (Hall's Equation) software for Shimadzu X-ray diffractometer. The Hall's Equation is as follows (Eq.5-1):

$$\frac{\beta \cos\theta}{\lambda} = \frac{1}{\varepsilon} + 2\eta \frac{\sin\theta}{\lambda} \qquad (5\text{-}1)$$

where θ is the Bragg angle, β is the expanse of the diffraction line width (integral width), ε is the average size of crystal particles, λ is the wavelength of the X-ray and η is the grating distortion. The particle size in the direction perpendicular to the (hkl) plane is $D_{hkl} = K\,\varepsilon$, where *K* is the Scherrer's constant which is different depending on the crystal (1.05 is typical). Using these equations, the average crystallite size, d_{xrd}, is calculated. The β value to be substituted for this Equation is the value obtained by correcting the integral width according to the integral width curve using the "Jones Correction" method by which the inherent expansion of the system is corrected.

A Perkin Elmer, Paragon 1000 spectrometer was used for FTIR spectra collection. The sample scans ranged from 400 to 4000cm^{-1} with 4.0cm^{-1} resolution and were obtained as 128 scans. IR spectra were obtained as dry samples mixed with KBr corresponding to 8mg of sample in approximately 40mg of spectral grade KBr. A typical room temperature measurement of the magnetization vs. applied magnetic field was obtained with a vibrating sample magnetometer.

Measurements of the specific surface area were made by the BET (Brunauer-Emmett-Teller) – Multipoint method using a nitrogen gas sorption analyzer NOVA 1000 Quantachrome. Prior to the measurements the samples were massed, degassed by placing them into a glass cell under vacuum for at least 24 h at 100ºC, and massed again. The BET analyzer was configured and its Dewar flask filled with liquid nitrogen

and set into place. Each degassed sample was load and the results of the analysis collected. Transmission electron microscopy (TEM) images of the samples were obtained using a Tecnai-G2-20-FEI 2006 microscope in the Center of Microscopy at the *Universidade Federal de Minas Gerais* (UFMG). A UV–visible spectrophotometer (Varian Cary 50) was employed to monitor degradation of dyes spectroscopically. Sampling of the solutions was measured at different times in an optical quartz cell (1.0cm).

5.3 Results and Discussion

Raman and FTIR spectroscopy results confirm that the magnetite particles synthesis was well performed. Sample mag shows a pronounced Raman band at 672cm^{-1} attributed to the A_{1g} vibrational mode of magnetite and two weak bands at 316cm^{-1} and 546cm^{-1} assigned to the T_{1g} vibrational mode of magnetite (Jubb et al., 2010). Moreover, sample mag shows two broad FTIR absorption bands (Fig. 5-1(b)) centered at about 575cm^{-1} and 400cm^{-1} also related to magnetite (Mürbe et al., 2008). Powder X-ray diffraction (XRD) pattern of sample mag is typical of single phase spinel oxides and shows broad peaks that correspond to a cubic spinel structure of magnetite (Fe_3O_4) (Fig. 5-2(a)). The structure has been refined (Rietveld refinement, GSAS 2001) in the cubic space group, $Fd\bar{3}m$, and has the following cell parameters: a_0=8.3617Å and V=584.645Å^3 (Fig. 5-2(a)). The sample presents crystallite size d_{XRD} calculated with Hall's equation of 13nm (Table 5-1), in agreement with those estimated by TEM images (Fig. 5-3(a)). The lattice constant of the magnetite nanocrystals reveal a significant change of unit cell dimension. The typical value for the lattice constant of bulk magnetite is a_0=8.3918Å, but for smaller particles the lattice constant tends to decrease (Mürbe et al., 2008). Surface area measurement of the magnetite particles via nitrogen gas absorption yielded a Brunauer, Emmett and Teller (BET) surface area of 92m^2.g^{-1} (Table 5-1). We have also observed the morphology of magnetite nanoparticles with TEM. Aggregated, octahedral magnetite nanoparticles with an average size of about 10nm (Fig. 5-3(a)).

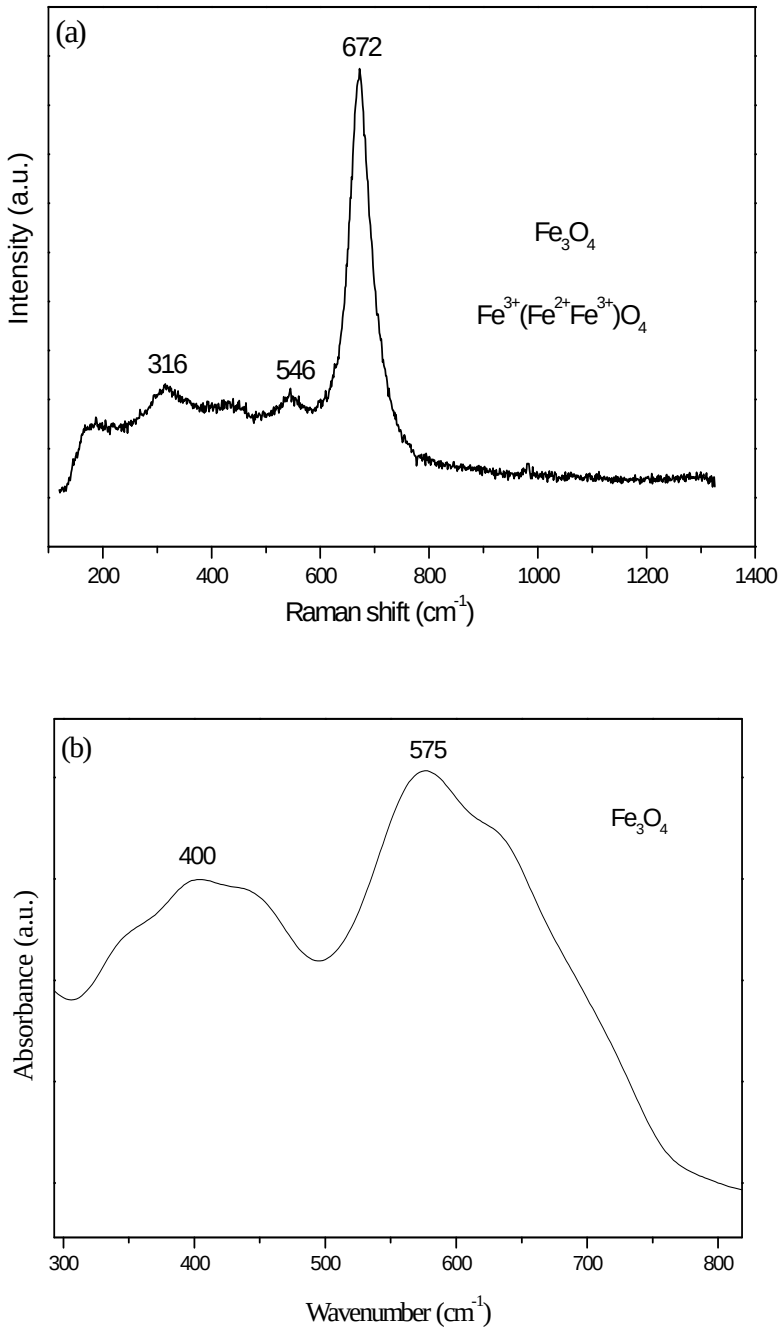

Fig. 5-1: (a) Raman and (b) FTIR spectra of synthesized magnetite nanoparticles.

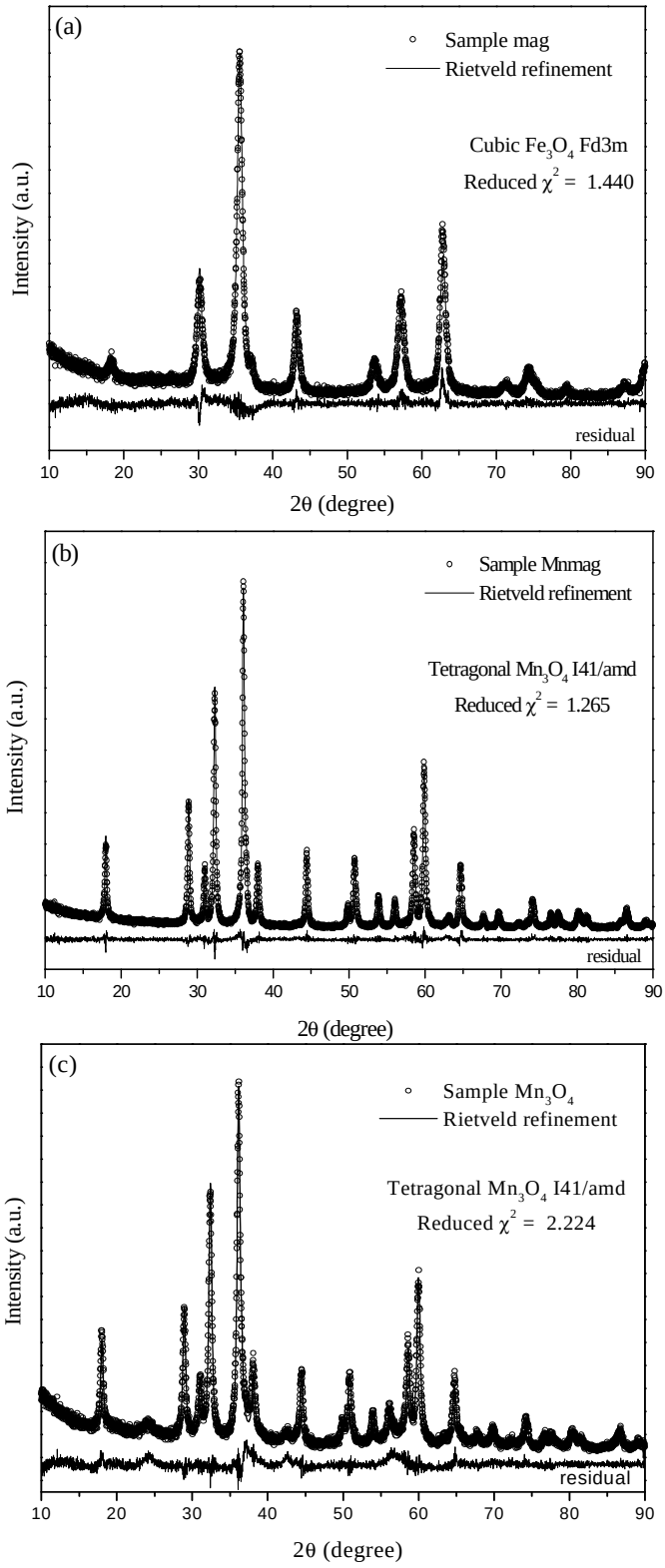

Fig. 5-2: Powder X-ray diffraction pattern of: (a) synthesized magnetite (mag3 – Chapter 3), (b) synthesized magnetic Mn_3O_4 composite (Mnmag3 – Chapter 3) and (c) Mn_3O_4 particles.

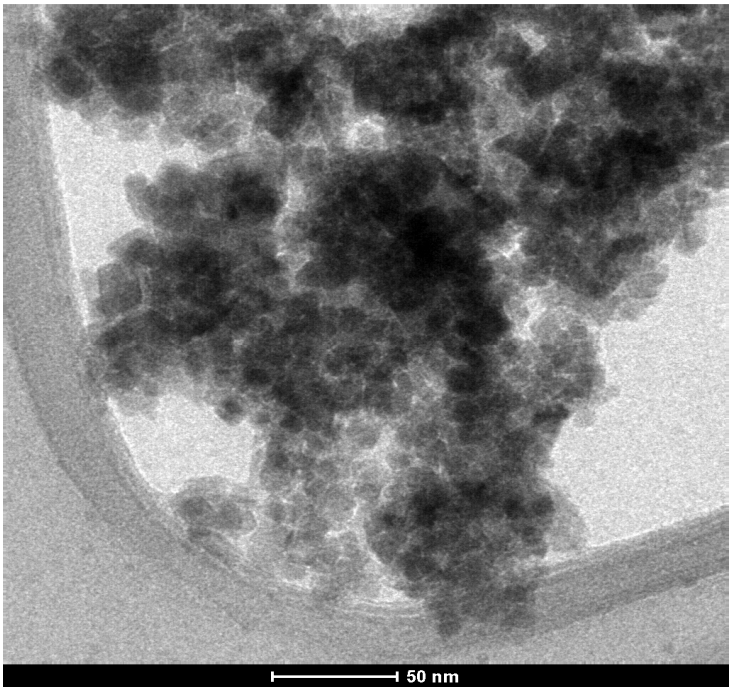

(a)

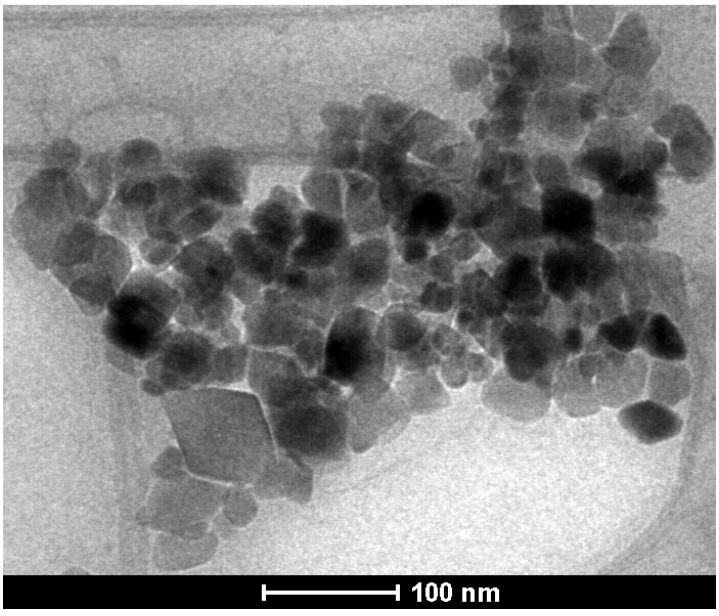

(b)

Fig. 5-3: TEM images of the (a) magnetite particles (mag3 – Chapter 3) and the (b) composite (Mnmag3 – Chapter 3).

Table 5-1: BET surface areas (S_{BET}), crystallite size (d_{XRD}), saturation magnetization (M_S) and coercive field (H_C) of the samples.

SAMPLE	**S_{BET} ($m^2.g^{-1}$)**	**d_{XRD} (nm)**	**M_S ($emu.g^{-1}$)**	**H_C (Oe)**
mag	92	13	70	0
Mnmag	40	27	3.75	0
Mn_3O_4	54	21	-	-

The magnetic hysteresis curve of magnetite nanoparticles was recorded at 300K (room temperature) (Fig. 5-4(a)). The saturation magnetization (Ms) at 300 K is about 70emu.g^{-1}, lower than that of bulk magnetite particles (92emu.g^{-1}, Mürbe et al., 2008) (Table 5-1). The possible causes of the decrease in Ms compared with bulk magnetite could be chemical changes on the surface, magnetic degradation of the surface or the decrease of particle size. The magnetite nanoparticles exhibit a superparamagnetic state at room temperature which is indicated by the disappearance of hysteresis (zero coercive filed, Table 5-1). Advantages of the superparamagnetic particles are easy resuspension, large surface area, slow sedimentation and uniform distribution of the particles in the suspension media. Once magnetized, the particles behave like small permanent magnets, so that they form aggregates due to magnetic interaction.

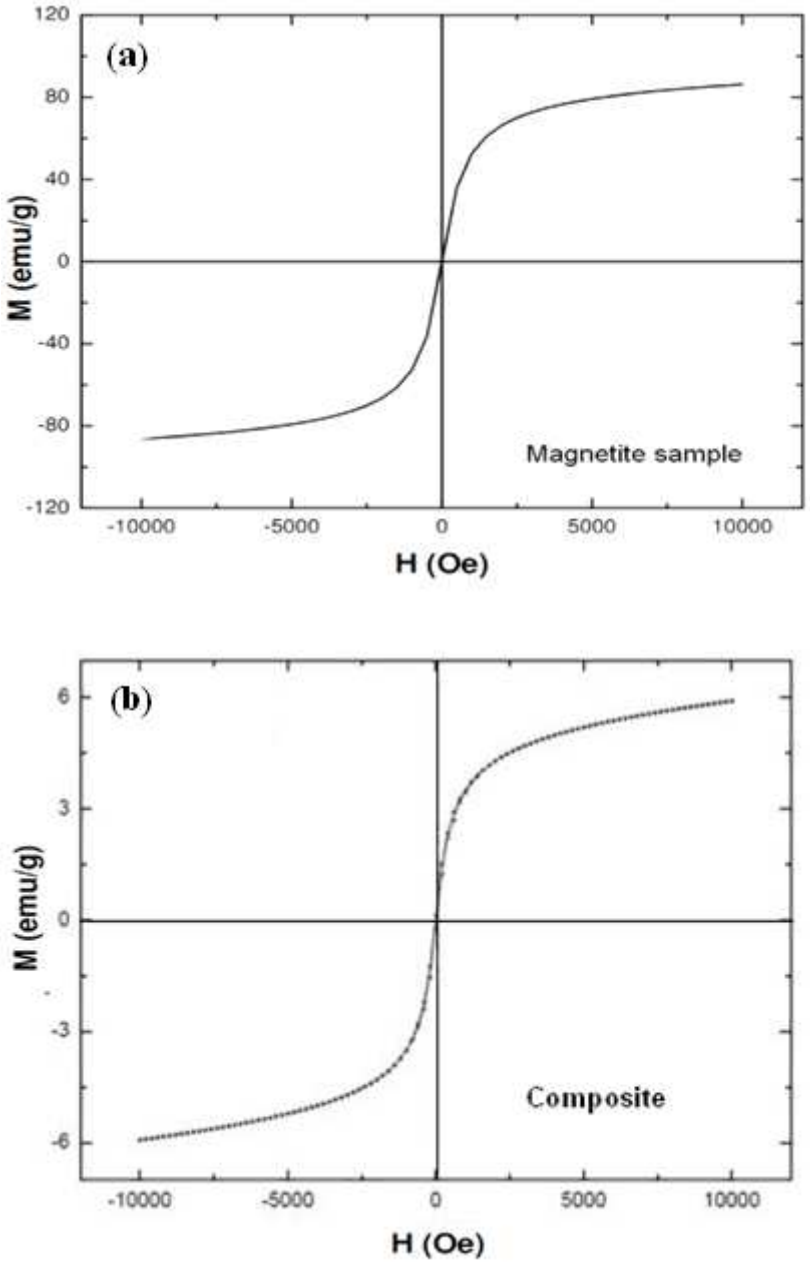

Fig. 5-4: Room temperature magnetization curves of: (a) synthesized magnetite (mag3- Chapter 3) and (b) magnetic Mn_3O_4 composite (Mnmag3 – Chapter 3).

The synthesis of Mn_3O_4 in presence and absence of magnetite is confirmed by the presence of diffraction peaks corresponding to a tetragonal structure of Mn_3O_4. Rietveld refinement of the structure in the tetragonal space group, I41/amd, shows the following cell parameters: a=b=5.7639Å, c=9.4650Å and V=314.449Å^3 for the composite and a=b=5.7586Å, c=9.4462Å and V=313.229Å^3 for Mn_3O_4 nanoparticles (Fig. 5-2(b)). The Mnmag3 sample presents crystallite size d_{XRD} of 27nm, while Mn_3O_4 particles sample presents crystallite size d_{XRD} of 21nm (Table 5-1). The synthesis in presence of magnetite favors the formation of a pure, highly ordered Mn_3O_4 material. Raman spectra of manganese oxide and Mnmag samples show only the main bands reported in literature for Mn_3O_4 (Fig. 3-3, Mnmag3) (Han et al., 2006). The composite dispersed in water solution can be separated from water by using magnets (Fig. 5-5). The reduced M_S (3.75emu.g^{-1}) of the composite can be understood as a result of the presence of much more Mn_3O_4 paticles than Fe_3O_4 particles (Fig. 5-4(b)). The TEM image of the composite shows particles with dominantly octahedral morphology, and diameters varying from 10 to 50nm (Fig. 5-3(b)). Significant agglomeration took place during synthesis and the Mn_3O_4 and Fe_3O_4 particles appear as large agglomerates, with the Fe_3O_4 particles being covered by Mn_3O_4 particles. Lack of magnetite (Fe_3O_4) contribution in the diffractogram and Raman spectra of the composite, and also the BET surface area value of the Mnmag3 composite, 40m^2.g^{-1} (approaching to that of Mn_3O_4 particles, 54m^2.g^{-1}), confirm the formation of agglomerates (Table 5-1).

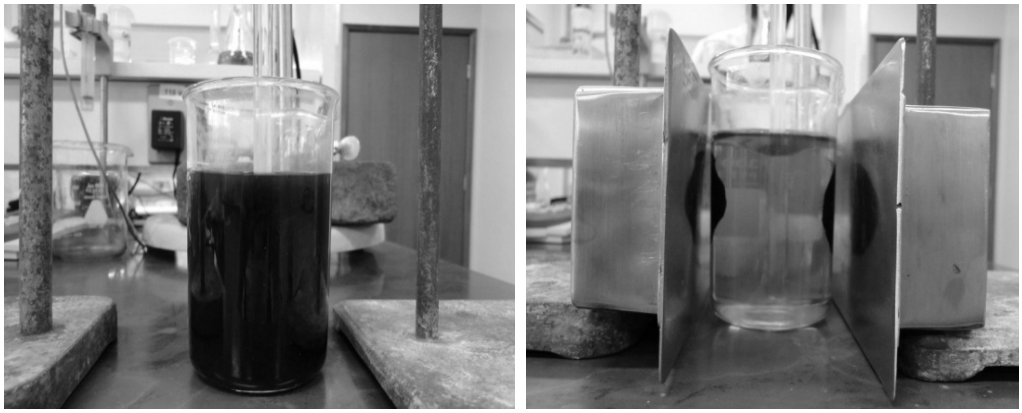

Fig. 5-5: Magnetic Mn_3O_4 composite (Mnmag3 – Chapter 3) dispersed water solution and magnetic separation.

Decolorization of MB by Mn_3O_4 nanoparticles and Mn_3O_4 magnetic composites (Mnmag) was investigated spectroscopically through UV–visible (UV-vis) spectroscopy and the discoloration efficiency (%) of the samples at different times of reaction was calculated according to the following equation (Eq. 5-2):

$$Dicoloration\ efficiency\ (\%) = \frac{(A_{0(\lambda \max)} - A_{(\lambda max)})}{A_{0(\lambda \max)}} \times 100 \qquad (5\text{-}2)$$

with $A_{0(\lambda max)}$: initial absorbance and $A_{(\lambda max)}$: absorbance at time t.

According to the literature, it has been well established that oxidative degradation of organic matter by Mn oxides proceeds via a surface mechanism, that is, the organic compound is adsorbed on surface of Mn oxides to form a surface precursor complex, electron transfer then occurs within the surface from organic reductant to the surface bound Mn^{3+}/Mn^{4+}, followed by release of organic oxidation products and Mn^{2+} arising from reductive dissolution of Mn oxides (Chowdhury et al., 2009; Zaied et al., 2011). Zaied et al. (2011) have used thin layers of birnessite (manganese dioxide) to degrade methylene blue (MB) contained in aqueous solutions and revealed the presence of intermediate reaction products (azure A (AA), azure B (AB), azure C (AC), and thionin (Th)) (Fig. 5-6) during interaction. The characteristic UV-vis λ_{max} of AA, AB, AC, and Th were identified as 628, 638, 618 and 601nm, respectively (Zaied et al., 2011). The following equations (Eqs. 5-3 to 5-7) show the Mn_3O_4 reductive dissolution reaction and *N*-demethylation reactions of MB and its derivatives. Mn_3O_4 favors electron transfers leading to the *N*-demethylation oxidative reaction of MB to form colored intermediary compounds:

$Mn_3O_4 + 8H^+ + 2e^- = 3Mn^{2+} + 4H_2O$ ($Eh^0 = 1.82V$) (5-3)

$AB + e^- + CH_3 = MB + H^+$ ($Eh^0 \sim 1.00V$) (5-4)

$AA + e^- + CH_3 = AB + H^+$ ($Eh^0 \sim 1.00V$) (5-5)

$AC + e^- + CH_3 = AA + H^+$ ($Eh^0 \sim 1.00V$) (5-6)

$Th + e^- + CH_3 = AC + H^+$ ($Eh^0 \sim 1.00V$) (5-7)

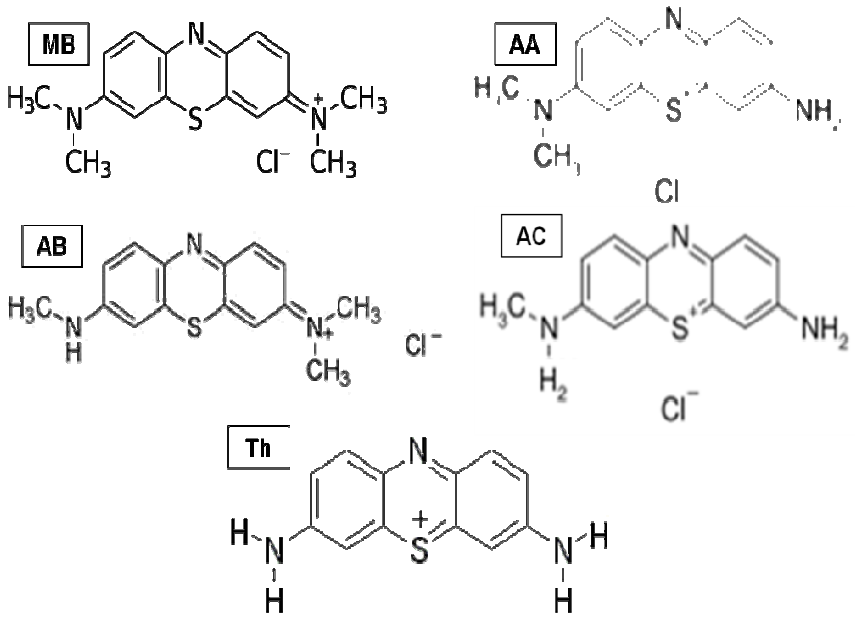

Fig. 5-6: Methylene blue (MB) and its N-demethylated derivatives.

UV-vis spectra of the $1.4x10^{-5}$mol.L^{-1} MB solution before and after charging Mn_3O_4 nanoparticles and Mnmag suspensions (0.7 and 1.4g.L^{-1}) at pH 3.0 are shown in Fig. 5-7. Spectra of dye solution, before adding the solids, clearly exhibit the characteristic λ_{max} (maximum wavelength) peak of MB at 667nm. As soon as the solids are added in the dye solution at pH 3.0, the peaks changed position and intensity indicating that MB was oxidized by Mn_3O_4. For Mn_3O_4 nanoparticles (Fig. 5-7(a)), after 5min of reaction with MB, λ_{max} becomes 634nm, which is close to λ_{max} of AB. After 10min, λ_{max} shifts to 627nm, which is close to λ_{max} of AA. After 15min and 20min, λ_{max} shifts to 613 and 612nm, close to λ_{max} of AC. After 30min until 180min, λ_{max} remains constant at ~600nm, which is close to λ_{max} of Th. For 0.7 g.L^{-1} Mnmag (Fig. 5-7(b)), MB is oxidized only after 20min, when it is transformed to AB. Then, MB is transformed to AA after 30min, to AC after 60min and to Th after 90min. For 1.4g.L^{-1} Mnmag (Fig. 5-7(c)), MB is oxidized to AB after 10min and to Th after 60min. The UV-Vis spectra of the $1.4x10^{-5}$mol.L^{-1} MB solution before and after charging Mn_3O_4 nanoparticles suspension (0.7g.L^{-1}) at pH 4.0 and pH 6.0 shows that the MB peaks only changed in intensity, remaining in the same positions with time (Fig. 5-8).

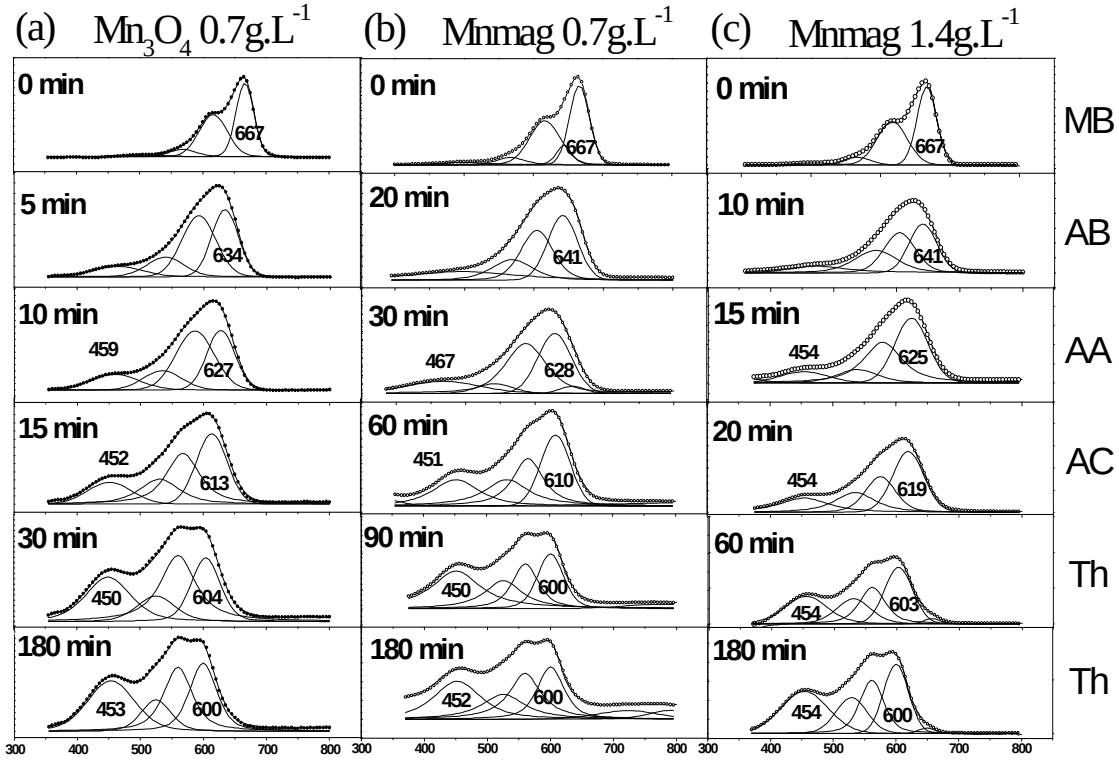

Fig. 5-7: UV-vis spectra peak fitting of 1.4 x 10^{-5}mol.L^{-1} MB solution before and after charging (a) Mn_3O_4 nanoparticles (0.7g.L^{-1}) and the magnetic Mn_3O_4 composite (Mnmag3 – Chapter 3) (b) 0.7g.L^{-1} and (c) 1.4g.L^{-1} suspensions at pH 3.0.

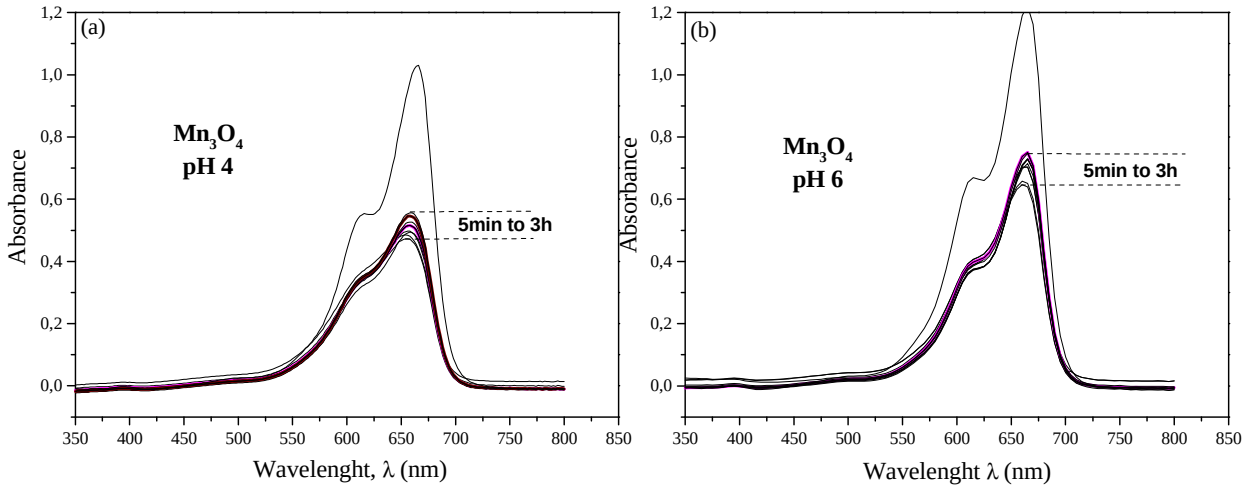

Fig. 5-8: UV-vis spectra of 1.4 x 10^{-5}mol.L^{-1} MB solution before and after charging Mn_3O_4 nanoparticles suspension (0.7g.L^{-1}) at (a) pH 4.0 and (b) pH 6.0.

Fig. 5-9(a) shows the discoloration efficiency (%) versus time for Mn_3O_4 nanoparticles and Mnmag suspensions at pH 3.0. For 0.7g.L^{-1} Mn_3O_4 nanoparticles, 86% of color disappeared after 60min and remained constant until 180min. For 0.7g.L^{-1} Mnmag, 83% of color have disappeared after 90min and remained constant until 180min. For 1.4g.L^{-1} Mnmag, 85% of color disappeared after 60min and remained constant until 180min. For Mn_3O_4 nanoparticles, at pH 4.0 and pH 6.0, the discoloration remained constant at ~50% (Fig. 5-9(b)).

The results show that at pH 4.0 and pH 6.0, MB was not oxidized by Mn_3O_4, indicating that the role of acid is very important in the decolorization reaction, what is explained by the H^+ dependent Mn_3O_4 reductive reaction (Eq.5-3). Futhermore, the oxidative reaction is slightly faster and discoloration is slightly higher for the 0.7g.L^{-1} Mn_3O_4 nanoparticles than for 0.7g.L^{-1} Mnmag suspension. However, when the Mnmag concentration is duplicated (1.4g.L^{-1}), the oxidation reaction rate and discoloration increase. Therefore, the lowering of oxidative reaction rate and discoloration for 0.7g.L^{-1} Mnmag is explained by the less quantity of Mn_3O_4 in the composite. About 1/3 of the composite mass consists of Fe_3O_4, so 50mg of the composite consists of ~33mg (0.5g.L^{-1}) of Mn_3O_4, while 100mg of the composite consists of ~67mg (1.0mg.L^{-1}) of Mn_3O_4.

Methanol (MeOH) was used to dissolve organic compounds present onto the solids after interaction in the aim to identify them. The solids were immersed during 24h. The identification of the organic compounds was made by UV–vis spectroscopy. Fig. 5-10 presents the absorbance measurements obtained with the MeOH solution. The measured value of λ_{max}=600nm is the characteristic λ_{max} of thionin (Zaied et al., 2011), indicating that the MB fully demethylated derivative is the adsorbed organic compound after MB oxidation.

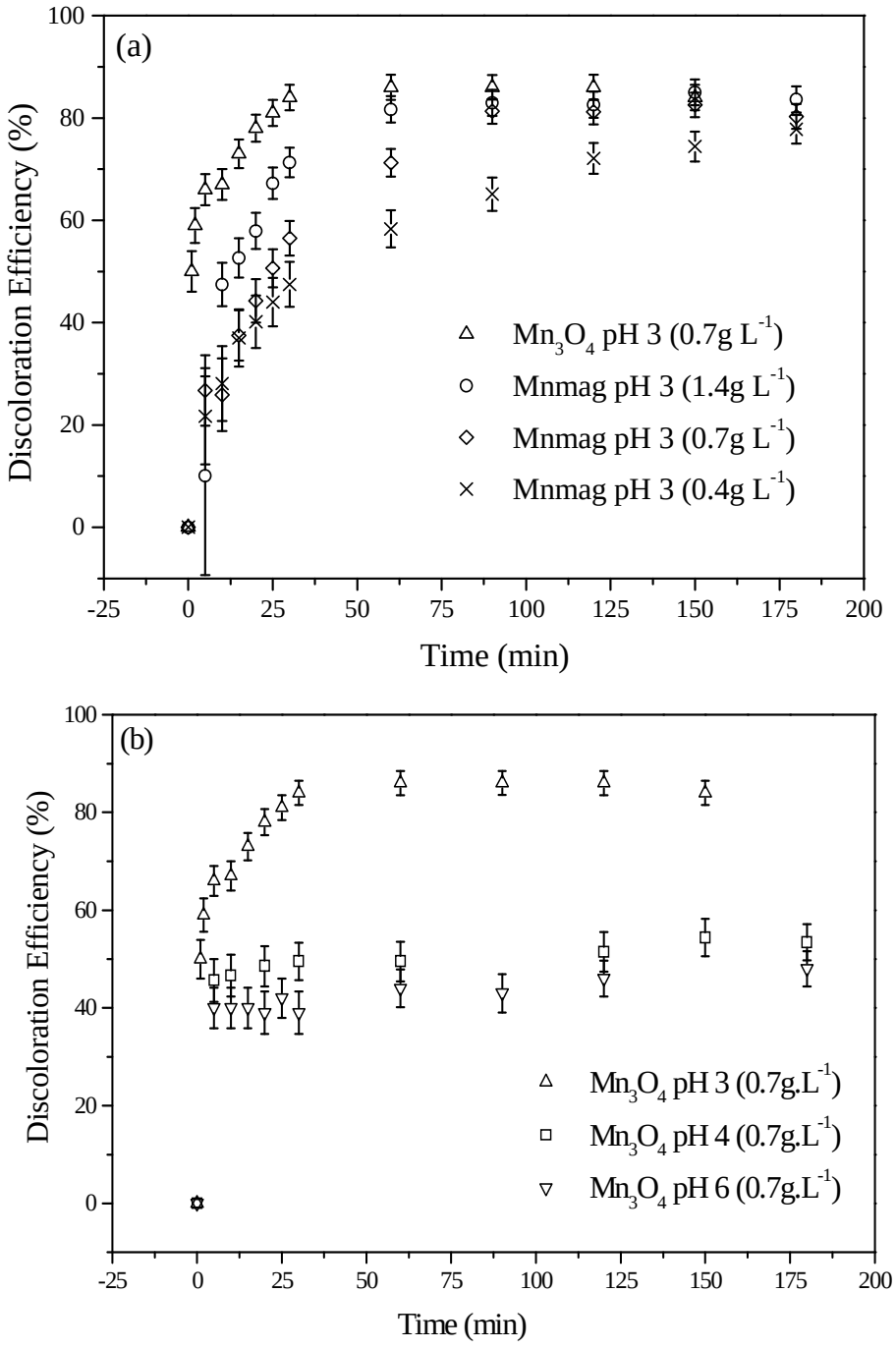

Fig. 5-9: Discoloration efficiency (%) versus time of 1.4 x 10^{-5}mol L^{-1} MB solution in interaction with (a) 0.4g.L^{-1}, 0.7g.L^{-1} and 1.4g.L^{-1} Mnmag suspensions at pH 3.0, and (b) with 0.7g $L^{-1}$$Mn_3O_4$ nanoparticles at pH 3.0, 4.0 and 6.0.

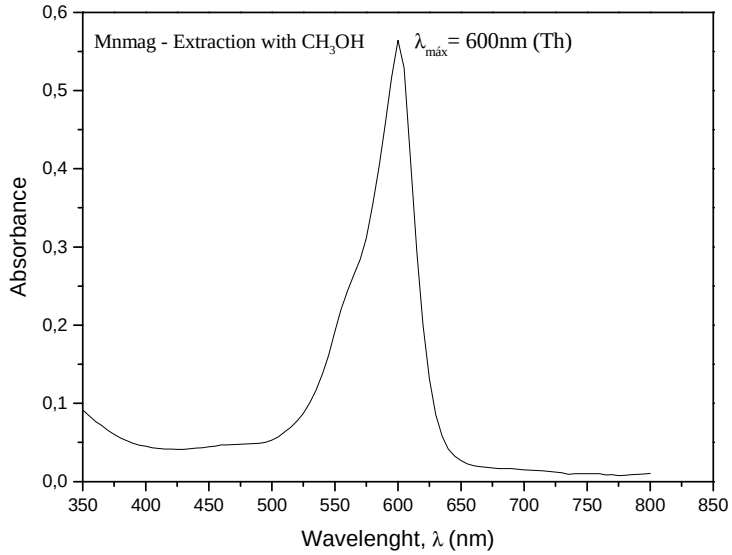

Fig. 5-10: UV–vis spectrum of MeOH solution after 24h of leaching reaction of Mnmag sample which have interacted with MB solution containing 1.4×10^{-5}mol.L^{-1} during 48h.

5.4 Conclusion

Mn_3O_4-Fe_3O_4 composites were synthesized via co-precipitation of Mn_3O_4 in presence of synthesized magnetite particles. Raman and FTIR spectroscopy results show the main magnetite bands confirming that the magnetite particles synthesis was well performed. The synthesized magnetite particles with 70emu.g^{-1} of saturation magnetization and a superparamagnetic state at room temperature present a cubic spinel structure with a_0=8.3617Å, and a particle diameter of ~10nm. The Mn_3O_4 synthesis in presence of these magnetite nanoparticles favors the formation of a pure, highly ordered magnetic Mn_3O_4 composite. The composite is superparamagnetic at room temperature and can be separated by an external magnetic field. The BET surface area value of the composite, 40m^2.g^{-1} (approaching to that of Mn_3O_4 particles, 54m^2.g^{-1}) and lack of magnetite (Fe_3O_4) contribution in the spectra of the composite indicates the formation of agglomerates.

The composite was tested in the degradation of MB in water. Results showed that the pH of the decolorization medium exerts significant effect on the degree of dye decolorization. At lower pH, the Mn_3O_4 nanoparticles show superior capacity of decolorization; the degrees of decolorization of MB in acidic media reached 85% within 60min for Mn_3O_4 magnetic composite. Therefore, the composite is usable for organic dyes oxidation and removal from water.

Chapter 6 Final Considerations

6.1 Summary of results

The overall objective of this thesis was to develop a magnetic adsorbent and oxidant for the removal of contaminants from aqueous solutions which exhibits features that significantly improve the solid-liquid separation needed after the process. Manganese oxide, Mn_3O_4, precipitated by O_2, an eco-friendly oxidant, was successfully deposited onto magnetite used as core material. XRD and Raman spectroscopy confirm that the magnetic particles were well covered by manganese oxide particles. The composites were applied to oxidize and remove As(III) and MB, and could be separated from solution by applying a magnetic field.

The maximum sorption capacity and affinity of arsenic ions onto magnetic Mn_3O_4 composites (synthesized with magnetite particles of different surface areas) were evaluated from the sorption isotherms by the Langmuir, Freundlich and combined Langmuir and Freundlich models. The composite and the Mn_3O_4 samples have shown high ($b > 1$ and $n > 1$ – Table 3-3) and similar affinity for As(III), which is desired for the removal of trace and sub-trace arsenic from water. XANES results show that the As adsorbed is in the oxidized arsenic form, As(V), and Raman and IR results indicate the formation of monodentate and bidentate mononuclear complexes. During the As oxidation-adsorption process, iron is not released and part of the Mn^{2+} released to solution is being adsorbed or precipitated, or both, which implies in a less contaminants release to solution. The Mn_3O_4 magnetic composite was also capable of catalyzing the complete *N*-demethylation of MB, forming thionine as the final product and removing 85% of the dye in 60min. The oxidation took place only in acidic media. At pH>3, MB was not oxidized by Mn_3O_4 and only 50% of the dye was removed.

Hence, it can be concluded that a main objective of this investigation, which comprised an environmentally friendly synthesis of a manganese oxide composite with magnetic properties to be recovered from aqueous solution environmental systems was achieved.

Moreover, the Mn_3O_4 magnetic composite could be efficiently applied to oxidize and remove inorganic (arsenite) and organic (MB dye) compounds from water.

6.2 Original contribution from this Thesis

1) “Preparation and application of a magnetic composite (Mn_3O_4/Fe_3O_4) for removal of As(III) from aqueous solutions”
- Authors: Gabriela C. Silva, Virgínia S. T. Ciminelli, Fabiana S. Almeida, and Angela M. Ferreira.
- Paper published by *Materials Research* Journal.

2) “Raman and IR spectroscopic investigation of magnetic Mn_3O_4 As-containing samples”
- Authors: Gabriela C. Silva, Virgínia S. T. Ciminelli, Maria S. S. Dantas, Fabiana S. Almeida, and Angela M. Ferreira.
- Paper published by *Spectrochimica Acta Part A: Molecular and Biomolecular Spectroscopy* Journal.

3) “Magnetic Mn_3O_4 Nanocomposites for Degradation of Methylene Blue”
- Authors: Gabriela C. Silva, Virgínia S. T. Ciminelli, Fabiana S. Almeida, Nathália C. Pissolati and Angela M. Ferreira.
- Paper to be submitted to the *ACS Nano* Journal.

4) “REMOÇÃO DE As(III) POR UM COMPÓSITO MAGNÉTICO DE Mn_3O_4”
- Authors: Gabriela C. Silva, Virgínia S. T. Ciminelli, Fabiana S. Almeida, and Angela M. Ferreira.
- Extended Abstract published in the Proceedings of the *XXIV Encontro Nacional de Tratamento de Minérios e Metalurgia Extrativa*, Salvador, Brazil - October 2011.

6.3 Future perspectives

The results of this PhD thesis have demonstrated that arsenic and dyes can be effectively removed from aqueous solutions by sorption process using manganese oxide (Mn_3O_4) with magnetic properties. The tests were carried out in batch operation systems. For testing the performance of the composite in industrial scale, a continuously operated scale-up system needs to be designed. Considering a large scale application, an almost complete separation of the magnetic composite could be achieved using a high gradient magnetic separation (HGMS) device. Additionally, the composite may be tested for other environmental systems, such as heavy metals removal, and for treating real effluents.

Considering arsenic adsorption mechanism investigations, EXAFS data of the As-loaded composites should be analyzed to confirm Raman and IR spectroscopy results.

References

ABDELAZEZ K, AHMED M, ZENG Q, WU K, HUANG K, 2010. Mn_3O_4 nanoplates and nanoparticles: Synthesis, characterization, electrochemical and catalytic properties. *J. Solid State Chem*, 183, 744–751.

AHN M Y, FILLEY T R, JAFVERT C T, NIES L, HUA I, BEZARES-CRUZ J, 2006. Photodegradation of decabromodiphenyl ether adsorbed onto clay minerals, metal oxides, and sediment. *Environmental Science and Technology*, 40, 215-220.

ANDREOZZI R, INSOLA A, CAPRIO V, MAROTTA R, TUFANO V, 1996. The use of manganese dioxide as a heterogeneous catalyst for oxalic acid ozonation in aqueous solution. *Applied Catalysis A: General*, 138, 75-81.

BAJPAI S, CHAUDHURI M, 1999. Removal of arsenic from ground water by manganese dioxide-coated sand. *Journal of Environmental Engineering*, 125(8),782-784.

BARRETT K A, MCBRIDE M B, 2005. Oxidative degradation of glyphosate and aminomethylphosphonate by manganese oxide. *Environmental Science and Technology*, 39, 9223-9228.

BOCHKAREV G R, PUSHKAREVA G I, KOVALENKO K A, 2010. Journal of Mining Science, 46, 197-202.

BROCK S L, DUAN N, TIAN Z R, GIRALDO O, ZHOU H, SUIB S L, 1998. A review of porous manganese oxide materials. *Chemistry of Materials*, 10, 2619-2628.

CAETANO M, CIMINELLI V, ROCHA S, SPITALE M, CALDEIRA C, 2009. Batch and continuous precipitation of scorodite from dilute industrial solutions. *Hydrometallurgy (Amsterdam)*, 95, 44-52.

CALDEIRA C L, CIMINELLI V S T, OSSEO-ASARE K, 2010. The role of carbonate ions in pyrite oxidation in aqueous systems. *Geochimica et Cosmochimica Acta*, 74, 1777-1789.

CARVALHO-FILHO A, CURI N, MARQUES J-J G S M, SHINZATO E, DE FREITAS D-A F, DE JESUS E A, MASSAHUD R T R, 2011. Óxidos de manganês em solos do Quadrilátero Ferífero (MG). *R. Bras. Ci. Solo*, 35, 793-804.

CHAKRAVARTY S, DUREJA V, BHATTACHARYYA G, MAITY S, BHATTACHARJEE S, 2002. Removal of arsenic from groundwater using low cost ferruginous manganese ore. *Water Research*, 36, 625-632.

CHANDRA V, PARK J, CHUN Y, LEE J W, HWANG I C, KIM K S.2010. Water-Dispersible Magnetite-Reduced Graphene Oxide Composites for Arsenic Removal. *ACS Nano, 4* (7), 3979–3986.

CHANG Y C, CHEN D H, 2005a. Preparation and adsorption properties of monodisperse chitosan-bound Fe_3O_4 magnetic nanoparticles for removal of Cu^{2+} ions. *Journal of Colloid and Interface Science*, 283(2), 446-451.

CHANG Y C, CHEN D H, 2005b. Adsorption kinetics and thermodynamics of acid dyes on a carboxymethylated chitosan conjugated magnetic nano-adsorbent. *Macromolecular Bioscience*, 5(3), 254-261.

CHANG Y C, CHANG S W, CHEN D H, 2006a. Magnetic chitosan nanoparticles: Studies on chitosan binding and adsorption of Co^{2+} ions. *Reactive and Functional Polymers*, 66, 335-341.

CHANG C F, LIN P H, HÖLL W, 2006b. Aluminum-type superparamagnetic adsorbents: Synthesis and application on fluoride removal. *Colloids and Surfaces A: Physicochem. Eng. Aspects*, 280, 194-202.

CHANG C F, CHANG C Y, HSU T L, 2008. Preparation and adsorptive application of novel superparamagnetic zirconia material. *Colloids and Surfaces A: Physicochem. Eng. Aspects*, 327, 64-70.

CHANG C F, WU Y L, HOU S S, 2009. Preparation and characterization of superparamagnetic nanocomposites of aluminosilicate/silica/magnetite. *Colloids and Surfaces A: Physicochem. Eng. Aspects*, 336, 159-166.

CHAUDHURY G R, CHATTOPADAHYAY P, DAS R P, MUIR D M, Singh P, 2003. Sorption of arsenate from aqueous solution with manganic ferric oxyhydroxide. *Hydrometallurgy 2. Young, C.A., et al. (Eds.), TMS, Warrendale, PA.*, 1913-1922.

CHEN H, CHU P K, HE J, HU T, YANG M. 2011. Porous magnetic manganese oxide nanostructures: Synthesis and their application in water treatment. *Journal of Colloid and Interface Science*. 359, 68-74.

CHEN H, HE J, 2008. Facile synthesis of monodisperse manganese oxide nanostructures and their application in water treatment. *The Journal of Physical Chemistry C*, 112, 17540-17545.

CHEN H, HE J, ZHANG C, HE H, 2007. Self-assembly of novel mesoporous manganese oxide nanostructures and their application in oxidative decomposition of formaldehyde. *The Journal of Physical Chemistry C*, 111, 18033-18038.

CHOWDHURY A N, AZAM M D S, AKTARUZZAMAN M D, RAHIM A, 2009. Oxidative and antibacterial activity of Mn_3O_4. *J. Hazard. Mater*, 172, 1229–1235.

CLARK C M, 2012. X-ray Powder Diffraction (XRD). Available in: <http://serc.carleton.edu/research_education/geochemsheets/techniques/XRD.html> Last Modified: February 01, 2012.

CONAMA, 2011. RESOLUÇÃO N^{o} 430, DE 13 DE MAIO DE 2011. Dispõe sobre as condições e padrões de lançamento de efluentes, complementa e altera a Resolução n^{o} 357, de 17 de março de 2005, do Conselho Nacional do Meio Ambiente-CONAMA.

DAHLKE T, CHEN Y H, FRANZREB M, HÖLL W H, 2006. Continuous removal of copper ions from dilute feed streams using magnetic weak-base anion exchangers in a continuous stirred tank reactor (CSTR). *Reactive & Functional Polymers*, 66, 1062-1072.

DEAN, J A, 1999. Lange`s Handbook of Chemistry. Fifteenth Edition, McGRAW-HILL, INC, 1536 pp.

DENIZLI A, TANYOLAC D, SALIHA B, ÖZDURAL A, 1998. Cibacron Blue F3GA-attached polyvinylbutyral microbeads as novel magnetic sorbents for removal of Cu^{2+}, Cd^{2+} and Pb^{2+} ions. *Journal of Chromatography A*, 793, 47-56.

DESCHAMPS E, CIMINELLI V S T, HÖLL W H, 2005. Removal of As(III) and As(V) from water using a natural Fe and Mn enriched sample. *Water Research*, 39(20), 5212-5220.

DIAS A, SÁ R G, SPITALE M C, ATHAYDE M, CIMINELLI V S T, 2008. Microwave hydrothermal synthesis of nanostructured Na-birnessites and phase transformation by arsenic3+ oxidation. *Materials Research Bulletin*, 43, 1528-1538.

DLUGOSCH T M, 2001. Development, testing and characterization of manganese coated magnetic sorbents for the elimination of arsenic species from water. *M. Sc Thesis, International Institute for Infrastructural Hydraulic and Environmental Engineering.*

DONIA A M, ATIA A A, ELWAKEEL K Z, 2007. Recovery of gold(III) and silver(I) on a chemically modified chitosan with magnetic properties. *Hydrometallurgy*, 87(3-4), 197-206.

DRIEHAUS W, SEITH R, JEKEL M, 1994. Oxidation of arsenite with manganese oxides in water treatment. *Water Research*, 29(1), 297-305.

DUARTE, G, CIMINELLI V S T, DANTAS M S S, DUARTE H A, VASCONCELOS I F, OLIVEIRA A F, OSSEO-ASARE K, 2011. As(III) immobilization on gibbsite: investigation of the complexation mechanism by combining EXAFS analyses and DFT calculations. *Geochimica et Cosmochimica Acta*, 00, 00-00 (in press, available online).

DUTROW B L, 2012. Louisiana State University Geochemical Instrumentation and AnalysisX-ray Powder Diffraction (XRD).

EARY L E, RAI D, 1987. Kinetics of chromium(III) oxidation to chromium(VI) by reaction with manganese dioxide. *Environmental Science and Technology*, 27, 1187-1193.

EBNER A D, RITTER J A, HARRY J P, 1999. New magnetic field-enhanced process for the treatment of aqueous wastes. *Separation Science and Technology*, 34(6/7), 1277-1300.

ERNI R, ROSSELL M D, KISIELOWSKI C, DAHMEN U, 2009. Atomic-Resolution Imaging with a Sub-50-pm Electron Probe. *Phys. Rev. Lett*., 102, 96-101.

FAN F L, QIN Z, BAI J, RONG W D, FAN F Y, TIAN W, WU X L, WANG Y, ZHAO L, 2012 Rapid removal of uranium from aqueous solutions using magnetic Fe_3O_4-SiO_2 composite particles. *Journal of Environmental Radioactivity*, 106, 40-46.

FENG X H, ZHAI L M, TAN W F, 2005. The syntheses of several Mn oxide minerals and their adsorption and redox characteristics for heavy metals. *Acta Petrologica Et Mineralogica*, 24(6): 531-536.

FERRARO J R, NAKAMOTO K, BROWN C W, 2003. Introductory Raman Spectroscopy, 2nd edition, Academic Press, Chapter 1.

FOSTER A L, BROWN J R G E, PARKS G A, 2003. X-ray absorption fine structure study of As(V) and Se(IV) sorption complexes on hydrous Mn oxides. *Geochimica et Cosmochimica Acta*, 67(11), 1937-1953.

GOLDSTEIN J, 2003. Scanning electron microscopy and x-ray microanalysis. *Kluwer Adacemic/Plenum Pulbishers*, 689.

GORRIA P, SEVILLA M, BLANCO J A, FUERTES A B, 2006. Synthesis of magnetically separable adsorbents through the incorporation of protected nickel nanoparticles in an activated carbon. *Carbon*, 44, 1954-1957.

GRAU P, 1991. Textile industry wastewater treatment. *Water Sci. Technol* , 24 (1), 97–103.

GUIMARÃES A M F, CIMINELLI V, VASCONCELOS W, 2009. Smectite organofunctionalized with thiol groups for adsorption of heavy metal ions. *Applied Clay Science*, 42, 410-414.

GUPTA V K, CARROTT P J M, RIBEIRO CARROTT & SUHAS M M L, 2009. Low-Cost Adsorbents: Growing Approach to Wastewater Treatment—a Review. *Critical Reviews in Environmental Science and Technology*, 39:10, 783-842.

GÜTLICH P, 2012. Fifty Years of Mössbauer Spectroscopy in Solid State Research - Remarkable Achievements, *Future Perspectives. Z. Anorg. Allg. Chem*, 638(1), 15–43.

HAN R, ZOU W, ZHANG Z, SHI J AND YANG J, 2006. Removal of copper II and lead II from aqueous solution by manganese oxide coated sand I. Characterization and kinetic study, *Journal of Hazardous Materials*, 137B, 384-395.

HAN Y F, CHEN F X, ZHONG Z Y, RAMESH K, CHEN L W, WIDJAJA E. 2006. Controlled Synthesis, Characterization, and Catalytic Properties of Mn_2O_3 and Mn_3O_4 Nanoparticles Supported on Mesoporous Silica SBA-15. *J. Phys. Chem. B.* 110, 24450-24456.

HÖLL W H, FRANZREB M, 2000. Development of the application of magnetic microsorbents for the elimination of hazardous inorganic contaminants from natural waters. *Forschungsvorhaben nach AZK, ITC-WGT, Karlsruhe.*

HSC CHEMISTRY® 6.0. Outokumpu Research Oy Antti Roine.

HU S Q, WANG H P, CHEN Y H, LIU P, Synthesis and Adsorption Properties of Ethylenediamine Modified Chitosan/Nano-Iron Magnetic Microspheres. *Advanced Materials Research*, 399-401, 1135-1138.

JANSEN D, STABLER C H, GOETZ-NEUNHOEFFER F, DITTRICH S, NEUBAUER J, 2011. Does Ordinary Portland Cement contain amorphous phase? A quantitative study using an external standard method. *Powder Diffr*, 26, 31.

JOHNSON B, HALLBERG K B, 2005. Acid mine drainage remediation options: a review. *Science of the Total Environment*, 338, 3-14.

JOHNSON K L, YOUNGER P L, 2005. Rapid Manganese Removal from Mine Waters Using an Aerated Packed-Bed Bioreactor. *Journal of Environmental Quality*. 34, 987-993.

JUBB A M, ALLEN H C, 2010. Vibrational Spectroscopic Characterization of Hematite, Maghemite, and Magnetite Thin Films Produced by Vapor Deposition. *ACS Appl. Mater. Interfaces*. 2 (10), 2804-2812.

JULIEN C M, MASSOT M, POINSIGNON C, 2004. Lattice vibrations of manganese oxides. Part I. Periodic structures. *Spectrochimica Acta Part A*, 60(3), 689-700.

JULIEN C, MASSOT M, BADDOUR-HADJEAN R, FRANGER S, BACH S & PEREIRA-RAMOS J P, 2003. Raman spectra of birnessite manganese dioxides. *Solid State Ionics*, 159, 345-356.

KATAFIAS A, FENSKA J, 2011. Oxidation of phenothiazine dyes by manganese3+ in sulfuric acid solution. *Transition Met. Chem*, 36, 801-809.

KIMA S C, SHIM W G, 2010. Catalytic combustion of VOCs over a series of manganese oxide catalysts. *Appl. Catal B,* 98, 180–185.

KIRILLOV S A, ALEKSANDROVA V S, LISNYCHA T V, DZANASHVILI D I, KHAINAKOV S A, GARCÍA J R, VISLOGUZOVA N M, PENDELYUK O I, 2009. Oxidation of synthetic hausmannite (Mn_3O_4) to manganite (MnOOH). *Journal of Molecular Structure*, 928, 89-94.

LADEIRA A C, CIMINELLI V S T, 2004. Adsorption and desorption of arsenic on an oxisol and its constituents. *Water Research*, 38, 2087-2094.

LAFFERTY B J, GINDER-VOGEL M, ZHU M, LIVI K J, SPARKS D L. 2010. Arsenite Oxidation by a Poorly Crystalline Manganese-Oxide. 2. Results from X-ray Absorption Spectroscopy and X-ray Diffraction *Environmental Science & Technology*, 44, 8467-8472.

LARKIN P J, 2011. IR and Raman Spectroscopy: Principles and Spectral Interpretation. Elsevier Inc.

LENOBLE V, LACLAUTRE C, SERPAUD B, DELUCHAT V, BOLLINGER J C, 2004. As(V) retention and As(III) simultaneous oxidation and removal on a MnO_2-loaded polystyrene resin. *Science of the Total Environment*, 326, 197-207.

LIM S F, CHEN J P, 2007. Synthesis of an innovative calcium-alginate magnetic sorbent for removal of multiple contaminants. *Applied Surface Science*, 253, 5772-5775.

LIM S F, ZHENG Y M, ZOU S W, CHEN J P, 2008. Characterization of Copper Adsorption onto an Alginate Encapsulated Magnetic Sorbent by a Combined FT-IR, XPS, and Mathematical Modeling Study, *Environmental Science & Technology*, 42, 2551-2556.

LOVETT R J, 1992. Removal of manganese from acid mine drainage. *Proceedings Thirteenth Annual West Virginia Surface Mine Drainage Task Force Symposium.*

MA W, YA F Q, HAN M, WANG R, 2007. Characteristics of equilibrium, kinetics studies for adsorption of fluoride on magnetic-chitosan particle. *Journal of Hazardous Materials*, 143(1-2), 296-302.

MAJUSTE D, CIMINELLI V S T, DANTAS M S S, MAGALHÃES-PANIAGO R, OSSEO ASARE, K, 2012. Electrochemical dissolution of chalcopyrite: detection of bornite by synchrotron small angle X-ray diffraction and its correlation with the hindered dissolution process. *Hydrometallurgy*, 111-112, 114-123.

MANNING B A, FENDORF S E, BOSTICK B, SUAREZ D L, 2002. Arsenic3+ oxidation and arsenic^{5+} adsorption reactions on synthetic birnessite. *Environmental Science & Technology*, 36, 976-981.

MARTIN S T, 2005. Precipitation and Dissolution of Iron and Manganese Oxides, in *Environmental Catalysis (V H Grassian, Ed), CRC press: Boca Raton*, 61-81.

MARTINS I, LIMA I V, 2001. Ecotoxicologia do manganês e seus compostos. *Série Cadernos de Referência Ambiental, 7, Salvador: CRA*.

MCMULLAN D, 1993. SCANNING ELECTRON MICROSCOPY 1928 – 1965. Full version of a presentation at the 51st Annual Meeting of the Microscopy Society of America, Cincinnati, August 1993.

MOHAN D, PITTMAN JR C U, 2007. Arsenic removal from water/wastewater using adsorbents-A critical review. *Journal of Hazardous Materials*, 142, 1-53.

MOSKOWITZ B M, 1991. Hitchhiker's Guide to Magnetism for the Environmental Magnetism Workshop held 5-8 June at the Institute for Rock Magnetism.

MÜLLER K, CIMINELLI V S T, DANTAS M S S, WILLSCHER S, 2010. A comparative study of As(III) and As(V) in aqueous solutions and adsorbed on iron oxy-hydroxides by Raman Spectroscopy. *Water Research*, 44, 5660-5672.

MÜRBE J, RECHTENBACH A, TÖPFER J, 2008. Synthesis and physical characterization of magnetite nanoparticles for biomedical applications. *Materials Chemistry and Physics*, 110(2–3), 426–433.

MYNENI S C B, TRAINA S J, WAYCHUNAS G A, LOGAN T J, 1998. *Geochimica et Cosmochimica Acta*. 62, 3285-3300.

NAUMOV G B, RYZHENKO B N, KHODAKOVSDSKY I L, 1974. Handbook of thermodynamic data, Nat. Tech. Inf. Service, 226, 722/7 GA, U.S. Dept. of Commerce, 328 pp.

NAVARRA A, GRAHAM J T, SOMOT S, RYAN D H, FINCH J A, 2010. Mössbauer quantification of pyrrhotite in relation to self-heating. *Minerals Engineering*, 23(8), 652–658.

NAVARRA A, GRAHAM J T, SOMOT S, RYAN D H, FINCH J A, 2011. Mössbauer quantification of pyrrhotite in relation to self-heating. *Catalysis Today*, 175(1, 25), 238–244.

NESBITT H W, CANNING G W, BANCROFT G M, 1998. XPS study of reductive dissolution of 7Å-birnessite by H_3AsO_3 with constraints on reaction mechanism. *Geochimica et Cosmochimica Acta*, 62(12), 2097-2110.

NEWBURY D E, 1986. Advanced scanning electron microscopy and X-ray microanalyses. *New York: Plenum*, 454p.

NEWVILLE, M. (2004): Fundamentals of X-ray Absorption fine Structure, Consortioum for Advanced Radiation Sources – University of Chicago, Version 1.6.1.

NGOMSIK A F, BEE A, SIAUGUE J M, CABUIL V, COTE G, 2006. Nickel adsorption by magnetic alginate microcapsules containing an extractant. *Water Research*, 40, 1848-1856.

NOUBACTEP C, 2009. Characterizing the discoloration of methylene blue in Fe^0/H_2O systems. *J. Hazard. Mat*, 166, 79-87.

O'KEEFE M A, ALLARD L F, BLOM D A, 2005. HRTEM imaging of atoms at sub-Ångström resolution. *J Electron Microsc*, 54(3), 169-180.

OLIVEIRA A, LADEIRA A, CIMINELLI V S T, HEINE T, DUARTE H, 2006. Structural model of arsenic3+ adsorbed on gibbsite based on DFT calculations. *Journal of Molecular Structure: TEOCHEM*, 762(1-3), 17-23.

OLIVEIRA L C A, PETKOWICZ D I, SMANIOTTO A, PERGHER S B C, 2004. Magnetic zeolites: a new adsorbent for removal of metallic contaminants from water. *Water Research*, 38, 3699-3704.

OLIVEIRA L C A, RIOS R R A, FABRIS J D, GARG V, SAPAG K, LAGO R M, 2002. Activated carbon/iron oxide magnetic composites for the adsorption of contaminants in water. *Carbon*, 40, 2177-2183.

OLIVEIRA L C A, RIOS R V R A, FABRIS J D, SAPAG K, GARG V K, LAGO R M, 2003. Clay-iron oxide magnetic composites for the adsorption of contaminants in water. *Applied Clay Science*, 22, 169-177.

OSCARSON D W, HUANG P M, DEFOSSE C, HERBILLON A, 1981. Oxidative power of Mn(IV) and Fe(III) oxides with respect to As(III) in terrestrial and aquatic environments. *Nature*, 291, 50-51.

OSCARSON D W, HUANG P M, HAMMER U T, 1983. Oxidation and sorption of arsenite by manganese dioxide as influenced by surface coatings of iron and aluminum oxides and calcium carbonate. *Water, Air, and Soil Pollution*, 20, 233-244.

PANTUZZO F L, CIMINELLI V S T, 2010.Arsenic association and stability in long-term disposed arsenic residues. *Water Research (Oxford)*, 44, 5631-5640.

PARSONS J G, LOPEZ M L, PERALTA-VIDEA J R, GARDEA-TORRESDEY J L, 2009. Determination of arsenic(III) and arsenic(V) binding to microwave assisted hydrothermal synthetically prepared Fe_3O_4, Mn_3O_4, and $MnFe_2O_4$ nanoadsorbents. *Microchemical Journal*, 91, 100-106.

PENG X J, LUAN Z K, DI Z C, ZHANG Z G, ZHU C L, 2005. Carbon nanotubes-iron oxides magnetic composites as adsorbent for removal of Pb^{2+} and Cu^{2+} from water. *Carbon*, 43, 855-894.

PENG X J, LUAN Z K, ZHANG H M, 2006. Montmorillonite–Cu^{2+}/Fe^{3+} oxides magnetic material as adsorbent for removal of humic acid and its thermal regeneration. *Chemosphere*, 63, 300-306.

PORTER S K, SCHECKEL K G, IMPELLITTERI C A, Ryan J A, 2004. Toxic metals in the environment: Thermodynamic considerations for possible immobilization strategies for Pb, Cd, As, and Hg. *Critical Reviews Environmental Science and Technology*, 34, 495.

POST J E, 1999. Manganese oxide minerals: Crystal structures and economic and environmental significance. *Proceedings of the National Academy of Sciences - Colloquium Paper*, 69, 3447-3454.

PRESNIAKOV I A, RUSAKOV V S, DEMAZEAU G, SOBOLEV A V, GLAZKOVA Y A S, GUBAIDULINA T V, GAPOCHKA A M, VOLKOVA O S, VASILIEV A N, 2012. Magnetic exchange interactions and supertransferred hyperfine fields at Sn probe atoms in $CaCu_3Mn_4O_{12}$. *physical review*, 85, 024406.

QU J, 2008. Research progress of novel adsorption processes in water purification: A review. *Journal of Environmental Sciences*, 20, 1-13.

RAMDANI A, STEINMETZ J, GLEITZER C, COEY J M D, FRIEDT J M, 1987. Perturbation de l'échange électronique rapide par les lacunes cationiques dans $Fe_{3-x}O_4$ ($x<0.09$). J. Phys. Chem. Solids, 48, 217-228.

RHADFIA T, PIQUEMAL J Y, SICARD L, HERBST F, BRIOT E, BENEDETTI M, 2010. Atlamsani, A. Polyol-made Mn_3O_4 nanocrystals as efficient Fenton-like catalysts. Appl. Catal., A. 386, 132–139.

RIBEIRO T S, SASAKI J M, VASCONCELOS I F, 2012. Structural disorder of ball-milled, nanosized, Fe-doped SnO_2: X-ray diffraction and Mössbauer spectroscopy characterization. *Journal of Materials Science*, 47, 2630-2636.

RIETVELD H M.1969. A Profile Refinement Method for Nuclear and Magnetic Structures J. *Appl. Cryst*, 2, 65-71.

ROCHA M J S, FILHO M C C, THEOPHILO K R B, DENARDIN, VASCONCELOS I F, ARAÚJO I B, SOMBRA A S B, 2012. Ferrimagnetism and Ferroelectricity of the Composite Matrix: $SrBi_2Nb_2O_9$ (SBN) X-BaFe12019(BFO)100–X. *Materials Sciences and Applications,* 3, 6-17.

ROCHER V, SIAUGUE J M, CABUIL V, BEE A, 2008. Removal of organic dyes by magnetic alginate beads. *Water Research*, 42, 1290-1298.

RODRIGUEZ A F R, ESCOSIO F, LÓPEZ J L, AZEVEDO R B, MORAIS P C, 2010. Mössbauer characterization of magnetite/polyaniline magnetic nanocomposite. *AIP Conference Proceedings*, 1311, 3-7.

ROSAS C A C, FRANZREB M, VALENZUELA F, HÖLL W H, 2010. Magnetic manganese dioxide as an amphoteric adsorbent for removal of harmful inorganic contaminants from water. *Reactive & Functional Polymers*. 70, 516-520.

SAFARÍK I, NYMBURSKA, SAFARIKOVA M, 1997. Adsorption of watersoluble organic dyes on magnetic charcoal. *Journal of Chemical Technology and Biotechnology*, 69, 1-4.

SCOTT M J, MORGAN J J, 1995. Reactions at oxide surfaces. 1. Oxidation of As(III) by synthetic birnessite. *Environmental Science & Technology*, 29, 1898-1905.

SEKINE Y, 2002. Oxidative decomposition of formaldehyde by metal oxides at room temperature. *Atmospheric Environment*, 36, 5543-5547.

SHAUGHNESSY D A, NITSCHE H, BOOTH C H, 2003. Molecular interfacial reactions between Pu(ε) and manganese oxide minerals manganite and hausmannite. *Environmental Science and Technology*, 37, 3367-3374.

SI Y, REN T, DING B, YU J Y, SUN G, 2012. Synthesis of mesoporous magnetic Fe_3O_4-carbon nanofibers utilizing in situ polymerized polybenzoxazine for water purification. *J. Mater. Chem.*, Advance Article

SILVA G C, VASCONCELOS I F, CARVALHO R P, DANTAS M S S, CIMINELLI V S T, 2009. Molecular modeling of iron and arsenic interactions with carboxy groups in natural biomass. *Environ. Chem.*, 4, 350–356.

SILVA A C, PEREIRA M C, OLIVEIRA L C A, CAVALCANTE L C D, FABRIS J D, MURAD E, 2012. An unusually thermally stable magnetite from a niobium mine in Brazil. *Clay Minerals*, 47(1), 69-79.

SMEDLEY P L, KINNIBURGH D G, 2002. A review of the source, behavior and distribution of arsenic in natural waters. *Applied Geochemistry*, 17(5), 517-568.

SOLOMONS T W G, 1996. Organic Chemistry, 6th Edition, New York: John Wiley and Sons, pp. 55-65.

SOLTI A, KOVÁCS K, BASA B, VÉRTES A, SÁRVÁRI E, FODOR F**,** 2012. Mössbauer quantification of pyrrhotite in relation to self-heating**.** *Plant Physiology and Biochemistry*, 52, 91–97.

STOBBE E R, DE BOER B A, GEUS J W, 1999. The reduction and oxidation behaviour of manganese oxides. *Catalysis Today*, 47, 161-167.

STUMM W AND MORGAN J J, 1981. Aquatic Chemistry. Wiley, New York.

SUN H, CAO L, LU L, 2011. Magnetite/reduced graphene oxide nanocomposites: One step solvothermal synthesis and use as a novel platform for removal of dye pollutants. *NANO RESEARCH*, 4 (6), 550-562.

TEIXEIRA M-C, CIMINELLI V S T, 2005. Development of a Biosorbent for Arsenite: Structural Modeling Based on X-ray Spectroscopy. *Environmental Science & Technology*, 39 (3), 895-900.

TEIXEIRA M, CIMINELLI V S T, DANTAS M, DINIZ S, DUARTE H, 2007. Raman spectroscopy and DFT calculations of As(III) complexation with a cysteine-rich biomaterial. *Journal of Colloid and Interface Science*, 315, 128-134.

THIRUNAVUKKARASU O S, VIRARAGHAVAN T, SUBRAMANIAN K S, CHAALAL O, ISLAM M R, 2005. Arsenic Removal in drinking water - impacts and novel removal technologies. *Energy Sources*, 27, 209-219.

THOSAR B V, 1983. Advances in Mössbauer spectroscopy: applications to physics, chemistry and biology. *Amsterdam*, Oxford, 924.

TIAN Z R, TONG W, WANG J Y, DUAN N G, KRISHNAN V V, SUIB S L, 1997. Manganese Oxide Mesoporous Structures: Mixed-Valent Semiconducting Catalysts. *Science*, 276, 926–929.

TRIPATHY S S, BERSILLON J L, GOPAL K, 2006. Adsorption of Cd^{2+} on hydrous manganese dioxide from aqueous solutions. *Desalination*, 194, 11-21.

TUUTIJARVI T, LUB J, SILLANPAS M., CHEN G, 2009. As(V) adsorption on maghemite nanoparticles. *Journal of Hazardous Materials*, 166, 1415-1420.

TYE F L, 1976. Manganese dioxide electrode-III relationship between activities and stoichiometry for compositions near to MnO_2. *Electrochimica Acta*, 21(6),415-420.

VACLAVIKOVA M, GALLIOS G P, HREDZAK S, JAKABSKY S, 2008. Removal of arsenic from water streams: an overview of available techniques *Clean Techn Environ Policy*, 10, 89-95.

VASCONCELOS I F, SILVA G C, CARVALHO R P, DANTAS M S S, CIMINELLI V S T, 2010. Mössbauer and EXAFS spectroscopy investigation of iron and arsenic adsorption to lettuce leaves. *Hyperfine Interact*., 195, 111-115.

VELSEN VAN A F M, VOS VAN DER G, 1991. High gradient magnetic separation technique for wastewater treatment. *Water Science and Technology*, 24(10), 195-203.

WANG Y, WANG X, LUO G, DAI Y, 2008. Adsorption of bovin serum albumin (BSA) onto the magnetic chitosan nanoparticles prepared by a microemulsion system. *Bioresource Technology*, 99, 3881-3884.

WEHRLI B, 1990. In: Aquatic Chemical Kinetics: Reaction Rate Processes in Natural Waters, W Stumm, ed. New York: Wiley, 311-336.

WEI Y Q, YAO W, WANG W, 2012. Effects of Internal Standards and Peak Profile Functions on Quantitative XRD Phase Analysis of Cement and its Hydrates Key *Engineering Materials*, 492, 424-428.

WOOLFSON M M, 1997. An introduction to X-ray crystallography. 2nd Ed. Cambridge: University Press.

WORLD HEALTH ORGANIZATION, 2008. Guidelines for Drinking Water Quality, Volume 1 - Recommendations, 3nd edition, Geneva.

WU R C, QU J H, 2004. Removal of Acid Red B from water by surface modified Fe_3O_4. *Acta Scieniae Circumstantiae*, 24(3), 435-439.

WU R C, QU J H, CHEN Y S, 2005. Magnetic powder $MnOFe_2O_3$ - A novel material for the removal of azo-dye from water. *Water Research*, 39, 630-638.

WU R, QU J H, HE H, YU Y, 2004. Removal of azo-dye Acid Red B (ARB) by adsorption and catalytic combustion using magnetic $CuFe_2O_4$ powder. *Applied Catalysis B: Environmental*, 48, 49-56.

XU H Y, XU S L, WANG H, YAN H, 2005. Characterization of Hausmannite Mn_3O_4 Thin Films by Chemical Bath Deposition. *Journal of The Electrochemical Society*, 152(12), C803-C807.

XU L, XU C, ZHAO M, QIU Y, SHENG G D, 2008. Oxidative removal of aqueous steroid estrogens by manganese oxides. *Water Res*, 42, 5038–5044.

YAVUZ C T, MAYO J T, YU W W, PRAKASH A, FALKNER J C, YEAN S, CONG L, SHIPLEY H J, KAN A, TOMSON M, NATELSON D, COLVIN V L, 2006. Low-Field magnetic separation of monodisperse Fe_3O_4 nanocrystals. *Science*, 314, 964-967.

YIN H, FENG X, QIU G, TAN W, LIU F, 2011. Journal of Hazardous Materials 188, 341-349.

ZAERA F, 2012. Probing Liquid/Solid Interfaces at the Molecular Level. *Chemical Reviews*, in press.

ZAIED M, PEULONA S, BELLAKHAL N, DESMAZIÈRESD B, CHAUSSÉA A, 2011. Studies of *N*-demethylation oxidative and degradation of methylene blue by thin layers of birnessite electrodeposited onto SnO_2. *Appl. Catal. B*, 101, 441–450.

ZHAI Y, ZHAI J, ZHOU M, DONG S, 2009. Ordered magnetic core–manganese oxide shell nanostructures and their application in water treatment. *J. Mater. Chem.*, 19, 7030–7035.

ZHANG G S, QU J H, LIU H J, COOPER A T, WU R C, 2007a. $CuFe_2O_4$/activated carbon composite: A novel magnetic adsorbent for the removal of acid orange II and catalytic regeneration. *Chemosphere*, 68, 1058-1066.

ZHANG G S, QU J H, LIU H J, LIU R P, WU R C, 2007b. Preparation and evaluation of a novel Fe-Mn binary oxide adsorbent for effective arsenite removal. *Water Research*, 41, 1921-1928.

ZHANG H, LIANG C, TIAN Z, WANG G, CAI W J, 2010. Single Phase Mn3O4 Nanoparticles Obtained by Pulsed Laser Ablation in Liquid and Their Application in Rapid Removal of Trace Pentachlorophenol. *Phys. Chem. C*, 114, 12524-12528.

APPENDIX

Gibbs energy of formation, ΔG^{o}_{298} (kJ.mol^{-1}) of Eh-pH diagrams species.

Species	ΔG^{o}_{298} (kJ.mol^{-1})	Reference
Mn	0.0	Dean, 1999
MnO_2	-465.2	Dean, 1999
Mn_2O_3	-881.2	Dean, 1999
Mn_3O_4	-1283.2	Dean, 1999
MnOOH	-553.5	Tye, 1976
Mn^{2+}	-228.1	Dean, 1999
MnO_4^-	-447.3	Dean, 1999
O_2	16.3	Naumov et al., 1971
H_2O	-237.14	Dean, 1999
OH^-	137.3	Naumov et al., 1971
H^+	0.0	Dean, 1999
$H_2AsO_3^-$	-587.22	Dean, 1999
H_3AsO_3	-639.9	Dean, 1999
$HAsO_4^{2-}$	-714.7	Dean, 1999
$H_2AsO_4^-$	-753.29	Dean, 1999
H_3AsO_4	-766.1	Dean, 1999